Measurement of left ventricular deformation using 3D echocardiography

Johannes Just Hjertaas

Thesis for the degree of Philosophiae Doctor (PhD)
University of Bergen, Norway
2023

UNIVERSITY OF BERGEN

Measurement of left ventricular deformation using 3D echocardiography

Johannes Just Hjertaas

Thesis for the degree of Philosophiae Doctor (PhD)
at the University of Bergen

Date of defense: 05.06.2023

Year: 2023

Title: Measurement of left ventricular deformation using 3D echocardiography

Name: Johannes Just Hjertaas

Print: Skipnes Kommunikasjon / University of Bergen

Contents

List of abbreviations

2D	Two-dimensional
3D	Three-dimensional
ABr	Apical basal longitudinal strain ratio
ABS	Acrylonitrile butadiene styrene
AD	Axial Dimension
AF	Atrial fibrillation
ALS	Apical longitudinal strain
ANOVA	Analysis of variance
AS	Aortic stenosis
ATTR-CM	Transthyretin amyloid cardiomyopathy
AVA	Aortic valve area
BCS	Basal circumferential strain
BLS	Basal longitudinal strain
BMI	Body mass index
CA	Cardiac amyloidosis
CAD	Coronary artery disease
CoV	Coefficient of variation
CS	Circumferential strain
CT	Computed tomography
DCM	Dilated cardiomyopathy
E/e’	Filling pressure (peak early trans mitral blood flow to average mitral annular velocity ratio)
ECG	Electrocardiogram
ED	End diastole
EF	Ejection fraction
ES	End systole
FR	Frame rate
GCS	Global circumferential strain

GLS	Global longitudinal strain
HCM	Hypertrophic cardiomyopathy
HR	Heart rate
ICC	Intraclass correlation coefficient
LV	Left ventricle, Left ventricular
LS	Longitudinal strain
MCS	Mid circumferential strain
MLS	Mid longitudinal strain
MRI	Magnetic resonance imaging
P_g	Group factor
PVA	Polyvinyl alcohol
P_w	Within factor
ROI	Region of interest
RWT	Relative wall thickness
RS	Radial strain
SAVR	Surgical aortic valve replacement
SD	Standard deviation
STE	Speckle tracking echocardiography
SV	Stroke volume
TAVI	Transcatheter aortic valve implantation
TVI	Tissue velocity imaging
VPS	Volumes per second
VR	Volume rate

Scientific environment

This PhD project has been carried out within the *Bergen Hypertension and Cardiac Dynamics group* at the Department for Clinical Science, University of Bergen, Norway. The group is now coordinated within *Centre for Research on Cardiac disease in Women*, established in 2020, where activities within the group are organized.

The main supervisor for the PhD project has been professor Knut Matre (now emeritus) with professor Eva Gerdts as co-supervisor. In addition, the group consist of one associate professor, one senior researcher, 1 postdoctoral fellow, 6 PhD fellows, 1 medical research student, 2 master students, 1 study nurse and 1 engineer.

The group has experience in both experimental and clinical research within the areas of regional cardiac function, hypertensive heart disease and valvular heart disease, ischemic heart disease, and sex differences within cardiology and heart diseases. The main research tools have been non-invasive imaging techniques such as echocardiography, magnetic resonance imaging (MRI), and cardiac computed tomography (CT). The group uses a state-of-the-art echocardiography research laboratory for image analysis.

The experimental research setup was developed in collaboration with the *Department of Physics and Technology* at the University of Bergen.

Clinical research has been done in cooperation with the *department of Heart Disease* at *Haukeland University Hospital*, Helse Bergen, Norway. In addition, the group have research collaborations with both national and international partners.

Acknowledgements

The work of the present thesis was carried out in several stages, starting as a medical research student. I would like to express my sincere gratitude to professor Knut Matre, who I have been privileged to have as my main supervisor. I first met Knut during second year in medical school, before being enrolled in the medical student research program, and he has since patiently provided guidance and support. His background as a physicist has given me great insight into the principles of ultrasound and fundamental understanding of echocardiography techniques in experimental research. I have also been very fortunate to have professor Eva Gerdts as my co-supervisor, and I am very grateful for the time and resources she has invested in me and this project. Her dedication for scientific research and knowledge in clinical echocardiography has been truly helpful and inspiring.

Great help and input have been provided by Sahrai Saeed, Stig Urheim and Marina Kokorina in both practical and theoretical echocardiography. I have also had great help in my clinical work from research nurse Liv Himle and research engineer Hilde Jacobsen. I am also grateful for the input and discussions with professor Ketil Grong on statistical methods.

Almost from the start, I had the pleasure of working with fellow medical researcher Christian Arvei Moen, who included me in his research project, as well as Geir Olav Dahle, with whom I have had many very helpful and interesting discussions. This resulted in many project ideas and solutions. I have also been fortunate to collaborate with Eigir Einarsen on both our projects, with whom I had great discussions on statistics and analyzing methods. I have also had many interesting discussions with fellow researchers Umael Khan and Tom Omdal.

It has been a great pleasure of working in a group with experienced researchers including associate professor Dana Cramariuc and senior researcher Helga Midtbø, as well as all my fellow PhD colleagues and alumni Hilde Halland, Ester Kringeland,

Arleen Aune, Lisa Marie Grymyr, Anja Linde, Annabel Ohldieck and Rune Eilertsen. I have also received great help from master students Henrik Fosså and Grete Lunestad at the Department of Physics and Technology.

I have been very fortunate to know and work with Saied Nadirpour, Jessica Viland, and Christer Aase at the hospital in Haugesund for several years. They have given me much input and knowledge in cardiology, a field which they have inspired me to pursue.

I am thankful for the financial support granted by the Bergesen Foundation, which has been essential in conclusion of this project.

Lastly, I am grateful for all the support, encouragement and inspiration from my family and friends.

Sammendrag

Bakgrunn

3D speckle tracking ekkokardiografi (STE) er en hjerteultralydmetode som gir mulighet for måling av deformasjonsparametere, som strain, rotasjon, tvist og torsjon. Den største begrensningen for 3D STE er lav tids- og romlig oppløsning. Økes den ene oppløsingen vil den andre bli redusert. I tillegg vil andre faktorer som antall flettede bilder, sektorstørrelse og dybde påvirke begge oppløsningene. Denne avhandlingen har hatt som mål å finne tilstander og opptaksinnstillinger for å optimalisere nøyaktigheten til 3D STE-parametere i et kontrollert miljø. Videre har det vært som mål å finne regional deformasjon fra 3D STE i en klinisk studie på pasienter med aortaklaffestenose (AS) ved bruk av optimaliserte innstillinger.

Materiale og metode

Studie 1 og 2 utforsket nøyaktigheten til 3D STE ved bruk av et in vitro-oppsett med et fantom av venstre ventrikkel. Studie 1 sammenlignet 3D STE strain mot sonomikromertri som gullstandard i longitudinell, sirkumferensiell og radiell retning. Ved å bruke et annet fantom i studie 2 ble 3D STE tvist sammenlignet mot sonomikrometri tvist for å finne nøyaktigheten til 3D STE tvistmålinger. Studie 3 inkluderte 85 pasienter med variabel grad av AS i en tverrsnittstudie. 3D ekkokardiografi ble utført og 3D STE-parametere ble sammenlignet mellom grupper av pasienter med mild, moderat og alvorlig AS.

Resultater

Studie 1 fant godt samsvar mellom 3D STE og sonomikrometri med optimalt volum rate på 36,6 volumer per sekund (VPS) ved bruk av 6 sammenflettede bilder. I studie 2 hadde 3D STE godt samsvar ved bruk av både 4 og 6 sammenflettede bilder med volum rater på henholdsvis 20,3 og 17,1 VPS. Studie 3 fant lavere global longitudinal strain i pasienter med alvorlig AS sammenlignet med mild AS. Basal og midtre longitudinal strain var også lavere i alvorlig sammenlignet med mild AS. Apikal-

basal ratio var høyere for moderat i forhold til mild AS. Maks apikal-basal tvist var høyere hos pasienter med alvorlig sammenlignet med mild og moderat AS.

Konklusjon

Måling av venstre ventrikkelfunksjon med 3D STE er mest nøyaktig med volum rater < 40 VPS. Høy romlig oppløsning virker å være mer viktig enn tidsoppløsning. Pasienter med alvorlig AS har lavere global, basal og midtre longitudinal strain enn pasienter med mild AS, ved bruk av 3D STE. De har også høyere tvist enn mild og moderat AS. Områder som involverer apeks, har høyere spredning av data og har antagelig lavere nøyaktighet ved bruk av 3D STE.

Abstract

Background

3D speckle tracking echocardiography (STE) enables measurement of multiple parameters of deformation, such as strain, rotation, twist and torsion. The main limitation of 3D STE is low temporal and spatial resolution. Increasing resolution in time will decrease resolution in space, and vice versa. In addition, other factors such as number of stitched images, sector size and depth, influence the resolution. This thesis aimed to find conditions and acquisition settings to optimize accuracy for 3D STE parameters in a controlled in vitro environment. Secondly, it aimed to evaluate regional deformation by 3D STE in a clinical study on patients with aortic valve stenosis (AS) using optimized settings.

Materials and methods

Study 1 and 2 explored the accuracy of 3D STE using an in vitro setup with a left ventricle (LV) phantom. Study 1 compared 3D STE strain to strain by sonomicrometry as the gold standard. Measurements were compared in both longitudinal, circumferential and radial direction. Using a different twisting phantom in study 2, 3D STE twist was compared to twist by sonomicrometry to evaluate the accuracy of 3D STE twist. Study 3 was a cross-sectional analysis of 85 patients with variable degree of AS in a cross-sectional study. 3D echocardiography was done, and 3D STE parameters were compared between groups of patients with mild, moderate and severe AS.

Results

Study 1 found 3D STE strain to have good agreement with sonomicrometry. Optimal acquisition settings were found to be volume rate 36.6 volumes per second (VPS) obtained by 6 stitched images. Study 2 found 3D STE twist to have good agreement with sonomicrometry when using both 4 and 6 stitched images with volume rates 20.3 and 17.1 VPS, respectively. Study 3 found global longitudinal strain to be lower

in patients with severe AS compared to those with mild AS. Basal and mid longitudinal strains were also lower in severe AS than in mild AS. Apical basal ratio was higher for moderate than mild AS. Peak apical-basal twist was higher in patients with severe AS than in those with mild and moderate AS.

Conclusion

Assessment of LV function by 3D STE is most accurate at volume rates < 40 VPS. High spatial resolution seems to be more important than temporal resolution. Patients with severe AS have lower global, as well as lower regional basal and mid longitudinal strain compared to patients with mild AS, assessed with 3D STE. They also have higher twist than mild and moderate AS. Segments involving the apex have high dispersion and probably lower accuracy in 3D STE.

List of Publications

1. **Hjertaas JJ**, Fosså H, Dybdahl GL, Grüner R, Lunde P, Matre K. Accuracy of real-time single- and multi-beat 3-d speckle tracking echocardiography in vitro. *Ultrasound Med Biol.* 2013;39(6):1006-14.

2. **Hjertaas JJ**, Matre K. A left ventricular phantom for 3D echocardiographic twist measurements. *Biomed Tech (Berl)*. 2020 Apr 28;65(2):209-218.

3. **Hjertaas JJ**, Einarsen E, Gerdts E, Kokorina M, Moen CA, Urheim S, Saeed S, Matre K. Impact of aortic valve stenosis on myocardial deformation in different left ventricular levels: a three-dimensional speckle tracking echocardiography study. *Echocardiography 2022; Submitted*

1. Introduction

1.1 Background

The development of echocardiography has led to multiple new methods for evaluation of left ventricular (LV) function. Modern cardiology is highly dependent on these methods, as echocardiography has become the primary diagnostic tool for multiple conditions. Since Edler and Hertz first demonstrated the use of echocardiography in 1953[1], its clinical use has evolved to cover all types of heart disease, and new areas of clinical usage are continuously introduced. With new methods, there is also a need to evaluate and test the accuracy of these methods, as well as to investigate their clinical application. In particular, methods for accurate assessment of LV deformation are a major area for development, notably new methods for detection of early myocardial dysfunction in clinical practice. Such measures are requested, among others, in the management of aortic valve stenosis (AS) with normal LV ejection fraction (EF) to diagnose subtle LV dysfunction.

1.2 LV deformation

In a healthy heart, synchronized depolarization of myocardial cells cause the LV myocardium to contract in a coordinated fashion during systole, causing ejection of a proportion of its content. During diastolic filling, The LV revert to its pre-systolic state, and myocardial fibers are stretched to a relaxed state. While a single myocyte contracts in one direction, the compounded architecture of myocardial fiber network in the LV makes its cyclic deformation complex. As various parts of the LV contracts in different directions, the net effect is a twisting appearance. This helical arrangement of LV fibers was first described by Sir William Harvey in the 17th century, and has later been studied through anatomic studies[2]. The outer subepicardial layer is oriented in a left-handed helical orientation, becoming more circumferential towards the mid myocardium, and then turns towards a right-handed helical shape in

the subendocardium[3-6]. Longitudinal deformation is attributed to the endocardial and to a certain degree epicardial layers, while circumferential deformation depends more on the mid myocardium. This gives the subepicardial and subendocardial LV myocardial layers of the myocardium a more longitudinal shortening during the systole, while the mid myocardial level contributes to circumferential shortening.

The fiber orientation results in a wringing motion of the LV during contraction. This helps to produce a higher LV EF of about 60 %, despite the myocytes shortening of only 20 %[7]. The full effect of this mechanism is not completely understood, and several explanatory models have been proposed[8,9]. The fiber orientation results in the twisting property of the LV, with the apex turning counterclockwise and the base clockwise during systole, when observed from the apex.

In addition, the helical fiber orientation is a mechanism for storing energy, contributing to diastolic suction of blood into the LV during the rapid untwist in early diastole. Untwist is therefore essential for normal early diastolic function[10].

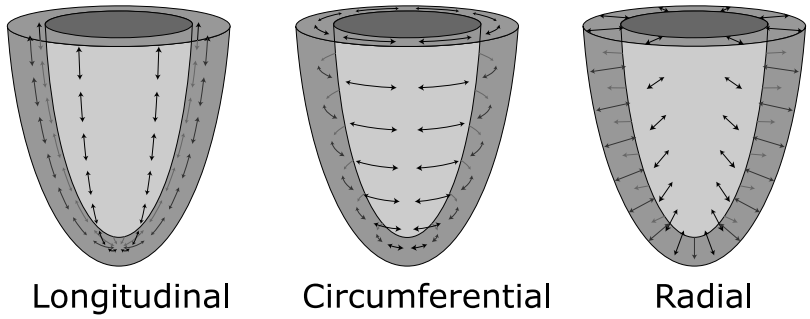

Figure 1. The LV coordinate system axis, where deformation is commonly measured in either longitudinal, circumferential or radial direction.

Deformation assessment may either be global, such as EF, or regional, such as measurements based on tissue velocity imaging (TVI). Deformation orientation is usually reported in either longitudinal, circumferential or radial direction (Figure 1). Any deformation may be influenced by pathology, usually resulting in reduced

deformation either regionally or globally. In AS, the severity of the disease may influence LV deformation differentially at individual levels of the LV.

1.2.1 3D speckle tracking echocardiography

3D speckle tracking echocardiography (STE) of the LV is a deformation measuring tool where pattern recognition is applied to 3D ultrasound myocardial volume regions. By tracking selected regions over time using a block-matching algorithm, a point-based model of the LV is produced[11]. This algorithm tracks patterns within a region of interest (ROI) in the 3D volume one volume to the next. The ultrasonic STE algorithm tracks multiple patterns of small irregularities in the myocardium that are consistent throughout the recording[12]. This speckle-like pattern makes a region of myocardium distinguishable and easily identifiable for the block-matching algorithm (Figure 2) from one frame to the next[13]. By tracking multiple regions in the myocardium, a point-based model of LV myocardium is produced, which further can be used to estimate deformation such as myocardial strain, twist and torsion.

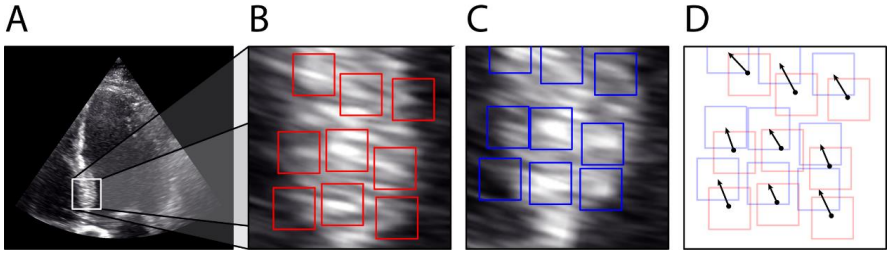

Figure 2. The principle of speckle tracking echocardiography, exemplified in 2D, using a block-matching algorithm in myocardium (A). Patterns are registered in one frame (B). At the next frame, adjacent areas are searched for patterns that matches the previous frame best (C) using the method of block-matching. The relative difference in position between each frame is then used to produce deformation patterns for strain and rotation (D).

1.2.2 Myocardial strain

Strain is defined as the fractional change of an objects dimension from the original dimension. Lagrangian strain can be defined as:

$$\varepsilon(t) = \frac{L(t) - L_0}{L_0}$$

Where $\varepsilon(t)$ is strain at a specific time t, L_0 is the initial dimension, while $L(t)$ is the dimension at the specified time. L_0 is typically defined at end-diastole (ED), while L is typically measured around end-systole (ES).

By using data from 3D STE, myocardial strain can be estimated. Myocardial strain is commonly measured in either longitudinal, circumferential or radial direction (Figure 1). Peak strain values are usually reported in percentage of systolic change relative to its original dimension in ED. If strain is known in two dimensions, strain in the third dimension can be estimated when assuming the material (myocardium) is incompressible. This assumption is commonly used by 3D STE algorithms, as only circumferential strain (CS) and longitudinal strain (LS) is measured, while radial strain (RS) is calculated from CS and LS[11].

1.2.3 Myocardial rotation

To understand the complex left ventricular rotational mechanics, it is essential to understand fiber orientation. The heart consists of myocardial fibers organized in a complex orientation (Figure 3). This has been verified in anatomic studies[2,6], and later *in vivo* studies has shown that magnetic resonance imaging (MRI) can also depict fiber orientation using Diffusion Tensor Imaging[10,14,15]. Later computer simulation models have shown to correlate well with these findings[8], giving a better understanding of the fiber orientation.

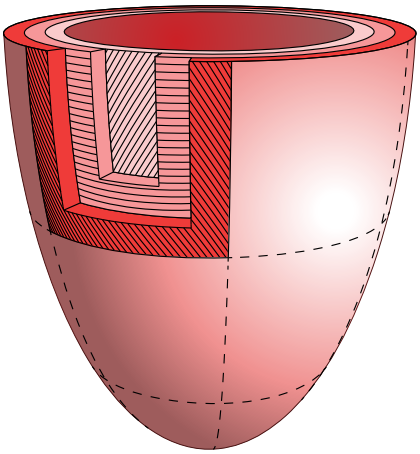

Figure 3. Fibers of the different layers of myocardium in the LV are oriented in different directions. Subepicardial and subendocardial layers have helical arrangement in opposite directions, while mid myocardial fibers have a more circumferential orientation.

As a consequence of the helical fiber arrangement in the myocardium, different LV levels rotate counterclockwise and clockwise throughout the heart cycle. By measuring STE data rotation around the longitudinal axis, myocardial rotation in a 2D plane can be estimated. In this context, the measured rotation is the object's change of angle relative to the observer, namely the ultrasound probe (Figure 4A). Although rotation alone is not a type of deformation, it provides the foundation for estimation of deformation parameters such as twist and torsion, when measuring rotation at different positions within the same object.

1.2.4 Myocardial twist

While rotation is the change of angle relative to the observer, twist is the change of angle relative to the object itself, measured in two different planes (Figure 4B). Using STE, this can be estimated by measuring rotation in two different planes along the longitudinal axis. Untwist is the rate of change when the LV twist return back to its original diastolic shape from ES.

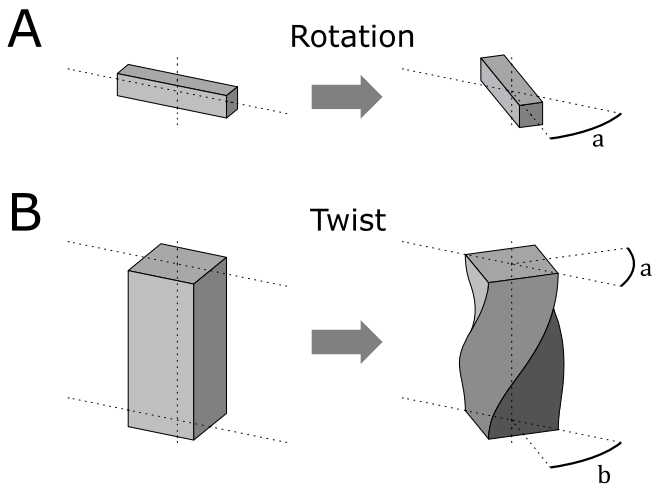

Figure 4. Rotation is measured as the change in angle (a) from a reference point (A). In echocardiography, the reference is the ultrasound probe. Twist is measured as the difference in angles between two planes $(a - b)$ (B). In cardiology this is usually the difference between apical rotation and basal rotation.

1.2.5 Myocardial torsion

Torsion is defined as twist, divided by the distance between the two planes (Figure 5). While torsion can be measured using 2D echocardiography using geographic markers[16], use of 2D is unreliable due to in and out of plane motion, and 3D echo could give a more accurate measurement[17].

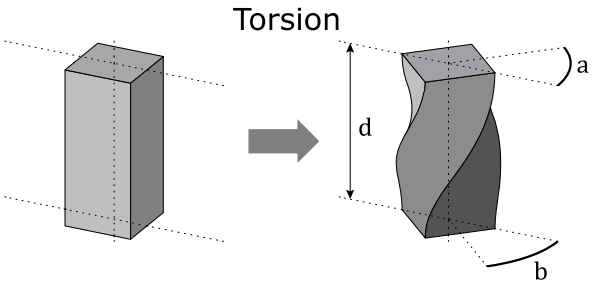

Figure 5. Torsion measures the difference in angles between two planes divided by the distance between them ($\frac{a-b}{d}$). In cardiology, this is the twist between the apex and basal level divided by the length between these two planes.

1.3 3D echocardiographic challenges

While 3D echocardiography has shown to be superior to 2D echocardiography in a number of areas[18,19], its major drawback is low temporal resolution, or volume rate, as well as limited spatial resolution, or number of beams per volume. This originates from the fact that 2D echocardiography only uses one lateral dimension in addition to the axial dimension (Figure 6A), while 3D echocardiography uses two lateral dimensions (Figure 6B).

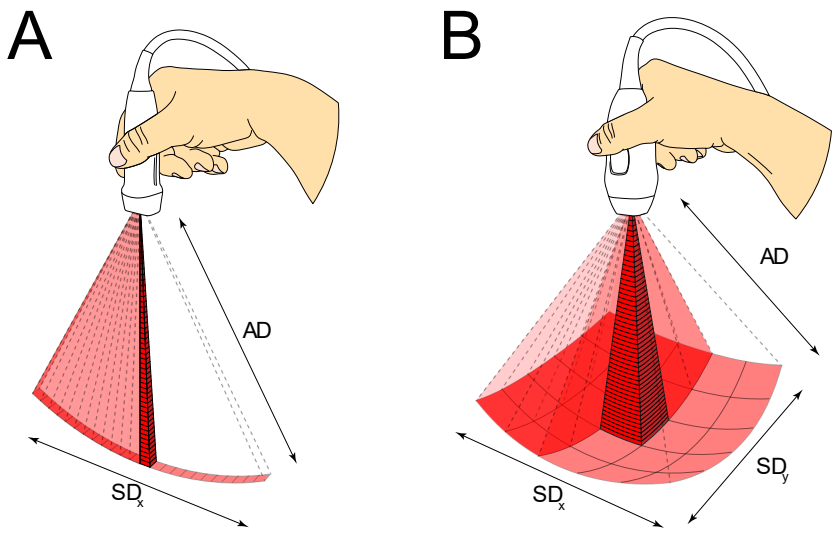

Figure 6. Spatial resolution of a 2D frame (A) versus a 3D volume (B), both consisting of 25 beams. While both methods have the same resolution in the axial dimension (AD), resolution in lateral dimension (SD_x and SD_y) is lower in 3D volumes.

A 3D volume consisting of 25 ultrasound beams only has 5 beams in each lateral dimension, while a 2D sector with the same number of beams has all 25 in its single lateral dimension, when acquired at the same frame rate (FR) (Figure 6). Therefore, the scanner probe must send out n^2 beams to account for the same spatial resolution as a 2D probe sending out n beams per frame. In the same setting, a 3D volume would have to send out 625 beams to accommodate for the same spatial resolution as a 2D sector of 25 beams. Any increase in spatial resolution comes at the cost of temporal resolution and vice versa. Both temporal and spatial resolution of 3D images thus depend on the number of beams chosen for each image as well as the sector width. It is also important to emphasize that spatial resolution is affected only in the lateral dimensions, while axial dimension resolution is relatively unaffected. Other factors, such as degree of beam focusing will also influence this balance.

A method now commonly used to increase both spatial and temporal resolution is volume stitched imaging. This technique uses multiple smaller 3D volumes, each acquired over a single heart cycle triggered by electrocardiogram (ECG) (Figure 7). The smaller volumes are then stitched together to one larger 3D volume[20,21]. However, this technique requires the length of the heart cycles to be near identical during acquisition, which may be challenging in a clinical setting. Although 3D strain has been compared at different number of stitched beats[22], no studies have evaluated accuracy and what acquisition settings gives the best accuracy.

A third parameter affecting temporal and spatial resolution is sector angle. While this can be adjusted, it may be more difficult in some clinical situations, such as with severely dilated LVs or large heart valves. Other factors, like sampling time, also affects both temporal and spatial resolution.

The balance between temporal and spatial resolution depends on what is to be measured. LS depends more on resolution in the axial direction, and may therefore be less affected by spatial resolution, while CS depends more on lateral resolution. This may result in different optimal resolutions for these two strain directions, even though both are measured using 3D STE. Increased lateral resolutions may also be important when measuring rotation and twist, which rely on deformation changes in the lateral direction. Another important factor is that lateral resolution decreases further away from the probe, because of increasing distance between the beams. Compared to 2D echocardiography, 3D is more sensitive to changes in either temporal or spatial resolution. Any increase in one resolution will reduce the other. With already restricted resolutions in both terms because of the third dimension, 3D echocardiography imaging needs to be optimized in order not to waste one type of resolution at the cost of the other. Few studies have evaluated the use of 3D STE in a controlled environment and what acquisition settings give best accuracy.

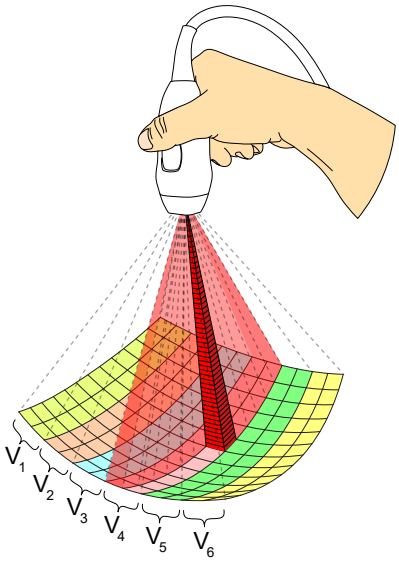

Figure 7. Volume stitched image technique. Multiple smaller 3D volumes (V_1-V_6) are recorded over 6 ECG triggered heart beats and stitched to one larger 3D volume.

1.4 Aortic valve stenosis

Degenerative AS is a progressive disease, characterized by fibrosis and calcification of the aortic valve leaflets. AS may be caused by rheumatic heart disease, which is the most prevalent type of heart valve disease in the developing world, or by congenital defects of the aortic valve, like bicuspid aortic valve disease. The primary cause of AS in the developed world, however, is fibro-calcific degeneration of the aortic valve leaflets, causing progressively increase in LV afterload. AS is the most prevalent form of valve disease requiring valve intervention or replacement, and the third most common cause of heart disease after coronary artery disease (CAD) and hypertension[23].

No pharmacological treatment of AS has proven effective so far, and the only curative therapy is removal of the stenotic valve, either by surgical aortic valve replacement (SAVR), or by transcatheter aortic valve implantation (TAVI). Untreated severe AS has a poor prognosis. The guidelines on management of AS recommend meticulous AS grading based on the pressure gradient, peak jet velocity and aortic valve area (AVA) to identify mild, moderate and severe AS[24,25]. The current guidelines recommend valve replacement in patients with severe, symptomatic AS or in asymptomatic severe AS when EF < 50 %. Low risk patients with EF < 55 % can also be considered for intervention [25]. However, in up to 30 % of patients, discordant grading of AS severity is found using these conventional measures. In particular for symptomatic patients with discordant grading, multimodality imaging methods for assessment of disease severity including aortic valve calcification score by computed tomography (CT), assessment of LV stroke volume (SV) and LV systolic function are recommended[25].

1.4.1 LV deformation and geometry in patients with AS

With progression of AS, chronic pressure overload exposes the LV to increased wall stress, causing it to adapt by remodeling. Such remodeling includes LV hypertrophy, reduced compliance and reactive myocardial fibrosis, which all affect the LV deformation. While the LV remodeling initially overcomes the chronic pressure overload, it gradually decompensates, leading to impaired LV systolic and diastolic function, and eventually symptoms of heart failure. While EF < 50 % is considered a mark of heart failure in AS, it usually presents late, and is often preceded by symptoms like exertional dyspnea, angina pectoris or syncope, the cardinal symptoms of severe AS. Furthermore, AS patients with preserved EF (EF > 50 %) may present with impaired contractility due to LV remodeling with increased wall thickness, reduced diameter or a compensated increased global circumferential strain (GCS) due to loss of global longitudinal strain (GLS)[26,27]. Patients with AS and preserved EF have shown to have reduced GLS[28,29], which may be a better marker of prognosis[30,31]. While GLS alone has not shown to be directly associated with severity or

symptomatic disease, reduced basal longitudinal strain (BLS) has been associated with symptomatic AS[32], and has been shown to predict future SAVR, independent of other parameters[33], suggesting that AS may affect regional LV deformation differentially. However, the impact of AS severity and LV remodeling on LV deformation at different LV levels has been less explored.

In moderate and severe AS, LV twist is higher than in mild AS[34-36]. This increased LV twist in severe AS severity may be due to concentric LV hypertrophy[37]. It has also been suggested that reduced flow in the subendocardial compared to the subepicardial arteries in more severe AS may contribute to this effect[38]. Furthermore, LV twist has been shown to decline after SAVR[39]. However, limited data have so far been published on the associations between LV twist and AS severity in such patients, as well as the accuracy and reproducibility of these 3D LV deformations.

2. Hypothesis and aim of thesis

2.1 Hypothesis

We hypothesized that 3D STE can accurately measure LV deformation using lower temporal resolution than conventional 2D STE. Moreover, 3D STE can be used to study level-specific differences of LV deformation in patients with variable degree of AS.

2.2 Aims

1. To investigate the accuracy of LV 3D STE strain using an *in vitro* setup, and to assess the best acquisition settings for best accuracy.

2. To develop an *in vitro* setup for rotational measurements, and to test the accuracy of LV 3D STE twist as well as the optimal acquisition settings for measuring LV 3D twist.

3. To analyze 3D STE deformation parameters at different LV levels in a clinical study of patients with variable degree of AS.

3. Materials and methods

3.1 Study 1 and 2

3.1.1 Study design

Both study 1 and 2 are in vitro studies with the objective to evaluate 3D STE using different spatial and temporal resolutions against a gold standard, and thereby the accuracy. In study 1, evaluation included 3D LS, CS and RS, and in study 2, the evaluation of 3D twist. Both studies used acoustic phantoms of the LV, and sonomicrometry as the gold standard.

3.1.2 In vitro pump setup

The setup consisted of a rig with two parallel pistons in a pump, driven by a stepper motor. The phantoms were submerged in a water container and connected to the pump via rigid pipes. An air buffer in an elastic hose connected to the pipe system acted as a damper of the strokes from the pump. The stepper motor driving the pump was controlled by custom written LabVIEW software[40] (LabVIEW 8.6, National Instruments, Austin, TX, USA), and allowed different settings such as pump rate (henceforth called heart rate [HR]), systolic-diastolic time ratio and SV. For study 1, the phantom was placed angled in the water container, with the 3D probe placed 4-5 cm directly perpendicular to the apex of the phantom (Figure 8). For study 2, a larger container was used, allowing the phantom to be mounted vertically with the probe 4 cm directly above the apex. For both studies, the same ultrasound probe (4V; GE Vingmed Ultrasound AS, Horten, Norway) was used, as well as the same scanner (Vivid E9; GE Vingmed Ultrasound AS).

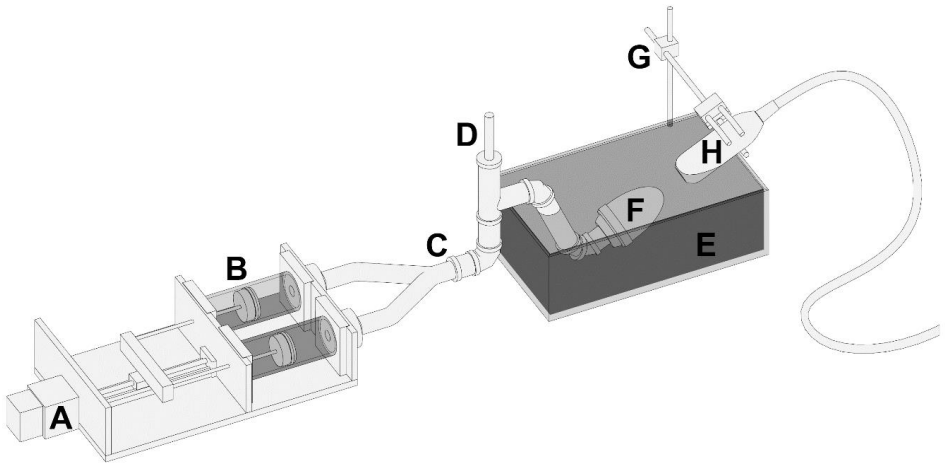

Figure 8. Pump rig setup. Stepper motor (A). Dual piston pump (B). Rigid pipes (C). Elastic hose for dampening (D). Water container ©. Phantom (F). Rigid stand with clamp (G). 3D ultrasound probe (H).

3.1.3 Phantom material

Polyvinyl Alcohol (PVA [M_w 89K-98K, 99+% hydrolyzed, Sigma-Aldrich, Saint Louis, MO, USA]) was used as the material for the phantoms. The PVA solution was prepared by adding 10 % by weight PVA to 90 % water, and then heated to 90° C while being stirred, dissolving the PVA. To solidify the material, freezing was done at -18° C for 24 hours followed by thawing at room temperature (+20° C), and then the cycle was repeated one more time before the phantom was ready for use.

3.1.4 Study 1 in vitro phantom

The phantom used in study 1 was based on a LV with a truncated prolate spheroid shape. Phantoms were casted using a 3D printed mold consisting of two parts, which had a wall thickness of 10 mm. After PVA was poured into the mold, it underwent a total of two freezing cycles of 24 hours. The internal diameter at rest (henceforth called end systole [ES]) was 50 mm. Three pairs of sonomicrometer crystals with a diameter of 2 mm (SL5-2, Triton Technologies Inc., San Diego, CA, USA) were

implanted mid-wall in longitudinal and circumferential direction with 10 mm distance between each crystal, and one pair with the crystals at each side of the wall for radial direction. The crystals positions were secured by a drop of cyanoacrylate glue. When connected to the rig, the phantom was inflated by the water pump, mimicking diastolic filling of the LV. Systolic contraction was mimicked as the water was pumped back out of the phantom. As the phantom material expanded when inflated, it mimicked myocardial relaxation, enabling simulation of strain imaging by echocardiography. Different strain values were achieved by using different SV.

3.1.5 Study 2 in vitro phantom

The phantom in study 2 was constructed to exert twist when inflated, so a different internal geometry was needed. As the phantom in the previous study, this was also made of PVA, but casted in two sessions, enabling different rigidity of the two cast layers. This permitted a more rigid internal helical structure in the phantom wall, that would force the phantom to twist and untwist when inflated and deflated, and at the same time avoid any external deformation attachment. The phantom mold was designed using computer-aided design software (Rhino 5, Robert McNeel & Associates, Seattle, WA, USA) (Figure 9A). The overall design was similar to the phantom in study 1, with slightly thicker wall around equator (12 mm) and thinner wall at the apex (8 mm). The internal diameter was 42 mm, and the length was 92 mm. A 3D printed threaded base of acrylonitrile butadiene styrene (ABS) was casted into the phantom for easy attachment to the rig. The spiral structure consisted of 8 continuous PVA-bands encircling inside the phantom wall in parallel at 45° to the longitudinal direction at the base and narrowing to 0° to meet at the apex. The spiral band thickness was 8 mm at the base and 4 mm at apex. Casting of the phantom was done in two steps. The PVA-solution was identical to the solution in the previous study. First, the inner spiral structure along with the inner parts of the phantom was casted using a 5-part 3D printed mold of ABS plastic (Figure 9B). The mold then underwent 5 freezing cycles at the same temperatures as in study 1, but with shorter duration of 12 hours freezing and then 12 hours thawing. The four pieces consisting

of the outer mold was then detached, and a wider outer mold was attached, allowing additional PVA-solution to be added before undergoing one additional freezing cycle with the outer layer (Figure 9C). This gave the spiral part of the phantom a total of 6 freezing cycles, and the outer part only one, resulting in a difference in rigidity between the inner and outer layer. This resulted in a phantom with an outer structure, similar to the previous phantom, but with a different inner structure, while still appearing as a cardiac LV on the ultrasound scanner (Figure 9D). When the phantom was connected to the rig pump, it inflated and deflated as the phantom in study 1. The helical structure inside the phantom forced the apex to be rotated clockwise during diastolic filling, and counterclockwise during systolic ejection when observed from the apex. As the basal level was stationary, this generated twisting deformation of the phantom. By increasing the SV, the angle of twist also increased.

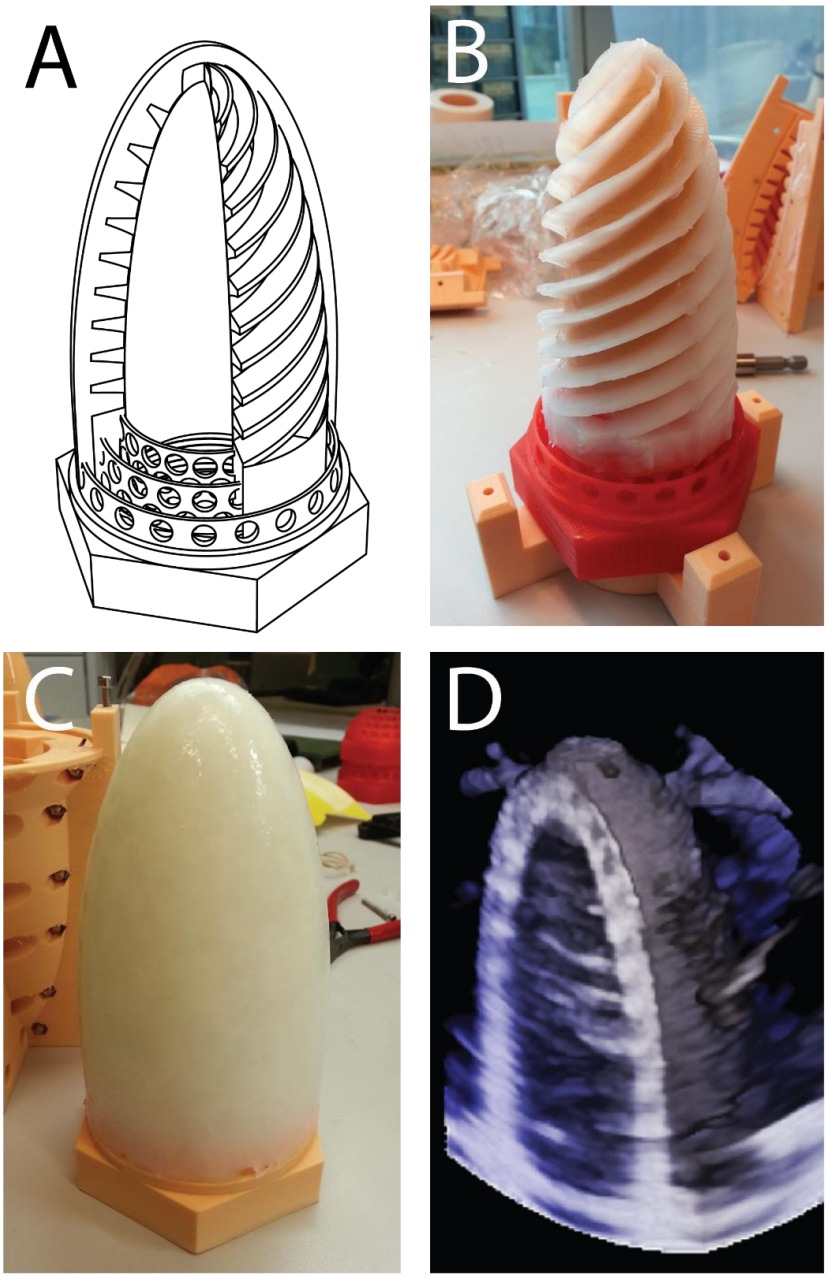

Figure 9. Design and production of the twisting phantom in study 2. Schematic view (A). The casted spiral body of the phantom, halfway through the process (B). The finished phantom with its outer layer (C). 3D ultrasound image of the phantom (D).

As for study 1, sonomicrometer crystals were used to measure distance. In this study however, we needed to measure rotation in two different planes of the phantom. To achieve this, a total of 6 crystals were placed in two group of triangles, one at the base, and the other at the apex, making the shape of a triangular antiprism (Figure 10).

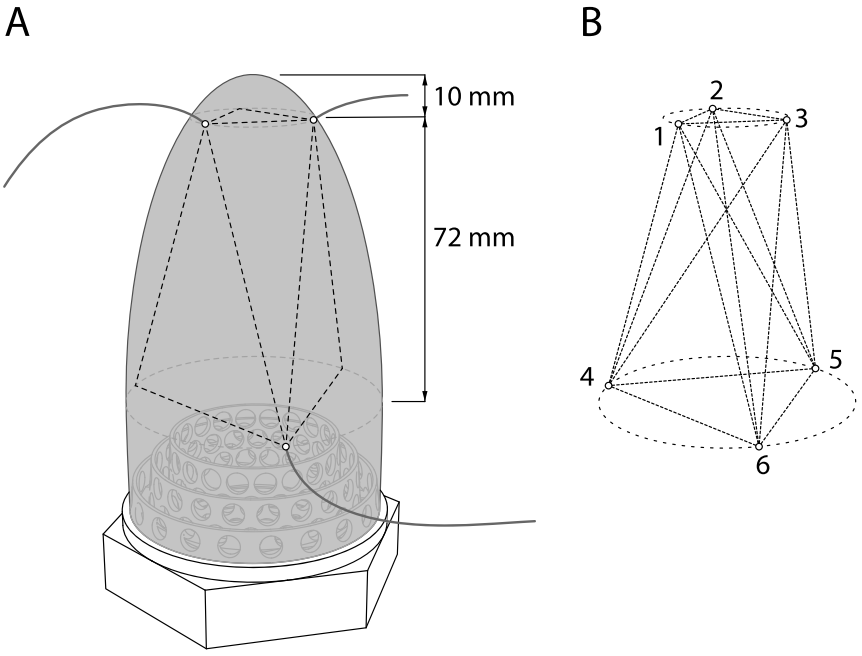

Figure 10. Sonomicrometer crystal setup for twist measurements. The crystals were placed in two triangles opposite to each other, to maximize the angle between each crystal. One triangle at the apex, and the other in the base (A). This resulted in the shape of a triangular antiprism, where all crystals could measure the distance to each other (B).

By setting the sonomicrometry up with this configuration, all crystals could measure the distance to each other, and thus make it possible to later calculate the cartesian coordinates of the crystals using the method of trilateration. Each crystal was placed mid-wall and kept in place with a drop of cyanoacrylate glue.

3.1.6 Monitoring and logging

All data from analog instruments were recorded using a digital data logger (PowerLab 8/30, AD Instruments, Sydney, Australia) at about 1000 samples/s. For study 1, sonomicrometry distance data was measured using a four-channel sonomicrometer (Type 120.2; Triton Technologies Inc. San Diego, CA, USA) by analog recording of three of the channels with a pair of crystals connected to each channel (Figure 11). For study 2, sonomicrometry data from all distances between the 6 crystals was measured using a digital Sonomicrometer and logging (DS3-8 and LabChart Pro v7, Sonometrics Corporation, Ontario, Canada), by digital recording using LabChart Pro at 192 samples/s. All sonomicrometer values were measured immediately before ultrasound recording, and then turned off because of ultrasound interference resulting in artifacts showing up on the ultrasound scanner. To ensure the pressure in the phantoms were identical for each recording a micro-tip pressure transducer was used (SPC-350, Millar Instruments, Houston, TX, USA). To enable stitched volume recordings on the ultrasound scanner, an ECG-signal for each pump cycle was required. This was achieved by sending a pulse from the pump to the analog data logger for each pump cycle. The signal was then transformed into a synthetic ECG-signal, and then fed to the ultrasound scanners ECG input.

3.1.7 Study 1 data acquisition and analysis

To create comparable data sets, two groups of recordings using different SVs to create variation of strain was carried out using different temporal and spatial resolutions. One dataset at HR 60 beats/min with SV ranging 10-150 ml with 10 ml step, and one group at 120 beats/min with SV ranging 10-80 ml with 10 ml step were recorded. In addition, 7 series were recorded in each group using different temporal and spatial resolutions (Table 1) by single-beat 3D echocardiography as well as 2- and 6-beat stitched images. In total 161 images were recorded. The different temporal resolutions were selected from available scanner presets when sector angle was set to 75° and the depth range was 0-12 cm. Other acquisition settings were kept constant throughout the recordings.

Echocardiographic analysis was performed using a commercial software (EchoPAC BT11; GE Vingmed Ultrasound AS). For analysis of strain, the 4D Auto LVQ-tool in EchoPAC was used. First the images were aligned to keep the LV axis parallel to the probe axis. Then, the inner ROI was selected, first in ED, then in ES. After the software had traced the lumen of the phantom in every volume recorded, the outer part, corresponding to the epicardial border was selected, at both ED and ES. The software then calculated STE in each volume. When completed, strain values were presented in a 17-segment bull's-eye-plot (6 basal segments, 6 mid segments, 4 apical segments and one segment for the apex), as well as global values for LS, CS, RS and area strain. Timings of ES and ED were calculated by the software, with ES being the frame with smallest volume and ED being the frame with largest volume. Segments adjacent to the crystals were picked to obtain strain in parts represented by the sonomicrometer readings, and strain values were read at ES for comparison.

The corresponding sonomicrometer values were read using a commercially available software (LabChart Pro; AD Instruments), with sonomicrometry strain values being calculated from the maximum and minimum values of measured lengths during the cycles (Figure 11).

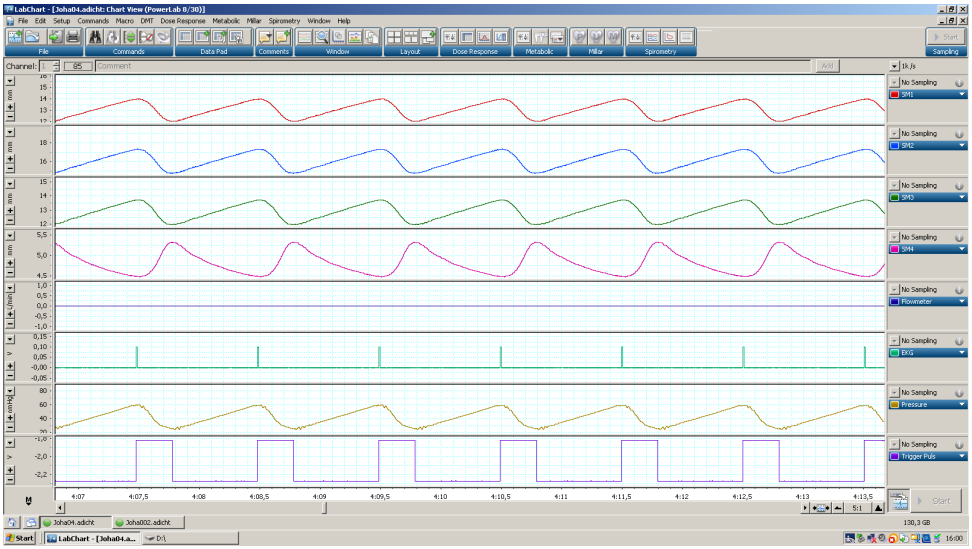

Figure 11. Screenshot from LabChart. Sonomicrometry curves in row 1-4. LS in row 1-2. CS in row 3. RS in row 4. ECG trigger pulse row 6. Phantom lumen pressure in row 7. Pump signal in row 8.

3.1.8 Study 2 data acquisition and analysis

As in study 1, multiple recordings were done using different SVs, with each series ranging from 5-105 ml with 5 ml steps. All recordings were done using 60 beats/min for a total of 11 series, each using different temporal resolutions (Table 1) by real-time 3D echocardiography as well as 2-, 4- and 6-beat stitched images. In total 321 images were recorded. As in study 1, the different temporal resolutions were selected from available scanner presets when sector angle was set to 75°. The depth was set 0-14 cm, and all other acquisition settings were kept constant for all recordings.

Table 1. Data acquisition setup for study 1 and 2

	Study 1		Study 2
	3D strain		3D twist
	Resting HR	Tachycardia	Resting HR
Simulated HR (min^{-1})	60	120	60
Volume range (ml)	10 – 150	10 – 80	5 – 105
Volume step (ml)	10	10	5
Number of SV (n)	15	8	21
Images pr SV (n)	7	7	11
Total images (n)	105	56	231
Volume rates			
Single-beat (VPS)	21.9		25.5
2-beat (VPS)	18.7, 41.5		14.4, 21.2, 47.9
4-beat (VPS)			20.3, 27.0, 42.4
6-beat (VPS)	30.2, 36.6, 52.3, 124.4		17.1, 30.4, 43.2, 63.6

HR, heart rate; SV, stroke volume; VPS, volumes per second; Comma-separated values indicate different volume rates tested.

Echocardiographic analysis was performed using a newer version of the same software (EchoPAC BT202; GE Vingmed Ultrasound AS) using the 4D Auto LVQ-tool. The procedures for analysis were the same as in study 1, but the improved software also provided values for rotation, twist and torsion in the result output.

To analyze twist by sonomicrometry, a custom-made software was written in MATLAB (MATLAB 2014b, MathWorks Inc., Natick, MA, USA). This software was fed with distance curves from all the sonomicrometer crystal channels, and then used the method of trilateration to create cartesian coordinates for each sample.

Knowing these coordinates, the relative angle between the two planes were calculate using trigonometric functions, outputting a twist curve at the same sample rate as the input values (192 samples/s). The sonomicrometry twist value was then measured as the difference between maximum and minimum of the twist curve.

3.1.9 Statistics

For both study 1 and 2, linear correlation coefficients were calculated to show the association between the two methods. Bland-Altman plots were performed to evaluate agreement between the two methods, showing the mean difference and limits of agreement (±1.96 standard deviations [SD]) as the absolute difference between the methods and was calculated for each series[41,42]. In addition, inter-observer variability was assessed in study 1, and reported as the mean difference between observer 1 and 2, and the intraclass correlation coefficient (ICC).

3.2 Study 3

Study 3 is a cross-sectional study using 3D echocardiography on patients with different degrees of AS. The aim of this study was to evaluate how 3D STE parameters at individual LV levels are affected at different AS stages. In addition, we wanted to assess how changes in temporal and spatial resolution would affect the 3D STE parameters at individual LV levels. A total of 120 patients previously diagnosed with AS at the out-patient clinic, Department of Heart Disease, Haukeland University Hospital, were recruited in the study. Inclusion criteria for the study was known AS with aortic valve peak jet velocity > 2.0 m/s[24]. Exclusion criteria were other significant valve disease, known CAD, atrial fibrillation (AF), and patients with known poor image quality. The study was approved by the Norwegian regional committee for medical health and research ethics (2014/1895/REK Nord) and all patients gave a written informed consent.

3.2.1 Echocardiography

Patients were examined using a standardized image 2D ultrasound protocol (Vivid E9 and M5S probe; GE Vingmed Ultrasound). In addition, 2-, 4-, and 6-beat volume stitched 3D images were obtained using a 3D probe (4V; GE Vingmed Ultrasound AS) with a target volume rate (VR) of 35 volumes per second (VPS), as this was close to the VR with highest correlation to sonomicrometer values in study 1 and 2. Patients were instructed to hold their breath during recording of each image to minimize respiratory image artifacts.

During image analysis, 7 patients were excluded because of irregular heart rate and 1 because of diagnosis of previously unknown myocardial infarction with regional scarring in the LV. In addition, if the 3D STE algorithm missed more than 3 of the 17 segments, during analysis, the images were considered of poor image quality by the analyzing software and the patient was excluded from the analysis. This accounted for 27 patients with 6-beat, 28 with 4-beat, and 48 with 2-beat images. As a result, the total number of patients arranged in 3 datasets were 85, 84, and 66, for 6-, 4-, and 2-beat images respectively. Of the patients in these 3 datasets, 62 overlapped, enabling comparison of images. This number was considered too small for segmentation into groups by AS severity, and further analysis therefore focuses on the image set with 85 patients, using 6-beat images. The image set with 62 patients was used to compare differences in STE parameters at different resolutions as a single patient group.

2D Images were analyzed using ImageArena 4.6 (TomTec Imaging Systems GmbH, Unterschleßheim, Germany). AS severity was assessed in accordance with ASA/ACC guidelines[24] by measuring peak jet velocity, mean aortic gradient and aortic valve area. Standard LV dimensions were measured using the current guidelines[43]. Filling pressure was estimated using the ratio of peak early trans-mitral blood flow to average mitral annular velocity (E/e')[44]. Relative wall thickness (RWT) was calculated from (2 x posterior wall thickness) / (LV internal diameter at ED)[43]. Initially, quantitative echocardiographic analysis was performed by a junior

investigator (EE), and then later proofread by an experienced reader (EG). To evaluate apical-basal relationship, apical basal longitudinal strain ratio (ABr) was calculated by dividing the mean LS of the 4 apical segments by the mean 6 basal segments.

3D images were analyzed using EchoPAC v202 (GE Vingmed Ultrasound AS). As multiple recordings were made, the images with least stitching artifacts were selected based on the multi-slice short axis view. All STE data were analyzed using the software 4D Auto LVQ tool. LV mass was estimated using 3D measurements from ED. 3D STE data containing strain, rotation, twist and torsion data was analyzed in the same manner as in study 1 and 2. The resulting data was stored in hierarchical data format (hdf5-files). These files provided strain curves in longitudinal, circumferential and radial direction as well as area strain for all 17 segments of the LV bull's-eye plot. In addition, it provided rotation curves for basal, mid, apical and apex level as well as torsion curves for basal, mid and apical level. The parameter called global twist was identical to the difference between apex rotation and basal rotation. In addition, rotation and torsion was available for each of the 17 segments.

3.2.2 Data analysis

All 3D STE data was provided in hdf-5 files from EchoPAC, with strain and rotation values for each of the 17 segments at each frame. Using Python (Python Software Foundation. Python Language Reference, version 3.0) and R (The R Foundation for Statistical Computing, Vienna, Austria), values for strain, rotation and torsion were obtained by averaging the segments involved (Figure 12). Further, twist for 6 possible combinations was calculated by subtracting one rotation level from another (Figure 13).

For LS and CS, the negative peak was recorded, while for RS, the positive peak was recorded. For rotation, positive peaks were recorded for apex, apical and mid-level, while basal peak rotation was recorded as the negative peak. Twist rate was

calculated as the derivative of the twist values, and the negative peak was recorded as peak untwist.

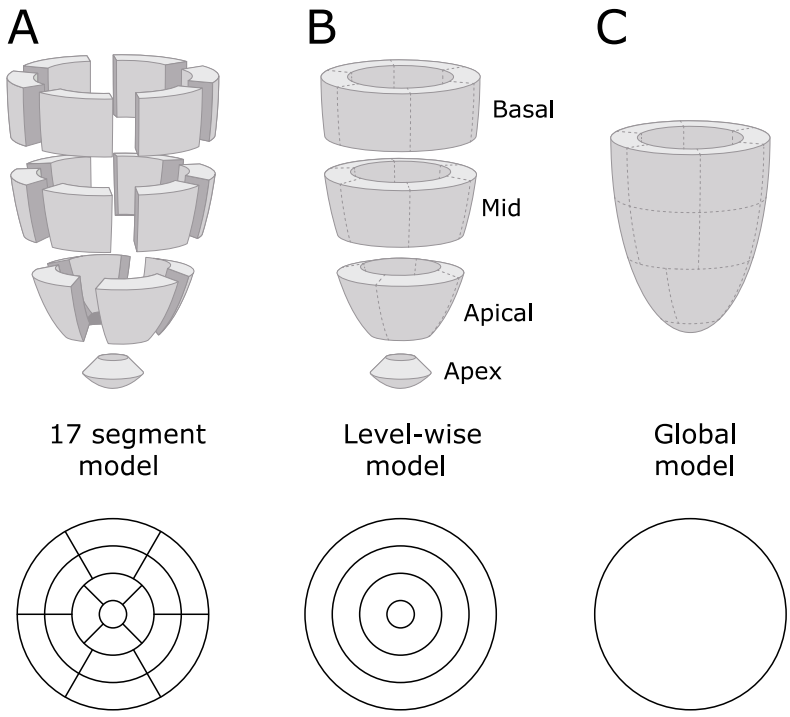

Figure 12. Segmental model containing 17 segments (A). Level model, containing 4 levels (basal, mid, apical and apex) (B). Global model (C). Corresponding bulls-eye plots at bottom.

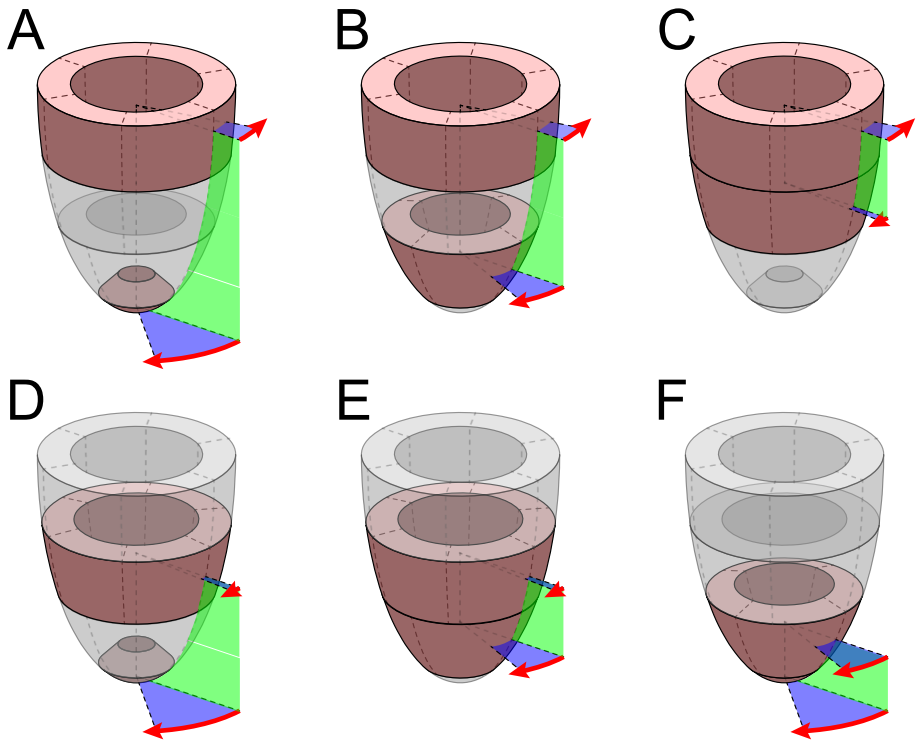

Figure 13. Combinations for measuring twist in the LV using 3D STE. Apex-basal (A), apical-basal (B), mid-basal (C), apex-mid (D), apical-mid (E), and apex-apical (F).

3.2.3 Statistics

For statistical analysis, R (R version 3.5.1; The R Foundation for Statistical Computing, Vienna, Austria) and SPSS (SPSS version 25; SPSS Inc., Chicago, IL, USA) were used.

Values were reported as mean ± SD. AS patients were divided into 3 groups of severity based on peak jet velocity. Mild AS (< 3.0 m/s), moderate AS (3.0-3.9 m/s) and severe AS (≥ 4.0 m/s). Comparison between groups was done using one-way analysis of variance (ANOVA) with Bonferroni post hoc test to show differences

between the groups. Parameters relative to the levels of the LV were compared using a mixed two-way ANOVA with AS severity being the group factor (P_g) and LV level being the within-factor (P_w). If Mauchly's test of sphericity was violated, the main effect was evaluated using Greenhouse-Geisser adjustment of freedom.

For data sets of patients where images in 2-, 4-, and 6-beat were available, the strain coefficient of variation (CoV) was calculated for each level, as SD / strain average of all patients. Resolutions with high CoV were considered of lesser quality, as a relatively uniform strain pattern was expected in this patient group. For rotation and torsion, the SD was registered for direct comparison.

Variable associations were assessed by linear regression, first using univariable linear regression. Variables with $P < 0.10$ were included in the multivariable linear regression models. In addition, some variables with $P > 0.10$ were forced into the models, if they were presumed relevant for the tested assumption. Multivariable linear regression was performed using the stepwise method with results reported as standardized beta coefficients (ß) and p.

Both inter and intraobserver variability were evaluated for 3D STE and reported as ICC and the mean difference between the results. $P < 0.05$ was considered statistically significant in all analyses.

4. Results

4.1 Study 1: Evaluation of 3D strain methods

The aim of this study was to evaluate the accuracy of 3D strain at different temporal and spatial resolutions, and to find optimal acquisition settings for best accuracy. A total of 161 images were compared from two groups with different HR, and 7 series in each group.

For the category of images at 60 beats/min, LS gave the best correlation at 36.6 VPS using 6-beat (Figure 14), with a correlation coefficient of 0.990 and agreement of 0.83 % ± 1.54 % (mean difference ± limits of agreement). An example of analysis of two different VRs is shown in Figure 15. For CS, the highest correlation was also found at 36.6 VPS, with a correlation coefficient of 0.989 and agreement of -0.78 % ± 1.75 %. For RS, the highest correlation was also found at 36.6 VPS, with a correlation coefficient of 0.897 and agreement of 16.10 % ± 22.26 % (see Table 1 in study 1 for details).

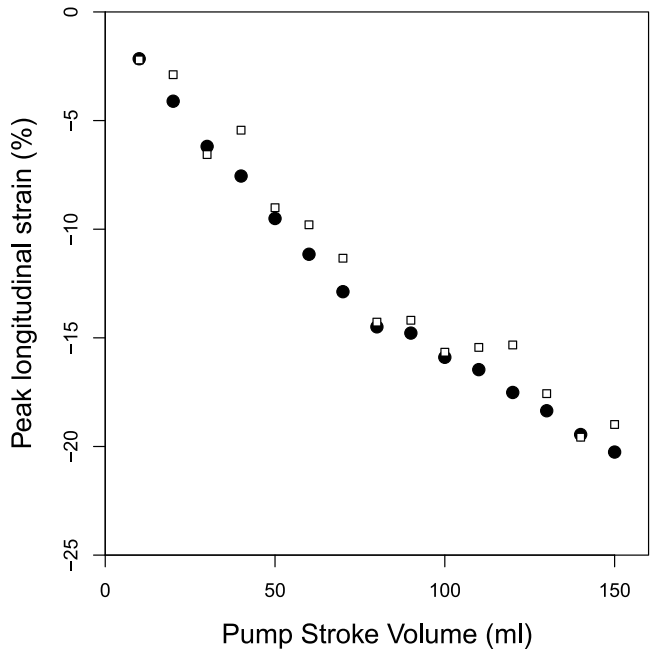

Figure 14. Sonomicrometer LS (filled circles) versus 3D STE LS at 36.6 VPS using 6-beat at HR 60 min^{-1} (white squares).

The category of images recorded at 120 beats/min showed LS with highest correlation at 36.6 VPS with 6-beat, with a correlation coefficient of 0.956 and agreement of 2.57 % ± 2.40 %. CS had highest correlation at 30.2 VPS at 6-beat, with a correlation coefficient of 0.967 and agreement of -1.20 % ± 2.26 %. RS had highest correlation at 36.6 VPS with correlation coefficient of 0.993 and agreement of 5.08 % ± 8.10 % (see Table 2 in study 1 for details).

As for intraobserver variability, the VR with highest correlation coefficient, 36.6 VPS with 6-beat, had a mean difference of -0.6 % ± 1.4 % for LS, -0.2 % ± 0.7 for CS and 1.1 % ± 2.0 % for RS at the same VR. Intraclass correlation was 0.97, 0.99 and 0.99, respectively.

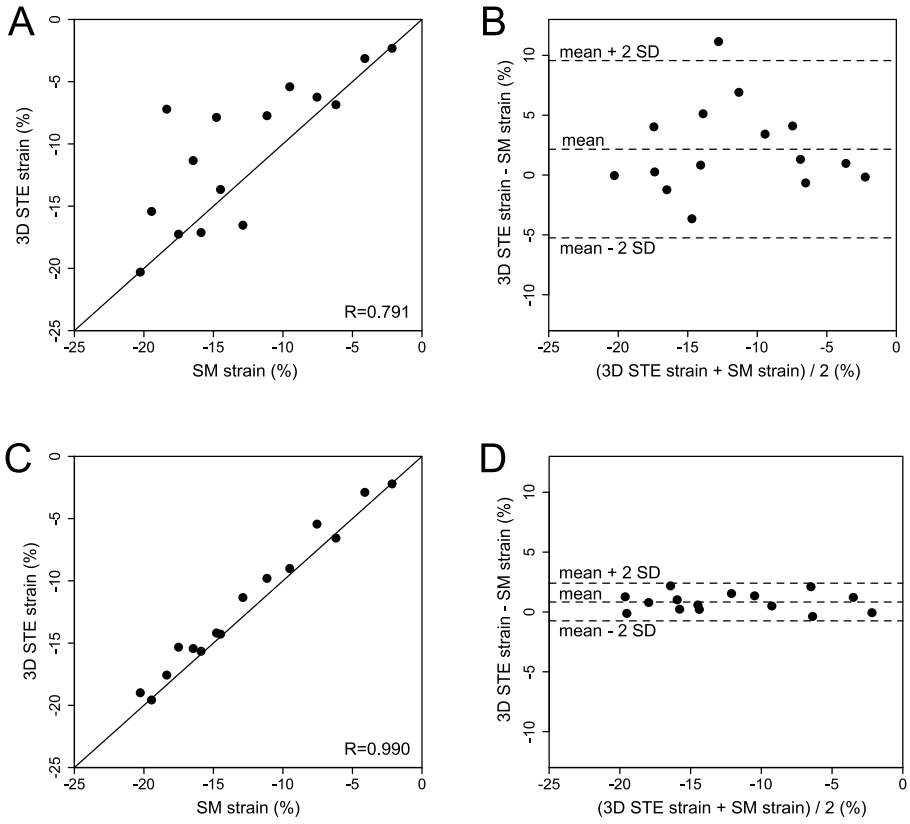

Figure 15. Scatter plots for 3D STE LS vs sonomicrometer LS (left) with corresponding Bland-Altman plots (right) for single beat at 21.9 VPS (A & B) and 6-beat at 36.6 VPS (C & D).

4.2 Study 2: Evaluation of 3D STE based rotation, twist and torsion methods

The aim of this study was to evaluate the accuracy of 3D STE derived twist, and to find the optimal temporal and spatial resolution. To achieve this, a total of 321 images were recorded in 11 series using different temporal and spatial resolutions, with 21 images in each series.

The recorded images of the phantom had an increasing sonomicrometer twist, from 2.0° to 13.8° with increasing SV. The corresponding 3D STE twist varied from 0.9° to 14.3° in 6-beat images with a VR of 17.1 VPS (Figure 16).

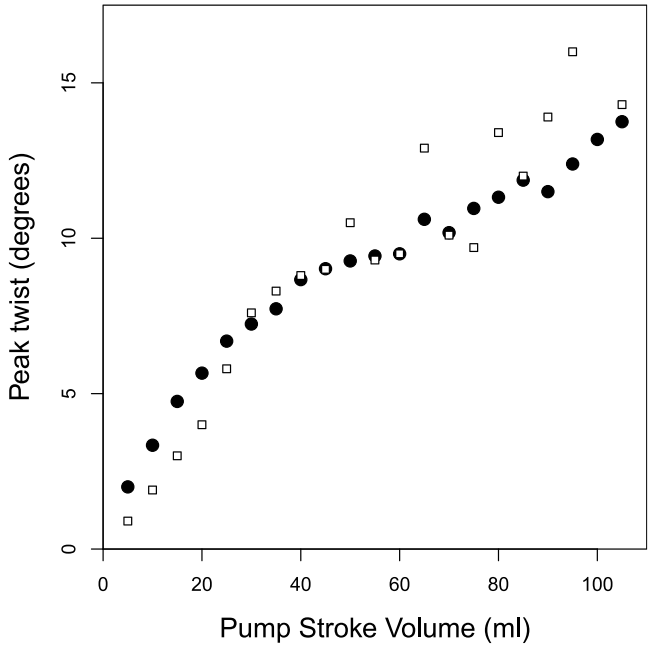

Figure 16. Sonomicrometer twist (filled circles) versus 3D STE twist at 17.1 VPS using 6-beat (white squares).

Correlation and Bland-Altman analysis showed the best correlation between 3D STE and sonomicrometry was found in recordings done at 17.1 VPS with 6-beat, with a correlation coefficient of 0.977 and agreement of 0.45° ± 1.31°. Best agreement was found at 20.3 VPS using 4-beat, with a correlation of 0.973 and an agreement of -0.17° ± 1.91°. Other series showing good correlation was 2-beat at 14.4 VPS, 4-beat at 27.0 VPS and 6-beat at 30.4 VPS with correlation coefficient of 0.960, 0.942, and

0.944, respectively. Two examples of twist with different VRs are shown in Figure 17.

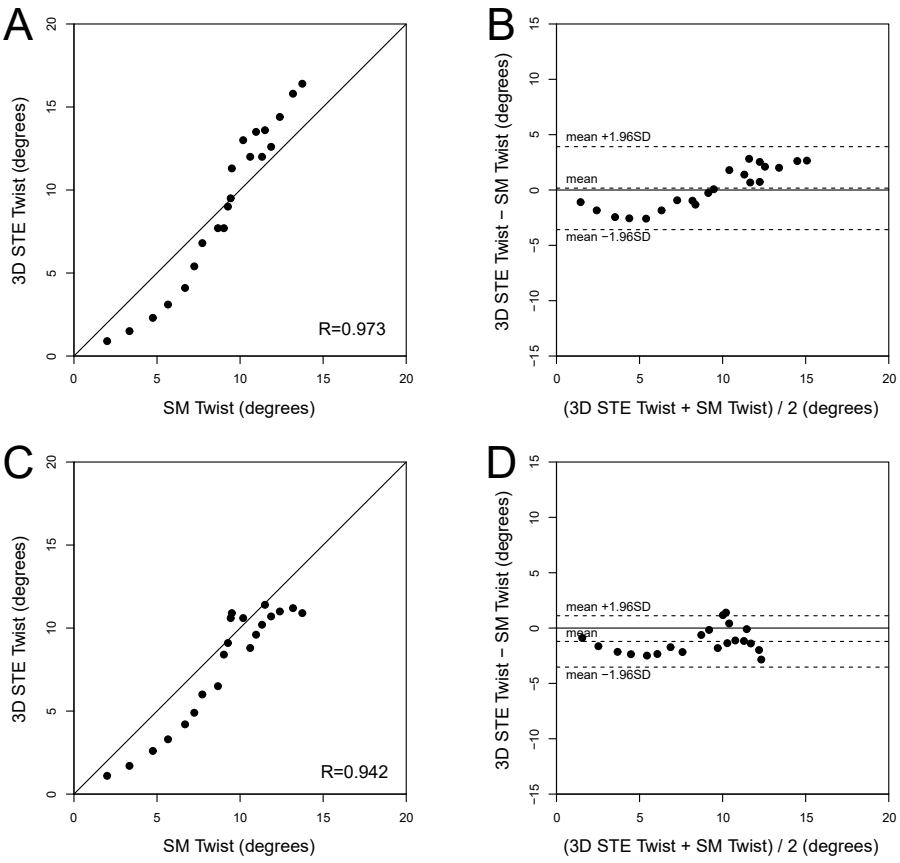

Figure 17. Scatter plots for 3D STE twist vs sonomicrometer twist (left) with corresponding Bland-Altman plots (right) for 4-beat at 20.3 VPS (A & B) and 4-beat at 27.0 VPS (C & D).

4.3 Study 3: Deformation at LV levels of AS patients

The aim of this study was to evaluate LV deformation at different levels of the LV in AS patients with different disease severity.

4.3.1 Comparison of groups by AS severity

A total of 85 patients were analyzed and divided into 3 groups based on AS severity graded by peak jet velocity in accordance with the American guidelines[24]. This resulted in 32 patients with mild, 31 with moderate and 22 with severe AS. Symptoms of dyspnea (New York Heart Association functional class II-III) were reported by 6 patients with moderate AS and 7 patients with severe AS, while no patient reported angina or syncope. Mean age was 72 ± 12 years, and 49 % were women.

Severe AS patients had higher LV filling pressure (E/e', P = 0.005) and RWT (P = 0.017) than patients with mild and moderate AS. GLS was found to be lower in patients with severe compared to mild and moderate AS (P = 0.002). No significant difference was found in GCS between the groups. Severe AS patients also had higher apical-basal peak twist than both mild and moderate AS patients (P = 0.003), while mid-basal peak twist in severe AS patients was higher than for moderate AS (P = 0.003). Peak untwist was higher in severe AS patients compared with the other groups (P = 0.002). Relative apical LS was higher in patients with moderate than mild AS (P = 0.012), which was the only parameter that was found to be different between these two groups.

Concerning level specific 3D STE results, LS was higher in the basal than apical level for all groups. Apical LS was lower in severe AS than in moderate AS, while both mid and basal LS was lower in severe AS than in mild AS (Figure 18). Also, CS was higher in apical than basal levels, while no differences were found between the groups. ABr showed significant difference between mild and moderate AS. For rotation, apex, apical, and mid-levels showed positive (counterclockwise) peak values, with apex being the highest, while the basal level showed negative (clockwise) peak values. Apex rotation showed higher dispersion than the other layers (Figure 19). Severe AS patients had higher peak values in basal rotation than mild AS patients. No difference in torsion was found between the groups.

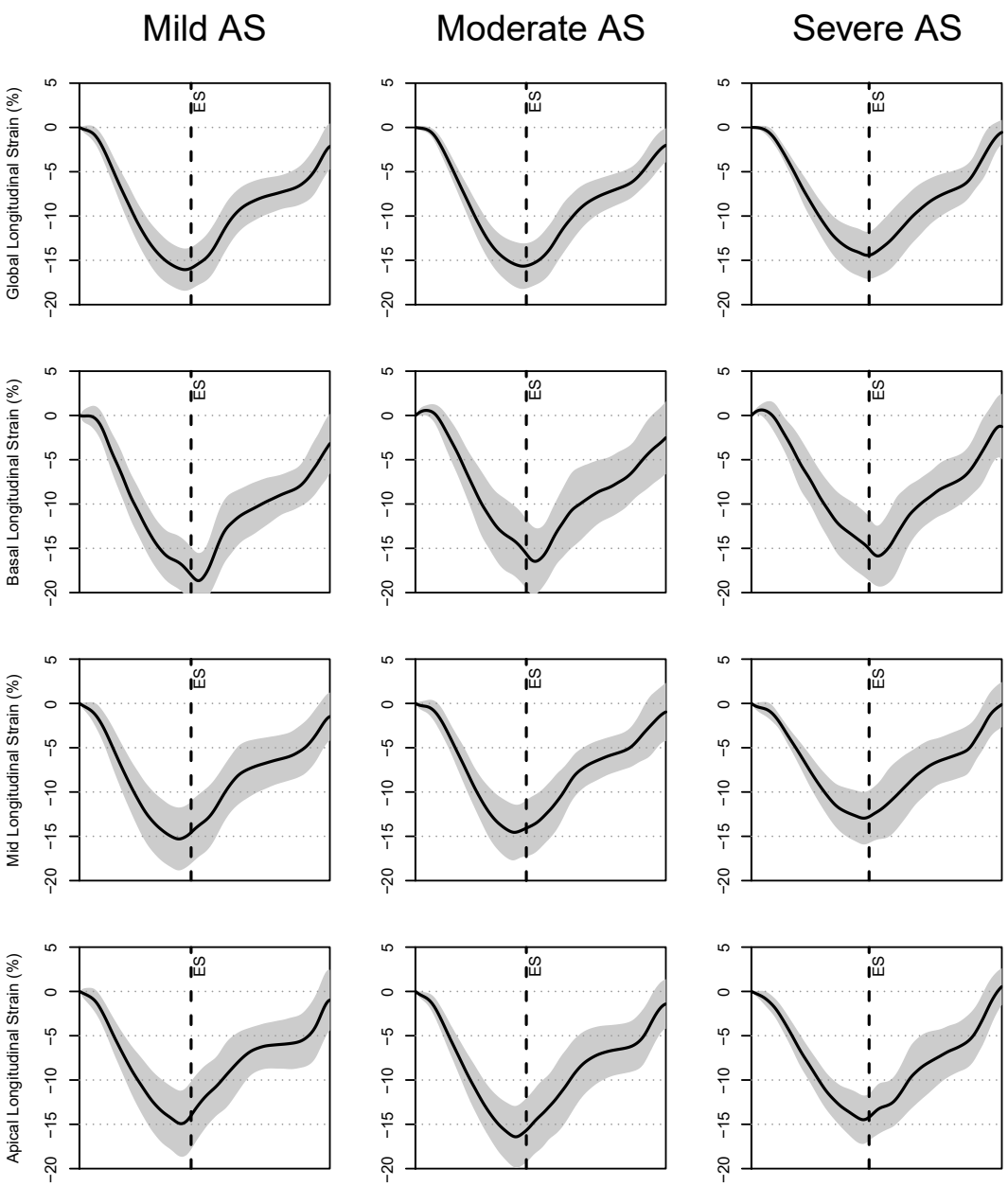

Figure 18. Curves for mean GLS and mean LS at apical, mid and basal level in the LV for mild, moderate and severe AS. The grey areas represent SD of the curves. n = 32, 31 and 22 for mild, moderate and severe AS respectively.

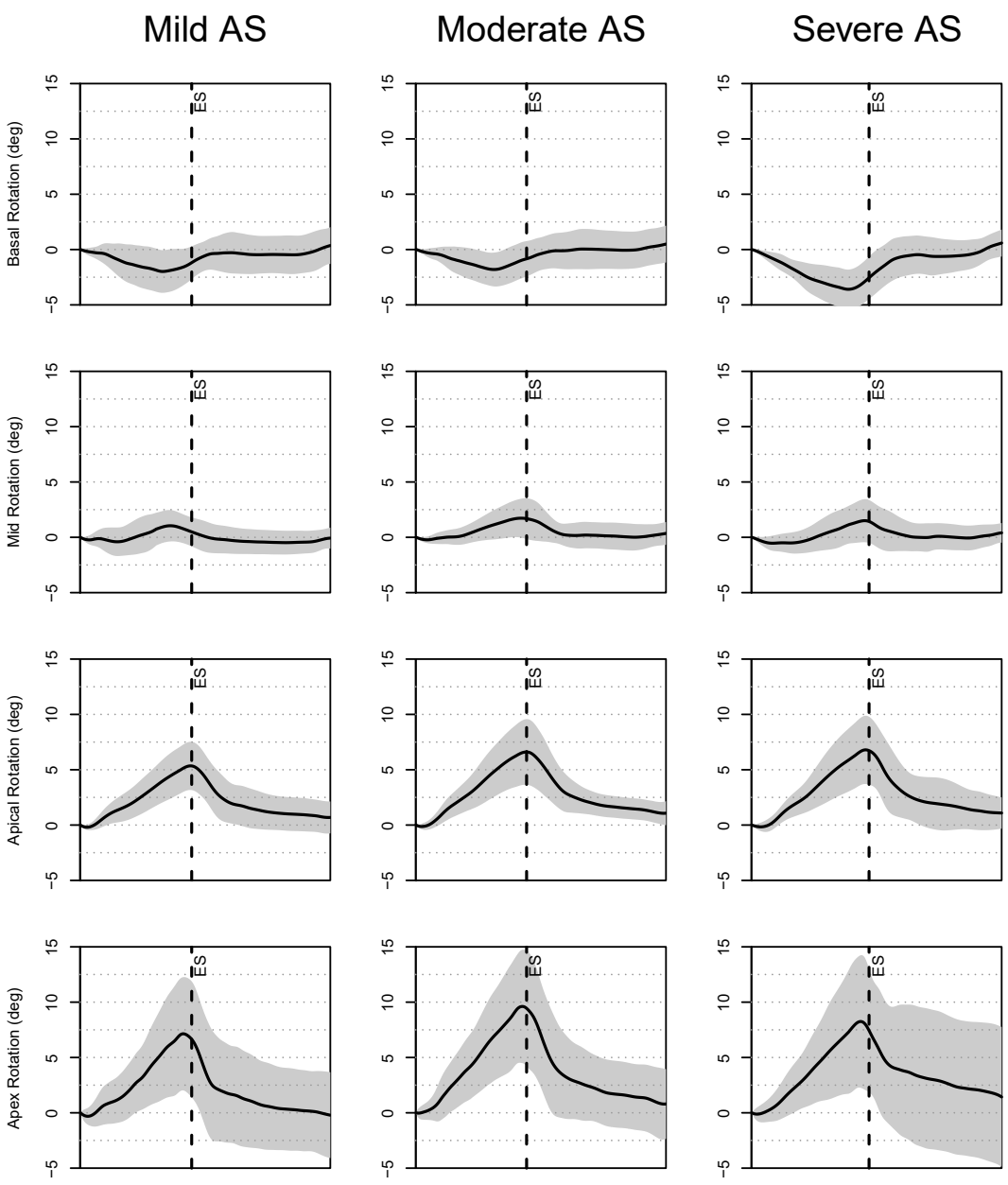

Figure 19. Mean peak rotation curves at apex, apical, mid and basal level in the LV for mild, moderate and severe AS. The grey areas represent SD of the curves. n = 32, 31 and 22 for mild, moderate and severe AS respectively.

In univariable linear regressions, lower 3D GLS, was associated with higher RWT (ß 0.33), peak jet velocity (ß 0.41), LV mass (ß 0.47), male sex (ß 0.42), and Body Mass Index (BMI) (ß 0.29), and with presence of AS symptoms (ß 0.35) (all $P < 0.05$). In multivariate linear regression, lower GLS was associated with higher peak jet velocity, BMI, and with male sex.

For apical-basal twist, higher RWT (ß 0.24), E/e' (ß 0.45) and peak jet velocity (ß 0.36), were associated with higher peak twist, while higher GCS (ß -0.48) and BMI (ß -0.36) were associated with lower peak twist. These associations were also significant in a multivariate model. No significant association between apical-basal twist and presence of AS symptoms was found, neither in uni- nor multivariate models.

4.3.2 Comparison of results by different number of stitched volumes

Images acquired using 2-, 4- and 6-beats had VRs of 22 ± 2, 29 ± 4, and 36 ± 6, respectively, with results shown in Table 2. For GLS, 2-beat had higher values than 4- and 6-beat images (-17.0 ± 3.5, -15.5 ± 2.8 and -15.3 ± 2.4 %, respectively). BLS had no difference between the methods, while both mid longitudinal strain (MLS) and apical longitudinal strain (ALS) had higher values for 2-beat than for 4- and 6-beat. Inter segmental CoV for LS was slightly higher for the 2-beat method than for 4- and 6-beat, with 6-beat ALS having the lowest inter segmental CoV.

GCS also had higher values for 2-beat than 4- and 6-beat (-18.8 ± 4.0, -17.3 ± 3.7 and -17.3 ± 3.6 %, respectively). Basal circumferential strain (BCS) and mid circumferential strain (MCS) had no difference between the methods while apical CS was higher for 2-beat than for 4- and 6-beat methods. For CS, BCS had higher inter-segmental CoV for all methods than MCS, and apical CS had the lowest inter segmental CoV.

Results for different number of stitched volumes for 3D STE rotation, twist and torsion using 2-, 4-, and 6-beat images are shown in Table 2. No difference in rotation

between the methods was found. Mid-level rotation showed 6-beat being lower than 2-beat. No difference between methods was found for apical rotation.

As for rotation, also mid-level torsion was lower for 6-beat than 2-beat, while there was no significant difference between the methods in the other levels, nor globally.

Table 2. Differences between 2-, 4-, and 6-beat, measuring different deformation parameters. n = 62.

		Mean ± SD				Inter-segmental CoV		
Deformation form	Level	2-beat	4-beat	6-beat	ANOVA P	2-beat	4-beat	6-beat
Longitudinal strain (%)	Basal	-17.8 ± 4.8	-16.8 ± 4.5	-17.1 ± 3.6	0.402	34.5	34.9	34.5
	Mid	-16.3 ± 4.3	-14.9 ± 3.6	-14.5 ± 3.5	0.019†‡	31.4	29.9	29.9
	Apical	-16.8 ± 4.3	-15.1 ± 3.1	-15.1 ± 3.0	0.008†‡	30.6	28.5	24.9
Circumferential strain (%)	Basal	-12.9 ± 4.4	-14.2 ± 4.2	-13.1 ± 3.2	0.168	106.7	71.7	74.4
	Mid	-12.9 ± 3.9	-16.7 ± 3.6	-17.0 ± 3.5	0.406	43.0	36.9	30.3
	Apical	-22.1 ± 6.2	-19.0 ± 4.8	-20.3 ± 5.4	0.008†‡	26.8	29.4	23.4
						Inter-segmental SD		
						2-beat	4-beat	6-beat
Rotation (°)	Basal	-2.3 ± 2.1	-2.2 ± 2.1	-2.4 ± 1.6	0.840	2.9	2.0	2.3
	Mid	2.1 ± 1.7	1.9 ± 1.6	1.7 ± 1.5	0.245	2.5	2.1	1.8
	Apical	7.0 ± 2.8	6.4 ± 3.4	6.5 ± 3.0	0.468	3.0	3.3	3.2
Torsion (°·cm^{-1})	Basal	1.2 ± 1.3	1.3 ± 1.2	1.3 ± 1.0	0.874	2.2	1.6	1.6
	Mid	2.8 ± 1.3	2.6 ± 1.1	2.4 ± 1.1	0.028†‡	2.1	1.6	1.5
	Apical	2.1 ± 2.5	2.5 ± 1.8	2.6 ± 1.8	0.102	2.3	2.4	2.4

SD, standard deviation; CoV, coefficient of variation; † denotes P value for difference between 2-beat and 4-beat; ‡ denotes P value for difference between 2-beat and 6-beat.

4.3.3 Inter and intra observer variability

Both inter- and intraobserver variability for strain showed good reproducibility with ICC 0.914, 0.879, 0.916, and 0.878, for inter-observer GLS, inter-observer GCS, intra-observer GLS, and intra-observer GCS, respectively. For rotation, best agreement was for apical rotation, with ICC of 0.972 and 0.973 for inter- and intra-observer, respectively.

5. Discussion

The use of 3D STE for LV deformation measurements depends on a chosen balance between spatial and temporal resolution to achieve the most accurate results. This balance may vary with different deformation parameters, and with the region of the LV under investigation. The current thesis demonstrates the accuracy of 3D STE, how its derived measurements can be evaluated, the optimal balance be found, and explores how 3D LV deformation parameters vary between groups of patients with variable degree of AS

5.1 Evaluation of 3D STE in LV phantoms

The purpose of the 3D STE evaluation in this thesis is not only to assess its accuracy, but also to determine the optimal balance between temporal and spatial resolution. To achieve this, an in vitro setup was needed, to assure maximum reproducibility in each situation. Methods evaluated in these setups need to be tested against known values of what is being measured; a gold standard. In most cases, gold standards are other methods being considered de facto standards, or the best known methods available.

Other setups include in vivo, such as animal setups, which allow highly invasive measurements for comparison[45-47]. Patient studies are rarely undertaken with high-risk invasive procedures, unless clinically indicated, although a few publications on clinical use of sonomicrometry was undertaken during cardiac surgery in the 1980's[48,49]. More frequent a comparison of two non-invasive methods, such as ultrasound, CT or MRI, that have low or no known risk of adverse effects or harm, is carried out[50]. Nonetheless, it is hard to ensure an identical situation when carrying out two different measurements in one patient, since multiple factors can influence the result of the measurements. Animal studies may to some degree be controlled, regarding factors influencing measurements, even though hemodynamic factors and unanticipated events may impair results. However, in vitro setups with high reproducibility will secure low dispersion of repeated measurements and assure

similar conditions for both methods being evaluated, and was therefore chosen for studies 1 and 2.

5.1.1 Phantom material

The ability to simulate "myocardial" ultrasound measurements in vitro requires a material that can produce a realistic ultrasound image resembling the myocardium, as well as being deformed without being impaired or weakened. For in vitro LV evaluation, both cadaver hearts[51,52] and synthetic models have been used[53,54]. Cadaver hearts are difficult to use in an in vitro model where you want to do repeated measurements, guaranteed to replicate the same values, as cadaver hearts gradually changes compliance with time.

Different synthetic materials have been suggested, such as gelatin[55] or combinations of glass-powder and agar[56], gelatin and dietary fiber[57,58], and silicone rubber[59], chosen for their near myocardial tissue sound velocity. Many of these phantoms, however, have poor mechanical qualities as they lack firmness, durability and the elasticity to be ideal for deformation studies.

A well tested phantom material for ultrasound studies is PVA, which is a synthetic polymer. As PVA also is water soluble, a liquid solution can be made, that crystallizes and solidifies after being frozen and then thawed. The property of PVA is then elastic, which enables it to be stretched or deformed. Additional freezing cycles increases the rigidity of the material, making it stiffer, as well as increasing the sound wave velocity. PVA was initially used as material in in vitro MRI phantom studies[60], but has since also been used as acoustic LV phantom material due to its ability to increase its firmness with increasing freeze-thaw cycles as a cryogel[54,61]. Sound velocity in PVA has been reported to range from 1520 to 1540 m/s, depending on number of freeze-thaw cycles[62,63]. Further increase of velocity up to 1570 m/s has been achieved by adding glycerol to the PVA solution[64], which is close to the acoustic velocity in healthy myocardium of 1597 ± 6 m/s[65]. Small differences in velocity may have an impact in direct distance measurements. B-mode ultrasound

images of PVA show small irregularities that resembles the speckles in conventional ultrasound images, making it usable for STE. To increase this scattering, some studies have added small amounts of graphite or glass powder to give the impression of more speckles[66]. Similar setups using inflating LV-phantoms of PVA have been used in other studies[53,63].

5.1.2 Phantom design

Both phantoms used in this thesis used the shape of a truncated prolate spheroid, which is frequently being used as a good model for left LV mechanics and has been used for simulations and similar settings in other studies[67-69]. Some other studies have also included a right ventricle in the phantoms[46,63], but we found this to be less relevant for strain evaluation, since the main purpose of the study was to evaluate the measurement of strain on a general basis, and a truncated prolate spheroid was less complex. Furthermore, this symmetric shape will ensure approximately even distribution of stress in the phantom wall during inflation.

Phantoms for evaluation of 2D STE twist have been used by simply twisting the phantoms mechanically from both ends[70] and acquiring the 2D images from short axis views at mid-level of the phantom. For 3D STE twist, the ultrasound probe needs to be oriented from the apex, requiring the twist force to come from elsewhere. Other studies by the same group performed 3D STE twist studies using mechanical appliances connected to the apex of cadaver hearts[51,52]. The apical attachment of this setup may however interfere with the ultrasonic image. Besides, as this was in cadaver hearts, it would be harder to attach high force mechanical appliances to the weaker PVA material of the phantom. Another solution explored was to have the twisting drive force from inside of the phantom, but this would also give ultrasonic artifacts as such a device would generate high echogenic signals.

5.1.3 Deformation reference

Sonomicrometry has been used as a method for measuring contractility both in vivo[50,71] and in vitro[46,72,73] for decades. The method uses two piezoelectric crystals

and measures the distance between them in a medium with known acoustic velocity using ultrasound.

Sonomicrometers are usually calibrated for myocardium or muscular tissue velocities, and when using other materials such as water, which has a lower acoustic velocity of around 1481 m/s, it may introduce a bias of increased length measurements in water. The acoustic velocity in water may be increased by adding salt. The velocity in our phantom material was slightly lower than in intact myocardium[74], but the difference was not considered to have any impact on our studies since both strain and twist measurements are relative measures, and any acoustic velocity bias should therefore not influence the results.

For deformation evaluation, strain can easily be calculated by using the Lagrangian formula. Evaluation of twist measurements is more challenging. The studies of Ashraf and Zhou[51,52,70] used the direct value from the driveshaft as a reference for rotation. One other method considered was using high framerate video of the phantom at the apex, to manually read the rotational value from optical images. The method chosen, using sonomicrometers for twist measurements, has been demonstrated in vivo in dogs, and compared to 2D rotation[71]. A similar setup has also been used in open-chest pigs, using 3D echocardiography[75].

5.1.4 Strain evaluation

The results of study 1 showed best accuracy for both LS and CS for images at 36.6 VPS using 6 beats at HR 60. Higher VR gave poorer spatial resolution and lower VR gave poorer temporal resolution. Optimal VR could be different at other HRs, but data from study 1 also showed best accuracy for HR 120 at low VRs. This finding suggests high temporal resolution is less important for 3D STE than for 2D STE.

We obtained an excellent correlation and small errors between 3D STE and strain from sonomicrometry. This shows that our setup was well suited for in vitro testing of strain measurements. Other studies have shown the dependence of FR for 2D STE

strain measurements[76,77] with lower FR giving lower strain values already at 30 FPS and require at least 40-60 FPS to measure strain accurately[78]. The 3D STE method seems not that sensitive to low VR with our best results at a VR of 36.6 VPS. The reason for this could be complex, but an important factor is that for 3D analysis we are following the movement of a speckle pattern in 3D space and not in 2D frames. This is even more important for CS where 2D recording involves the in-and-out of plane motion of the heart[79].

An in vivo study in animals by Seo et al using sonomicrometry also found good correlation for both LS, CS and RS[80], although different temporal and spatial resolutions were not evaluated. This was investigated for 3D STE in a clinical study by Yodwut et al, using different number of stitched images with VR from 5 to 25 VPS[22], who concluded low temporal resolution did not compromise the results in agreement with our study. The effect of number of stitched images is discussed further in section 5.3.2.

5.1.5 Twist evaluation

As early as 2005, Notomi et al showed a large variation in measured twist from 2D short axis recordings in normal individuals[81]. Thus, the obvious improvement was to introduce 3D recordings for twist measurements. However, 3D STE acquisition has its challenges with VR and resolution as Study 2 shows. The result of our study demonstrates that the accuracy of twist measurements with 3D STE depends both on the VR and on the number of beats included in the stitched analysis. Accuracy was good for both 4- and 6-beat images for VR as low as 17 VPS, and best accuracy was found with VR between 17 and 30 VPS for both 4- and 6-beats. Good accuracy was also found for 2-beat at 14.4 VPS. Higher VR had a slight tendency to underestimate 3D STE twist compared to sonomicrometry. Precision was in the same area for most measurements, except images with higher VR.

These findings suggest 3D STE twist is even less dependent on temporal resolution than 3D STE for LS and CS in study 1, where best accuracy was found at around 36.6

VPS. As with CS, 3D STE twist is mostly dependent on motion tracking in the lateral directions, and rotation accuracy should therefore be higher in the apex, where lateral resolution is better. This need for high beam density to include enough speckles for lateral tracking can explain why high spatial resolution is favorable for 3D STE twist.

Clearly, the method in both study 1 and 2 omits several obstacles that are present in clinical echocardiography, and ensures identical heart cycles, ideal for repetitive measurements in a controlled environment.

5.2 Use of 3D STE in patients with AS

Cardiac remodeling in pure AS consists of LV hypertrophy in response to chronic pressure overload, typically hypertrophy of concentric type, i.e., increased LV mass with increased RWT. However, cardiac remodeling may be influenced by co-morbidities like hypertension, obesity and CAD, or if a combined AS and regurgitation is present[82-84]. 3D STE is an ideal tool for evaluating the concomitant changes in LV deformation, both globally and regionally.

During AS progression, LV GLS is reduced and LV twist increase[36,85]. LV strain is affected as myocardial fibrosis progresses, and 2D studies have shown subclinical dysfunction to be detected by strain before AS patients develop symptoms[32]. Strain, and particular LS, may therefore better reflect the progressive changes in long axis function than EF in chronic pressure overload conditions, such as AS.

5.2.1 3D strain

Reduced global multidirectional strain, and particularly GLS, has been documented in severe AS in multiple studies, both for 2D[28,29,86,87] and 3D echocardiography[85]. These studies, however, were mainly focusing on global strain rather than regional differences, which may be evident at earlier stages of AS. Study 3 looked at 3D strain in patients with AS, both globally and at different LV levels. Although the findings in

study 3 indicated lower global strain in all directions in patients with severe AS, only 3D GLS was significantly reduced compared to mild and moderate AS.

3D longitudinal strain

One important reason for investigating LV deformation in patients with AS is finding the optimal timing of valve intervention. Describing changes in deformation at different stages of disease would be beneficial to identify earlier LV dysfunction in AS. 2D GLS reduction has shown to appear before EF reduction, which has led to the proposal of introducing 2D GLS in the regular follow-up and before intervention in patients with asymptomatic AS[88].

When looking at regional LS by level, our 3D STE study found significant differences between mild and severe AS in BLS and MLS, and between severe and moderate AS for ALS (Figure 20A). Although apical strain was not significantly higher for moderate than mild AS, the apex can still play a compensatory role in lost basal and MLS. This is supported by our findings of higher ABr in moderate compared to mild AS. In this case, regional strain would be more interesting than global strain in identifying early signs of LV dysfunction during AS follow up.

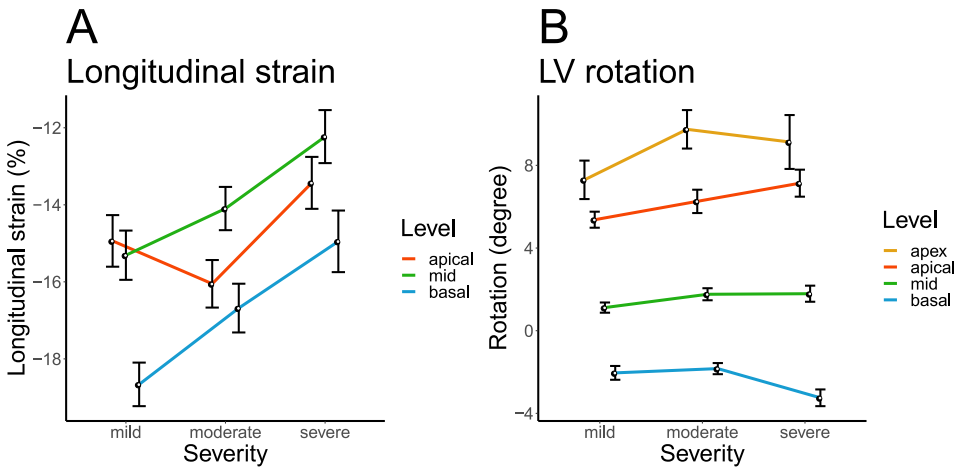

Figure 20. Peak LS for mild, moderate, and severe AS in basal, mid and apical level (A). Peak rotation for mild, moderate, and severe AS in basal, mid, apical and apex level (B). Mean ± SEM is shown.

Other studies have shown significant reduction of 2D STE BLS in patients with symptomatic compared to non-symptomatic AS[32,33]. Study 3 had too few patients for any direct comparison between asymptomatic and symptomatic AS patients.

Study 3 also investigated 3D CS in AS patients. As expected, CS was highest in apical and lowest in basal levels. However, no difference in GCS or level related CS was found between the AS-groups in this study, although a difference would be expected, as other studies have found GCS to increase in patients with AS. Carasso et al found GCS to increase, and then be reduced when patients became symptomatic[87], and they therefore proposed that CS has a compensatory mechanism for the loss of LS. This has also been found in a simulation study by Stokke et al[27] based on echocardiographic data from 100 patients with different types of heart disease other than AS, where GCS was shown to contribute more than twice as much as GLS in preserving EF and supported the hypothesis that loss in GLS is compensated by GCS. Indeed, one study claim to have found higher GCS using 3D STE in patients with AS compared to normal values from other studies in literature[89], however with other

equipment than in study 3. Another study using similar equipment as in study 3 found no difference in GCS between controls and severe AS using 3D STE[90]. A study on multidirectional strain in patients with variable degree of AS using 2D STE found lower strain in all 3 axes in patients with severe AS[91].

The failure of study 3 to find any difference in GCS may be related to higher variation in CS, since the apical short axis resolution of 3D STE is lower than for 2D STE parasternal short axis (Figure 21). 3D STE LS, on the other hand, had partially good resolution, as both 2D STE and 3D STE have high resolution in the axial direction (Figure 6).

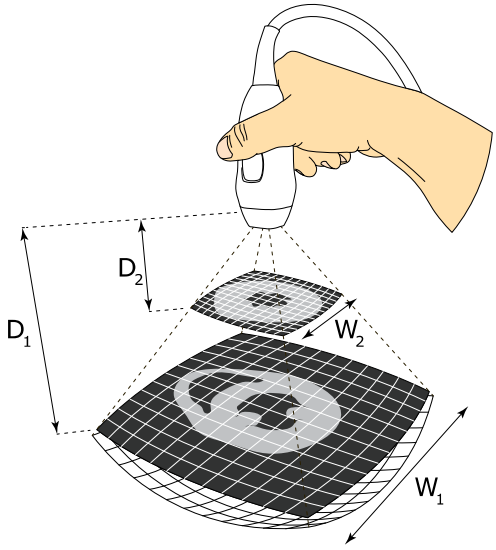

Figure 21. The difference in lateral resolution in short axis planes acquired by 3D echocardiography shown schematically. This poses a problem in STE-analysis of short axis images distant to the probe (D_1), where resolution is lower (W_1), while close images (D_2) have high resolution (W_2). Other factors, such as beam focusing may also influence spatial lateral resolution.

5.2.2 The role of deformation at different levels of the LV in AS

It has been shown that myocardial fibrosis in patients with AS initiates in the basal levels of the LV myocardium in mild cases and advance towards the apex in AS patients with severe myocardial fibrosis[92]. It therefore seems likely that LV deformation should be affected in these basal regions of the LV at an earlier stage than apical regions. Furthermore, global deformation measurements may mask any compensatory effect of other myocardial regions to account for any loss of function. Such effects may be present at early stages in disease, and gradually loss of deformation may be preserved by the work of compensatory regions up to a point where the work burden of these regions is overloaded, and the global function is affected.

At present, few studies are known to evaluate regional strain differences in patients with AS using echocardiography. One study by Dahl Pedersen[93] have directly compared ALS to BLS in patients with AS using 2D STE. This study retrospectively divided a population of 499 patients with AS into groups by ABr and compared them regarding survival after TAVI. Their study draws a direct connection of the findings to the relatively high prevalence of transthyretin amyloidosis cardiomyopathy (ATTR-CM) among patients with AS (16%) found in another study[94], although no data of ATTR-CM was reported in the study by Dahl Pedersen. Neither study 3 of this thesis included information on ATTR-CM (see also section 5.4.1). Dahl Pedersen also found that GLS is relatively unaffected by ABr, except when the ratio is extreme (ABr > 4), which can support the previous theory of ALS having a compensatory effect on the loss of BLS in severe AS.

Study 3 found higher ABr in mild than moderate AS. Reduced BLS with compensatory increase in ALS could explain this difference, and at the same time preserve GLS in patients with mild AS.

Some 3D STE studies have reported deformation at different levels of the LV in non-AS subjects. Kaku et al found LS to be highest in the apical and lowest in the basal

segments[95], while Kleijn et al found LS be highest in basal levels and lowest in mid levels[96], although both these studies were on normal subjects without AS. It is also worth mentioning that they used different ultrasound scanners and 3D STE analyzing software compared to the present study.

5.2.3 3D rotation, twist, and torsion

The fiber orientation of the LV result in the wringing motion of during contraction. This was observed in all 3 groups of AS patients, where the apex had positive peak systolic angle, while basal levels had negative peak systolic angle, resulting in positive systolic twist (Figure 20B). Computer models have shown that less sarcomere shortening is needed when twist is included in keeping normal EF[7]. The fully effect of this mechanism is not completely understood, and several explanation models have been proposed[8,9].

In line with previous 2D STE studies[35,37], study 3 also found increased twist in patients with severe AS. A significant change was found in apical-basal twist as well as mid-basal twist. A tendency of increased variation in peak rotation was observed towards the apex, which indicate a possible explanation of why no significant twist-change was observed in levels involving the apex, as illustrated in Figure 19. This is paradoxical regarding measurement accuracy, since increased variability would be expected distant from the probe, where lateral resolution is lower, as illustrated in Figure 21. This may be a limitation to current ultrasound equipment or the STE algorithms and is discussed in more detail in section 5.3.

In literature, the terms, rotation, twist and torsion are often used interchangeably for any rotational deformation of the LV, and several studies have been published using different rotational parameters in patients with AS. As most other studies on twist in AS patients used 2D echocardiography[35,37,97,98], they are not affected by resolution in the axial direction to the same degree as 3D, as lateral resolution distant to the probe can be kept higher than for 3D. Many 2D STE studies therefore exclusively look at apical rotation instead[87], which in many cases can be closely related to twist, since the

basal level contributes in a lesser degree to LV twist than the apex. Apex rotation is probably closer related to apex-mid twist, where the mid-level is close to stationary regarding rotation. Strictly speaking, rotation is not deformation, since the change is relative to the observer, not the object itself. For true deformation to be measured, the relative angular measurement planes need to be within the same deformation material.

Our study 3 also found that patients with severe AS had significant higher peak rotation in the basal level of the LV compared to both mild and moderate AS. This is notably, since significantly lower strain compared to mild AS was found in the same level. However, this may not need to be related, and it is hypothesized that an increase in wall thickness may lead to increased rotation and twist[4,38], which has been shown in patients with hypertrophic cardiomyopathy (HCM)[99,100] and hypertensive patients with concentric hypertrohy[101]. The opposite has been found in patients with dilated cardiomyopathy (DCM)[102], where LV twist is lower than normal subjects. While both subendocardial and subepicardial fibers are helically aligned in each direction , and the force of subendocardial fibers are stronger, the increased torque produced by the subepicardial fibers with their bigger radius causes them to dominate the twist direction[103]. This is relevant for AS, as the pressure overload leads to increased wall thickness, and a linear trend in LV twist has been shown at increasing afterloads for both HCM and AS[37]. Increased twist with increased wall thickness is also supported by both uni- and multivariable regression in study 3, where RWT was analyzed as a covariate of apical-basal twist.

The prognostic role of apical rotation in AS is undetermined as previous studies have found diverging results. A study by Holmes et al[97] on 82 patients using 2D STE found increased mortality to be associated with high apical rotation regardless of AVR-treatment. The same study hypothesized that apical rotation acts as a compensatory mechanism to maintain cardiac output in patients with AS and severe LV hypertrophy. A more recent study conducted by Erhart et al[98] on 146 patients

using 2D STE found survival to be greater in patients with high peak apical rotation, contradictory to the study of Holmes et al. The finding of increased twist in severe AS should therefore not necessarily be characterized as “good” or beneficial and could be a marker of early reduced LV function.

Study 3 had too low VR to evaluate untwist rate, with untwist taking place over just 2-3 volumes.

5.3 Optimal settings for 3D STE acquisition

For most echocardiographic equipment today, acquisition settings available for the operator are limited. Resolution is usually determined by the setting of VR, sector width, beam depth and fundamental/octave frequencies. In addition, the choice of either single, 2, 4 or 6 ECG-triggered stitched images can increase spatial resolution, but at the cost of potential splicing artefacts. To increase either temporal or spatial resolution, one can adjust any of these settings, usually resulting in a drop in the other resolution factor.

This resulted in a large gap between tested values of VR. While the spatial resolution had no quantifiable value on the scanner, it was just left assumed that the spatial resolution was higher when temporal resolution was low.

5.3.1 Accuracy, precision and reproducibility

In study 1 and 2, we assess accuracy of 3D STE strain and twist. We try to find out how close our measured data is to the true value, where the mean difference of repeated measurements could be defined as the accuracy of the method. In reality we have no true value, and therefore use sonomicrometry as a substitute method. We consider values from this substitute method as the closest available to the true value, defined as the gold standard. What we find in studies 1 and 2 is strictly not the methods accuracy as a quantifiable variable, but the agreement between sonomicrometry and 3D STE[41,42]. Even though we do not measure true accuracy, we

consider the method with values closest to the gold standard the most accurate method.

As we only rely on the mean value of repeated measurements for mean difference, our measured values could be imprecise, but still have a mean value very close to the gold standard. Other methods could have much less dispersion but have a mean difference further away from the gold standard. This is observed for 3D STE twist in Figure 17B, where difference between sonomicrometry and 3D STE twist using 4-beat at 20.3 VPS have a medium dispersion, while the mean difference is close zero. Figure 17D, showing 3D STE twist using 4-beat at 27.0 VPS, have less dispersed difference between methods, but the mean difference is further away from zero. The interpretation of the two methods in Figure 17 would thus be that 3D STE twist at 27.0 VPS have less accuracy, but better precision than 3D STE twist using 4-beat at 20.3 VPS.

If the mean difference between methods, as shown in figure Figure 17D, is reproduced by other observers and other equipment, the mean difference could be considered a consistent bias compared to the other method. The method could thus be calibrated to have better agreement.

Good accuracy is dependent on high reproducibility. Study 1 assessed inter observer variability to evaluate reproducibility with low difference between observers, indicating good reproducibility for both LS, CS and RS. Study 3 assessed both inter- and intra-observer variability to evaluate reproducibility in clinical use of 3D STE. For strain, both LS and CS had low difference for both inter and intra-observers for both global and regional measurements. For 3D STE twist, lower difference was found for both inter- and intra-observer in basal, mid and apical segments, but with more difference in the apex. This indicates good reproducibility for both in vitro and clinical 3D STE in basal to apical levels.

5.3.2 Number of stitched images

Study 1 and 2 did not consider the factor of splicing artefacts that can appear depending on the operator and patient, as it was not relevant to these studies. The results of these two studies must therefore be considered to apply under ideal conditions. The results of study 1 showed images at 36.6 VPS using 6 beat to give the most accurate LS-values, while in a clinical setting 4 beats may be more appropriate. Study 2, which used both 2, 4 and 6 beats, showed good accuracy for both 4 and 6 beats when measuring twist.

For the clinical data in study 3, accuracy could not be assessed without a gold standard, however the 3D STE data from 2-, 4- and 6-beat can be compared to each other directly (Table 2). In addition to ANOVA analysis, CoV was calculated for each level in the LV for LS and CS. For LS 2-beat showed higher values in mid and apical levels than 4- and 6-beat, while there was no difference between 4- and 6-beat. For LS, there was little difference between CoV, indicating that 4- and 6-beat is comparable in terms of LS accuracy.

For CS, apical strain was higher for 2- than 4- and 6-beat, but not in other levels. CoV for CS showed lower CoV in apical levels and highest CoV in basal levels. This finding is coherent with the fact that CS depends on lateral resolution, and that resolution decreases further away from the probe (Figure 21).

For rotation, there was no significant difference using different number of beats, although there is a tendency for 2-beat to have higher peak rotation values than 4- and 6-beat. Torsion values are also comparable for 4- and 6-beat. We also saw a larger number of 2-beat images with 3D STE tracing errors, probably due to the algorithm having problems tracking at lower spatial and temporal resolution.

These findings suggest 4- and 6-beat is comparable in terms of accuracy, which is consistent with the findings of Yodwut et al[22], although temporal resolution was much lower in that study.

5.3.3 Volume rate and heart rate

The patients HR will also affect 3D STE accuracy, with fewer volumes per cycle when HR increases. Study 1 included both HR 60 and 120 beats/min, while study 2 used HR 60. One might consider increasing VR to keep number of volumes per cycle at for example 30, when HR increases, but at the same time the spatial resolution drops. Both study 1 and 2 implies that spatial resolution might be more important than temporal resolution for 3D STE. This is evident in study 1, where best accuracy at HR 120 beat/min for LS and CS was found between 36.6 and 30.2 VPS.

5.3.4 Other factors influencing accuracy of 3D STE

Studies 1 and 2 have shown that 3D STE measurements have good agreement, even with low temporal resolution. While temporal and spatial resolution are the most important factors influencing 3D STE accuracy, other factors, such as transducer settings and frequency may also influence the results and accuracy[104].

Artifacts generated during acquisition affects image quality, and thus accuracy. Usually these can be patient movement or respiration, resulting in stitching artifacts. Recording images with the patient holding breath requires good cooperation between the patient and the operator.

Another factor affecting accuracy and reproducibility is the operator analyzing the images. Different experience and training may influence the results, and even experienced operators may have different habits when analyzing, such as defining limits and ROI of the LV.

One obvious factor affecting accuracy is the difference in software algorithms. Some algorithms allow changes in temporal and spatial smoothing, in which exaggerated smoothing may flatten the results, although studies on 2D STE have shown these changes to be minor[105]. 3D STE algorithms are different, and some may have more difficulties tracking the myocardial ROI than others. The same applies for calculation of variables, such as GLS and twist, from the speckle patterns generated by 3D STE,

which may be based on different algorithms. Most algorithms may also have different methods of defining ED and ES, and small changes in these variables may influence 3D STE parameters notably. These vendor differences in 3D echocardiography are well known[106], and must be considered when 3D STE results from different examinations with different vendors are being compared.

5.4 Limitations

Ultrasound phantom images in study 1 and 2 were used to mimic the movement and deformation of the LV. Although similar movement to the LV, there were many dissimilarities. The pressure cycle in the phantom was opposite to that of a LV with high pressure mimicking diastole and low-pressure mimicking systole. Consequently, at large volumes, the phantom had a more spherical shape. The 3D STE algorithm had difficulty tracking both phantoms at high SV when using high VR.

Speckles appearing in the PVA ultrasound images were different from the speckles in myocardium. The helical layer alignment in study 2 created visible artifacts in the ultrasound image which may influence tracking, and it is uncertain if it could influence the results. Regardless of these dissimilarities, the purpose of the phantom was not to simulate a beating LV in detail, but to mimic deformation which could be recognized and measured by the 3D STE algorithm.

The selection of VR in study 1 and study 2 was limited to the settings allowed by the ultrasound scanner manufacturer, typically 5 different VRs for a certain transmitted frequency. VRs and spatial resolution could be changed further by altering the sector width and to a lesser degree the depth of the image.

Study 1 did not include 4 beat images. The reason for selecting 6 beat was the assumption that 6 beat would be superior to 4-beat regarding image quality in an optimal setting, which may be true in an in vitro environment. Study 2 showed that 4-beat recordings could compete with 6-beat regarding twist accuracy. In a clinical

setting, 4 beat may be more relevant. Most of today's scanners support both 4- and 6-beat stitched images[107].

One disadvantage of using twist for rotational LV measurements is that there is no requirement for positioning of the two angular planes necessary for measuring twist. Usually, the placement can be based on anatomical landmarks, but the geometry may vary.

Although 3D STE torsion theoretically seem to be the appropriate deformation parameter for LV rotational measurements, considering the size of the LV, its present clinical use seems to be limited. This is likely due to the low spatial resolution in the short axis plane, which is depending on high lateral beam density. While torsion is calculated between two single short axis planes for 3D STE, twist uses the rotation from average STE rotation in the whole level of segments, and thus a larger ROI (Figure 22). Another argument for using twist instead of torsion is that by using anatomical landmarks, the results may be independent of LV size, which may be affected when using torsion. Such effects may be present in large LVs, which may have less torsion than a small LV, while both may have the same peak apical-basal twist angle.

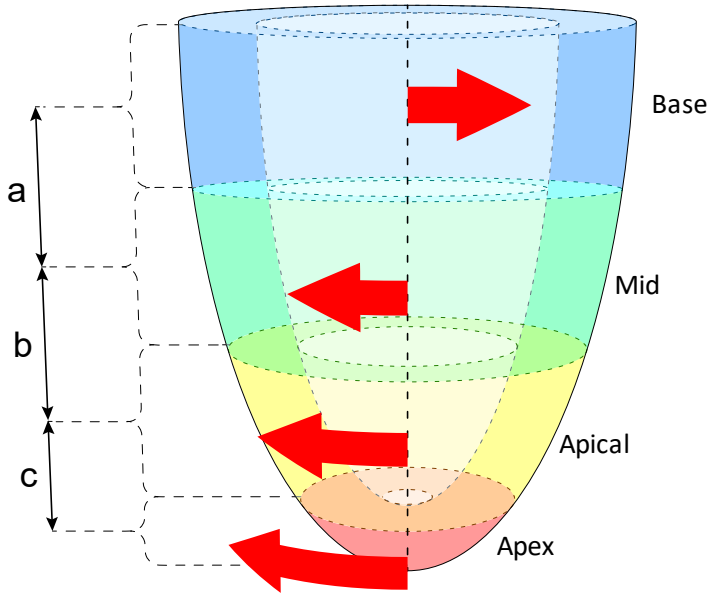

Figure 22. Twist was calculated by subtracting rotation of one level from another (a, b and c). Torsion was estimated within one level (base, mid, apical and apex), by subtracting rotation in the short axis plane in one end from the other end and the divide by the length of that level.

Study 3 evaluated 3D STE deformation in different levels of the LV in patients with AS. This was done based on the assumption that the chosen settings, found in study 1 and 2, were optimal for 3D STE acquisition. As found with apical rotation, shown for SD in Figure 19, there could be large variation in measured values, especially in the apex. This indicates that accuracy is variable depending on where deformation is measured in the 3D STE volume. One method that could address this issue is to evaluate deformation at different levels in the LV in a similar matter as in study 1 and 2.

CoV is used to estimate difference between the results of strain using different number of beats. This method only shows the difference in variation between the groups, and cannot compare different algorithms or equipment, where higher

smoothing would give lower variation, and could thus be interpreted as less noise. As some variation between segments would be expected[96], low CoV would only be expected in patients with a homogenous distribution of strain, and segmental smoothing could therefore be misinterpreted. In this setting however, the same images are compared in the same patients in the same conditions at nearly the same time. A good method for comparison would be MRI.

Although at least one has shown 3D STE to be superior to 2D STE, both for global and regional deformation[108], not every patient is suitable for acceptable quality 2D STE, and even fever for 3D STE. This is likely due to multiple factors resulting in poor image quality and artifacts. Experienced operators are even more important for 3D STE than for 2D STE.

5.4.1 Confounding effect with cardiac amyloidosis

As discussed in section 5.2.2, study 3 showed relatively lower LS in basal segments compared to apical segment in patients with moderate AS. This closely resembles the features seen in patients with advanced cardiac amyloidosis (CA). ATTR-CM is a specific type of CA, characterized by depositing protein fibrils, which can affect several organs. During recent years, new diagnostic methods have shown ATTR-CM to be much more prevalent than previously known[94], and specially in AS, where prevalence has been found in up to 16 % of patients with AS, and up to 30 % of patients with low-flow, low-gradient AS[94,109]. The findings in study 3 may thus be confounded by the effect of ATTR-CM. This relationship between AS and ATTR-CM is not completely understood[110,111]. However, in AS, in particular when hypertension is present as co-morbidity, it is common to find asymmetric septal hypertrophy with a sigmoid septum having particularly high interventricular septal thickness in the basal region which may contribute to lower LS in the basal segment[112].

5.5 Clinical implications and future perspectives

Today 95 % of echocardiography laboratories have access to 3D and STE, however only one third use it routinely as a supplement to conventional 2D echocardiography, while the majority use it in special cases[113]. While 3D echocardiography has proven superior to 2D for evaluation of multiple structural heart diseases, especially volume estimation[114], use of 3D STE has been debated due to factors like reduced spatial and temporal resolution, compared to 2D STE.

One objective of this thesis addressing the clinical usefulness, has been to investigate which scanner settings would give the most accurate results, both in vitro and in clinical setting. 3D STE seem to be more dependent on good spatial than temporal resolution, compared to 2D STE. While 6 beat stitched images may be hard to achieve in a clinical setting without getting stitching artifacts, both our in vivo and clinical data suggest accuracy of the same magnitude for 4- as for 6-beat, while 2-beat tends to give higher strain values than 4- and 6-beat.

Study 1 and 2 have demonstrated that 3D STE has good accuracy for both strain and twist, when used correctly. Reduced strain in severe AS is known from other studies, however knowledge about its clinical implication has been limited.

Study 3 shows that 3D STE can be used to grade deformation in different levels of the LV in patients with AS, a task which is difficult using conventional 2D STE. Our findings suggest LS has more reduction in the basal than other levels of the LV in patients with AS. Level LS, and especially BLS may be used in the evaluation of AS severity. However, further clinical evaluation is spoken for. The presence of reduced twist may also have a prognostic value in this group of patients. The search for early markers of reduced LV function in patients with AS and timing of intervention may in the future move away from EF, and subclinical features may become more important.

Compared to 2D STE, 3D STE can give a superior view with multiple additional parameters, once analyzed. This feature could give a clearer view of potential pathology and more features may be available in the future, as well as the potential for artificial intelligence to identify and evaluate such findings.

6. Conclusions

We hypothesized that 3D STE can accurately measure LV deformation using lower temporal resolution than conventional 2D STE. Moreover, 3D STE can be used to study level specific differences of LV deformation in patients with variable degree of AS.

In study 1, the aim was to investigate the accuracy of LV 3D STE strain using an in vitro setup, and to assess the best acquisition settings for best accuracy.
We found that phantoms can be used to evaluate 3D STE using sonomicrometry as a gold standard. Optimal settings using 6-beat was a VR of 36.6 VPS for LS and CS in a standardized setting with HR 60. While 2D STE is dependent on high temporal resolution to track myocardium both in and out of the 2D plane, 3D STE is less dependent on temporal, and more dependent on spatial resolution.

In study 2, the aim was to develop an in vitro setup for rotational measurements, and to test the accuracy of LV 3D STE twist as well as the optimal acquisition settings for measuring LV 3D twist.
We found that 3D STE twist can be evaluated using a twisting phantom, and that 3D twist correlates well to sonomicrometer twist. Optimal setting for multi beat acquisition was found at VR between 17.1 and 30.4 VPS. Good spatial resolution seems to be even more important for lateral than for longitudinal 3D STE movement.

In study 3, the aim was to analyze 3D STE deformation parameters at different LV levels in a clinical study of patients with variable degree of AS.
We found that using optimal settings derived from study 1 and 2, 3D STE deformation in LV levels can be used for regional investigation in a clinical setting for AS patients. To achieve high spatial resolution, using 4-beat is comparable to using 6-beat in terms of accuracy.

The main conclusion of this thesis is that 3D STE can be used with good accuracy and correlates well to sonomicrometry in an experimental setup. 3D STE is a good

option for evaluating both global and regional deformation in a clinical setting, when used correctly.

References

1. Edler I, Hertz CH. The use of ultrasonic reflectoscope for the continuous recording of the movements of heart walls. 1954. Clin Physiol Funct Imaging. 2004;24(3):118-36.
2. Grant RP. Notes on the Muscular Architecture of the Left Ventricle. Circulation. 1965;32:301-8.
3. Taber LA, Yang M, Podszus WW. Mechanics of ventricular torsion. J Biomech. 1996;29(6):745-52.
4. Sengupta PP, Khandheria BK, Narula J. Twist and untwist mechanics of the left ventricle. Heart Fail Clin. 2008;4(3):315-24.
5. Streeter DD, Jr., Spotnitz HM, Patel DP, Ross J, Jr., Sonnenblick EH. Fiber orientation in the canine left ventricle during diastole and systole. Circ Res. 1969;24(3):339-47.
6. Fernandez-Teran MA, Hurle JM. Myocardial fiber architecture of the human heart ventricles. Anat Rec. 1982;204(2):137-47.
7. Beyar R, Sideman S. Effect of the twisting motion on the nonuniformities of transmyocardial fiber mechanics and energy demand--a theoretical study. IEEE Trans Biomed Eng. 1985;32(10):764-9.
8. Bayer JD, Blake RC, Plank G, Trayanova NA. A novel rule-based algorithm for assigning myocardial fiber orientation to computational heart models. Ann Biomed Eng. 2012;40(10):2243-54.
9. Beyar R, Sideman S. A computer study of the left ventricular performance based on fiber structure, sarcomere dynamics, and transmural electrical propagation velocity. Circ Res. 1984;55(3):358-75.
10. Beladan CC, Calin A, Rosca M, Ginghina C, Popescu BA. Left ventricular twist dynamics: principles and applications. Heart. 2014;100(9):731-40.
11. Crosby J, Amundsen BH, Hergum T, Remme EW, Langeland S, Torp H. 3-D speckle tracking for assessment of regional left ventricular function. Ultrasound Med Biol. 2009;35(3):458-71.
12. Meunier J, Bertrand M. Echographic image mean gray level changes with tissue dynamics: a system-based model study. IEEE Trans Biomed Eng. 1995;42(4):403-10.
13. Meunier J. Tissue motion assessment from 3D echographic speckle tracking. Phys Med Biol. 1998;43(5):1241-54.
14. Hsu EW, Muzikant AL, Matulevicius SA, Penland RC, Henriquez CS. Magnetic resonance myocardial fiber-orientation mapping with direct histological correlation. Am J Physiol. 1998;274(5):H1627-34.
15. Scollan DF, Holmes A, Winslow R, Forder J. Histological validation of myocardial microstructure obtained from diffusion tensor magnetic resonance imaging. Am J Physiol. 1998;275(6):H2308-18.
16. Tischler M, Niggel J. Left ventricular systolic torsion and exercise in normal hearts. J Am Soc Echocardiogr. 2003;16(6):670-4.

17. Parisi V, Losi MA, Contaldi C, Chiacchio E, Pastore F, Scatteia A, et al. Speckle-tracking analysis based on 2D echocardiography does not reliably measure left ventricular torsion. Clin Physiol Funct Imaging. 2013;33(2):117-21.
18. Muraru D, Niero A, Rodriguez-Zanella H, Cherata D, Badano L. Three-dimensional speckle-tracking echocardiography: benefits and limitations of integrating myocardial mechanics with three-dimensional imaging. Cardiovasc Diagn Ther. 2018;8(1):101-17.
19. Voigt JU, Cvijic M. 2- and 3-Dimensional Myocardial Strain in Cardiac Health and Disease. JACC Cardiovasc Imaging. 2019;12(9):1849-63.
20. Brekke S, Rabben SI, Stoylen A, Haugen A, Haugen GU, Steen EN, et al. Volume stitching in three-dimensional echocardiography: distortion analysis and extension to real time. Ultrasound Med Biol. 2007;33(5):782-96.
21. Lang RM, Badano LP, Tsang W, Adams DH, Agricola E, Buck T, et al. EAE/ASE recommendations for image acquisition and display using three-dimensional echocardiography. Eur Heart J Cardiovasc Imaging. 2012;13(1):1-46.
22. Yodwut C, Weinert L, Klas B, Lang RM, Mor-Avi V. Effects of frame rate on three-dimensional speckle-tracking-based measurements of myocardial deformation. J Am Soc Echocardiogr. 2012;25(9):978-85.
23. Otto CM, Lind BK, Kitzman DW, Gersh BJ, Siscovick DS. Association of aortic-valve sclerosis with cardiovascular mortality and morbidity in the elderly. N Engl J Med. 1999;341(3):142-7.
24. Otto CM, Nishimura RA, Bonow RO, Carabello BA, Erwin JP, 3rd, Gentile F, et al. 2020 ACC/AHA Guideline for the Management of Patients With Valvular Heart Disease: A Report of the American College of Cardiology/American Heart Association Joint Committee on Clinical Practice Guidelines. Circulation. 2021;143(5):e72-e227.
25. Vahanian A, Beyersdorf F, Praz F, Milojevic M, Baldus S, Bauersachs J, et al. 2021 ESC/EACTS Guidelines for the management of valvular heart disease. Eur Heart J. 2021.
26. Aurigemma GP, Silver KH, Priest MA, Gaasch WH. Geometric changes allow normal ejection fraction despite depressed myocardial shortening in hypertensive left ventricular hypertrophy. J Am Coll Cardiol. 1995;26(1):195-202.
27. Stokke TM, Hasselberg NE, Smedsrud MK, Sarvari SI, Haugaa KH, Smiseth OA, et al. Geometry as a Confounder When Assessing Ventricular Systolic Function: Comparison Between Ejection Fraction and Strain. J Am Coll Cardiol. 2017;70(8):942-54.
28. Cramariuc D, Gerdts E, Davidsen ES, Segadal L, Matre K. Myocardial deformation in aortic valve stenosis: relation to left ventricular geometry. Heart. 2010;96(2):106-12.
29. Ng AC, Delgado V, Bertini M, Antoni ML, van Bommel RJ, van Rijnsoever EP, et al. Alterations in multidirectional myocardial functions in patients with

aortic stenosis and preserved ejection fraction: a two-dimensional speckle tracking analysis. Eur Heart J. 2011;32(12):1542-50.
30. Dahl JS, Videbaek L, Poulsen MK, Rudbaek TR, Pellikka PA, Moller JE. Global strain in severe aortic valve stenosis: relation to clinical outcome after aortic valve replacement. Circ Cardiovasc Imaging. 2012;5(5):613-20.
31. Salaun E, Casalta AC, Donal E, Bohbot Y, Galli E, Tribouilloy C, et al. Apical four-chamber longitudinal left ventricular strain in patients with aortic stenosis and preserved left ventricular ejection fraction: analysis related with flow/gradient pattern and association with outcome. Eur Heart J Cardiovasc Imaging. 2018;19(8):868-78.
32. Attias D, Macron L, Dreyfus J, Monin JL, Brochet E, Lepage L, et al. Relationship between longitudinal strain and symptomatic status in aortic stenosis. J Am Soc Echocardiogr. 2013;26(8):868-74.
33. Carstensen HG, Larsen LH, Hassager C, Kofoed KF, Jensen JS, Mogelvang R. Basal longitudinal strain predicts future aortic valve replacement in asymptomatic patients with aortic stenosis. Eur Heart J Cardiovasc Imaging. 2016;17(3):283-92.
34. Nagel E, Stuber M, Burkhard B, Fischer SE, Scheidegger MB, Boesiger P, et al. Cardiac rotation and relaxation in patients with aortic valve stenosis. Eur Heart J. 2000;21(7):582-9.
35. van Dalen BM, Tzikas A, Soliman OI, Kauer F, Heuvelman HJ, Vletter WB, et al. Left ventricular twist and untwist in aortic stenosis. Int J Cardiol. 2011;148(3):319-24.
36. Tumenbayar M, Yamaguchi K, Yoshitomi H, Endo A, Tanabe K. Increased apical rotation in patients with severe aortic stenosis assessed by three-dimensional speckle tracking imaging. J Echocardiogr. 2018;16(1):28-33.
37. Santoro A, Alvino F, Antonelli G, Zacà V, Benincasa S, Lunghetti S, et al. Left Ventricular Twisting Modifications in Patients with Left Ventricular Concentric Hypertrophy at Increasing After-Load Conditions. Echocardiography. 2014;31(10):1265-73.
38. Sengupta PP, Tajik AJ, Chandrasekaran K, Khandheria BK. Twist mechanics of the left ventricle: principles and application. JACC Cardiovasc Imaging. 2008;1(3):366-76.
39. Sandstede JJ, Johnson T, Harre K, Beer M, Hofmann S, Pabst T, et al. Cardiac systolic rotation and contraction before and after valve replacement for aortic stenosis: a myocardial tagging study using MR imaging. AJR Am J Roentgenol. 2002;178(4):953-8.
40. Dybdahl GL. Utvikling av testrigg for ultralyd volum og strainmålinger i hjarte [Master's thesis]:Department of Physics and Technology, University of Bergen; 2011.
41. Altman DG, Bland JM. Measurement in Medicine: The Analysis of Method Comparison Studies. Journal of the Royal Statistical Society: Series D (The Statistician). 1983;32(3):307-17.

42. Bland JM, Altman DG. Statistical methods for assessing agreement between two methods of clinical measurement. Lancet. 1986;1(8476):307-10.
43. Lang RM, Badano LP, Mor-Avi V, Afilalo J, Armstrong A, Ernande L, et al. Recommendations for cardiac chamber quantification by echocardiography in adults: an update from the American Society of Echocardiography and the European Association of Cardiovascular Imaging. J Am Soc Echocardiogr. 2015;28(1):1-39 e14.
44. Nagueh SF, Smiseth OA, Appleton CP, Byrd BF, 3rd, Dokainish H, Edvardsen T, et al. Recommendations for the Evaluation of Left Ventricular Diastolic Function by Echocardiography: An Update from the American Society of Echocardiography and the European Association of Cardiovascular Imaging. J Am Soc Echocardiogr. 2016;29(4):277-314.
45. Urheim S, Rabben SI, Skulstad H, Lyseggen E, Ihlen H, Smiseth OA. Regional myocardial work by strain Doppler echocardiography and LV pressure: a new method for quantifying myocardial function. Am J Physiol Heart Circ Physiol. 2005;288(5):H2375-80.
46. Heyde B, Bouchez S, Thieren S, Vandenheuvel M, Jasaityte R, Barbosa D, et al. Elastic image registration to quantify 3-D regional myocardial deformation from volumetric ultrasound: experimental validation in an animal model. Ultrasound Med Biol. 2013;39(9):1688-97.
47. Bouchez S, Heyde B, Barbosa D, Vandenheuvel M, Houle H, Wang Y, et al. In-vivo validation of a new clinical tool to quantify three-dimensional myocardial strain using ultrasound. Int J Cardiovasc Imaging. 2016;32(12):1707-14.
48. Chitwood WR, Jr., Hill RC, Sink JD, Kleinman LH, Sabiston DC, Jr., Wechsler AS. Measurement of global ventricular function in patients during cardiac operations using sonomicrometry. J Thorac Cardiovasc Surg. 1980;80(5):724-35.
49. Chitwood WR, Jr., Hill RC, Sink JD, Wechsler AS. Diastolic ventricular properties in patients during coronary revascularization. Intermittent ischemic arrest versus cardioplegia. J Thorac Cardiovasc Surg. 1983;85(4):595-605.
50. Amundsen BH, Helle-Valle T, Edvardsen T, Torp H, Crosby J, Lyseggen E, et al. Noninvasive myocardial strain measurement by speckle tracking echocardiography: validation against sonomicrometry and tagged magnetic resonance imaging. J Am Coll Cardiol. 2006;47(4):789-93.
51. Zhou Z, Ashraf M, Hu D, Dai X, Xu Y, Kenny B, et al. Three-dimensional speckle-tracking imaging for left ventricular rotation measurement: an in vitro validation study. J Ultrasound Med. 2010;29(6):903-9.
52. Ashraf M, Zhou Z, Nguyen T, Ashraf S, Sahn DJ. Apex to base left ventricular twist mechanics computed from high frame rate two-dimensional and three-dimensional echocardiography: a comparison study. J Am Soc Echocardiogr. 2012;25(1):121-8.
53. Heyde B, Cygan S, Choi HF, Lesniak-Plewinska B, Barbosa D, Elen A, et al. Regional cardiac motion and strain estimation in three-dimensional

echocardiography: a validation study in thick-walled univentricular phantoms. IEEE Trans Ultrason Ferroelectr Freq Control. 2012;59(4):668-82.
54. Langeland S, D'Hooge J, Claessens T, Claus P, Verdonck P, Suetens P, et al. RF-based two-dimensional cardiac strain estimation: a validation study in a tissue-mimicking phantom. IEEE Trans Ultrason Ferroelectr Freq Control. 2004;51(11):1537-46.
55. Burlew MM, Madsen EL, Zagzebski JA, Banjavic RA, Sum SW. A new ultrasound tissue-equivalent material. Radiology. 1980;134(2):517-20.
56. Martensson M, Winter R, Cederlund K, Ripsweden J, Mir-Akbari H, Nowak J, et al. Assessment of left ventricular volumes using simplified 3-D echocardiography and computed tomography - a phantom and clinical study. Cardiovasc Ultrasound. 2008;6:26.
57. Stigo A, Johansen P, Jensen MO, Sivesgaard K, Nygaard H, Sloth E. An automated in vitro model for the evaluation of ultrasound modalities measuring myocardial deformation. Cardiovasc Ultrasound. 2010;8:40.
58. Sivesgaard K, Christensen SD, Nygaard H, Hasenkam JM, Sloth E. Speckle tracking ultrasound is independent of insonation angle and gain: an in vitro investigation of agreement with sonomicrometry. J Am Soc Echocardiogr. 2009;22(7):852-8.
59. Matre K, Ahmed AB, Gregersen H, Heimdal A, Hausken T, Odegaard S, et al. In vitro evaluation of ultrasound Doppler strain rate imaging: modification for measurement in a slowly moving tissue phantom. Ultrasound Med Biol. 2003;29(12):1725-34.
60. Chu KC, Rutt BK. Polyvinyl alcohol cryogel: an ideal phantom material for MR studies of arterial flow and elasticity. Magn Reson Med. 1997;37(2):314-9.
61. Fromageau J, Brusseau E, Vray D, Gimenez G, Delachartre P. Characterization of PVA cryogel for intravascular ultrasound elasticity imaging. IEEE Trans Ultrason Ferroelectr Freq Control. 2003;50(10):1318-24.
62. Surry KJ, Austin HJ, Fenster A, Peters TM. Poly(vinyl alcohol) cryogel phantoms for use in ultrasound and MR imaging. Phys Med Biol. 2004;49(24):5529-46.
63. Lesniak-Plewinska B, Cygan S, Kaluzynski K, D'Hooge J, Zmigrodzki J, Kowalik E, et al. A dual-chamber, thick-walled cardiac phantom for use in cardiac motion and deformation imaging by ultrasound. Ultrasound Med Biol. 2010;36(7):1145-56.
64. Cournane S, Cannon L, Browne JE, Fagan AJ. Assessment of the accuracy of an ultrasound elastography liver scanning system using a PVA-cryogel phantom with optimal acoustic and mechanical properties. Phys Med Biol. 2010;55(19):5965-83.
65. O'Brien WD, Sagar KB, Warltier DC, Rhyne TL. Acoustic propagation properties of normal, stunned, and infarcted myocardium. Morphological and biochemical determinants. Circulation. 1995;91(1):154-60.

66. Larsson M, Kremer F, Heyde B, Brodin LA, D'Hooge J, editors. Ultrasound-based Speckle Tracking for 3D Strain estimation of the Arterial wall — An experimental validation study in a tissue mimicking phantom. 2011 IEEE International Ultrasonics Symposium; 2011 18-21 Oct. 2011.
67. Regen DM. Myocardial stress equations: fiberstresses of the prolate spheroid. J Theor Biol. 1984;109(2):191-215.
68. Rabben SI, Irgens F, Angelsen B. Equations for estimating muscle fiber stress in the left ventricular wall. Heart Vessels. 1999;14(4):189-96.
69. Usyk TP, Omens JH, McCulloch AD. Regional septal dysfunction in a three-dimensional computational model of focal myofiber disarray. Am J Physiol Heart Circ Physiol. 2001;281(2):H506-14.
70. Ashraf M, Li XK, Young MT, Jensen AJ, Pemberton J, Hui L, et al. Delineation of cardiac twist by a sonographically based 2-dimensional strain analysis method: an in vitro validation study. J Ultrasound Med. 2006;25(9):1193-8.
71. Helle-Valle T, Crosby J, Edvardsen T, Lyseggen E, Amundsen BH, Smith HJ, et al. New noninvasive method for assessment of left ventricular rotation: speckle tracking echocardiography. Circulation. 2005;112(20):3149-56.
72. Okrasinski SJ, Ramachandran B, Konofagou EE. Assessment of myocardial elastography performance in phantoms under combined physiologic motion configurations with preliminary in vivo feasibility. Phys Med Biol. 2012;57(17):5633-50.
73. Jhun CS, Reibson JD, Cysyk JP. Effective ventricular unloading by left ventricular assist device varies with stage of heart failure: cardiac simulator study. ASAIO J. 2011;57(5):407-13.
74. Fosså H. Ultrasound Phantom for Myocardium [Master's thesis]:Department of Physics and Technology, University of Bergen; 2011.
75. Ashraf M, Myronenko A, Nguyen T, Inage A, Smith W, Lowe RI, et al. Defining left ventricular apex-to-base twist mechanics computed from high-resolution 3D echocardiography: validation against sonomicrometry. JACC Cardiovasc Imaging. 2010;3(3):227-34.
76. Rosner A, Barbosa D, Aarsaether E, Kjonas D, Schirmer H, D'Hooge J. The influence of frame rate on two-dimensional speckle-tracking strain measurements: a study on silico-simulated models and images recorded in patients. Eur Heart J Cardiovasc Imaging. 2015;16(10):1137-47.
77. Risum N, Ali S, Olsen NT, Jons C, Khouri MG, Lauridsen TK, et al. Variability of global left ventricular deformation analysis using vendor dependent and independent two-dimensional speckle-tracking software in adults. J Am Soc Echocardiogr. 2012;25(11):1195-203.
78. Amzulescu MS, De Craene M, Langet H, Pasquet A, Vancraeynest D, Pouleur AC, et al. Myocardial strain imaging: review of general principles, validation, and sources of discrepancies. Eur Heart J Cardiovasc Imaging. 2019;20(6):605-19.

79. Wu VC, Takeuchi M, Otani K, Haruki N, Yoshitani H, Tamura M, et al. Effect of through-plane and twisting motion on left ventricular strain calculation: direct comparison between two-dimensional and three-dimensional speckle-tracking echocardiography. J Am Soc Echocardiogr. 2013;26(11):1274-81 e4.
80. Seo Y, Ishizu T, Enomoto Y, Sugimori H, Yamamoto M, Machino T, et al. Validation of 3-dimensional speckle tracking imaging to quantify regional myocardial deformation. Circ Cardiovasc Imaging. 2009;2(6):451-9.
81. Notomi Y, Lysyansky P, Setser RM, Shiota T, Popovic ZB, Martin-Miklovic MG, et al. Measurement of ventricular torsion by two-dimensional ultrasound speckle tracking imaging. J Am Coll Cardiol. 2005;45(12):2034-41.
82. Cramariuc D, Gerdts E, Hjertaas JJ, Cramariuc A, Davidsen ES, Matre K. Myocardial function in aortic stenosis--insights from radial multilayer Doppler strain. Cardiovasc Ultrasound. 2015;13:8.
83. Cramariuc D, Cioffi G, Rieck AE, Devereux RB, Staal EM, Ray S, et al. Low-flow aortic stenosis in asymptomatic patients: valvular-arterial impedance and systolic function from the SEAS Substudy. JACC Cardiovasc Imaging. 2009;2(4):390-9.
84. Rieck AE, Cramariuc D, Staal EM, Rossebo AB, Wachtell K, Gerdts E. Impact of hypertension on left ventricular structure in patients with asymptomatic aortic valve stenosis (a SEAS substudy). J Hypertens. 2010;28(2):377-83.
85. Li CM, Li C, Bai WJ, Zhang XL, Tang H, Qing Z, et al. Value of three-dimensional speckle-tracking in detecting left ventricular dysfunction in patients with aortic valvular diseases. J Am Soc Echocardiogr. 2013;26(11):1245-52.
86. Vollema EM, Sugimoto T, Shen M, Tastet L, Ng ACT, Abou R, et al. Association of Left Ventricular Global Longitudinal Strain With Asymptomatic Severe Aortic Stenosis: Natural Course and Prognostic Value. JAMA Cardiol. 2018;3(9):839-47.
87. Carasso S, Mutlak D, Lessick J, Reisner SA, Rakowski H, Agmon Y. Symptoms in severe aortic stenosis are associated with decreased compensatory circumferential myocardial mechanics. J Am Soc Echocardiogr. 2015;28(2):218-25.
88. Dahl JS, Magne J, Pellikka PA, Donal E, Marwick TH. Assessment of Subclinical Left Ventricular Dysfunction in Aortic Stenosis. JACC Cardiovasc Imaging. 2019;12(1):163-71.
89. Bi X, Yeung DF, Salah HM, Arciniegas Calle MC, Thaden JJ, Nhola LF, et al. Dissecting myocardial mechanics in patients with severe aortic stenosis: 2-dimensional vs 3-dimensional-speckle tracking echocardiography. BMC Cardiovasc Disord. 2020;20(1):33.
90. Cho EJ, Park SJ, Kim EK, Lee GY, Chang SA, Choi JO, et al. Effects of increased left ventricular wall thickness on the myocardium in severe aortic stenosis with normal left ventricular ejection fraction: Two- and three-

dimensional multilayer speckle tracking echocardiography. Echocardiography. 2017;34(4):511-22.
91. Fung MJ, Leung DY, Thomas L. Differential Myocardial Fibre Involvement by Strain Analysis in Patients With Aortic Stenosis. Heart Lung Circ. 2018;27(11):1357-67.
92. Weidemann F, Herrmann S, Stork S, Niemann M, Frantz S, Lange V, et al. Impact of myocardial fibrosis in patients with symptomatic severe aortic stenosis. Circulation. 2009;120(7):577-84.
93. Dahl Pedersen AL, Povlsen JA, Dybro A, Clemmensen TS, Larsen AH, Ladefoged B, et al. Prevalence and Prognostic Implications of Increased Apical-to-Basal Strain Ratio in Patients with Aortic Stenosis Undergoing Transcatheter Aortic Valve Replacement. J Am Soc Echocardiogr. 2020;33(12):1465-73.
94. Castano A, Narotsky DL, Hamid N, Khalique OK, Morgenstern R, DeLuca A, et al. Unveiling transthyretin cardiac amyloidosis and its predictors among elderly patients with severe aortic stenosis undergoing transcatheter aortic valve replacement. Eur Heart J. 2017;38(38):2879-87.
95. Kaku K, Takeuchi M, Tsang W, Takigiku K, Yasukochi S, Patel AR, et al. Age-related normal range of left ventricular strain and torsion using three-dimensional speckle-tracking echocardiography. J Am Soc Echocardiogr. 2014;27(1):55-64.
96. Kleijn SA, Pandian NG, Thomas JD, Perez de Isla L, Kamp O, Zuber M, et al. Normal reference values of left ventricular strain using three-dimensional speckle tracking echocardiography: results from a multicentre study. Eur Heart J Cardiovasc Imaging. 2015;16(4):410-6.
97. Holmes AA, Taub CC, Garcia MJ, Shan J, Slovut DP. Increased apical rotation in severe aortic stenosis is associated with reduced survival: a speckle-tracking study. J Am Soc Echocardiogr. 2015;28(11):1294-301.
98. Erhart L, Donati T, Anwer S, Schindler M, Gremminger M, Renzulli M, et al. Left ventricular twist predicts mortality in severe aortic stenosis. Heart. 2022;108(3):225-32.
99. Urbano Moral JA, Arias Godinez JA, Maron MS, Malik R, Eagan JE, Patel AR, et al. Left ventricular twist mechanics in hypertrophic cardiomyopathy assessed by three-dimensional speckle tracking echocardiography. Am J Cardiol. 2011;108(12):1788-95.
100. Zhang HJ, Wang H, Sun T, Lu MJ, Xu N, Wu WC, et al. Assessment of left ventricular twist mechanics by speckle tracking echocardiography reveals association between LV twist and myocardial fibrosis in patients with hypertrophic cardiomyopathy. Int J Cardiovasc Imaging. 2014;30(8):1539-48.
101. Cameli M, Lisi M, Righini FM, Massoni A, Mondillo S. Left ventricular remodeling and torsion dynamics in hypertensive patients. Int J Cardiovasc Imaging. 2013;29(1):79-86.
102. Popescu BA, Beladan CC, Calin A, Muraru D, Deleanu D, Rosca M, et al. Left ventricular remodelling and torsional dynamics in dilated

cardiomyopathy: reversed apical rotation as a marker of disease severity. Eur J Heart Fail. 2009;11(10):945-51.
103. Ingels NB, Jr., Hansen DE, Daughters GT, 2nd, Stinson EB, Alderman EL, Miller DC. Relation between longitudinal, circumferential, and oblique shortening and torsional deformation in the left ventricle of the transplanted human heart. Circ Res. 1989;64(5):915-27.
104. Olsen FJ, Svendsen JH, Kober L, Hojberg S, Haugan K, Jensen JS, et al. Impact of transducer frequency setting on speckle tracking measures. Int J Cardiovasc Imaging. 2018;34(3):457-63.
105. Moen CA, Salminen PR, Dahle GO, Hjertaas JJ, Grong K, Matre K. Is strain by Speckle Tracking Echocardiography dependent on user controlled spatial and temporal smoothing? An experimental porcine study. Cardiovasc Ultrasound. 2013;11:32.
106. Badano LP, Cucchini U, Muraru D, Al Nono O, Sarais C, Iliceto S. Use of three-dimensional speckle tracking to assess left ventricular myocardial mechanics: inter-vendor consistency and reproducibility of strain measurements. Eur Heart J Cardiovasc Imaging. 2013;14(3):285-93.
107. Hur DJ, Sugeng L. Integration of three-dimensional echocardiography into the modern-day echo laboratory. Echocardiography. 2022;39(7):985-1000.
108. Amzulescu MS, Langet H, Saloux E, Manrique A, Slimani A, Allain P, et al. Improvements of Myocardial Deformation Assessment by Three-Dimensional Speckle-Tracking versus Two-Dimensional Speckle-Tracking Revealed by Cardiac Magnetic Resonance Tagging. J Am Soc Echocardiogr. 2018;31(9):1021-33 e1.
109. Ternacle J, Gallet R, Champagne S, Teiger E, Gellen B, Dubois Rande JL, et al. Changes in three-dimensional speckle-tracking-derived myocardial strain during percutaneous coronary intervention. J Am Soc Echocardiogr. 2013;26(12):1444-9.
110. Galat A, Guellich A, Bodez D, Slama M, Dijos M, Zeitoun DM, et al. Aortic stenosis and transthyretin cardiac amyloidosis: the chicken or the egg? Eur Heart J. 2016;37(47):3525-31.
111. Fabbri G, Serenelli M, Cantone A, Sanguettoli F, Rapezzi C. Transthyretin amyloidosis in aortic stenosis: clinical and therapeutic implications. Eur Heart J Suppl. 2021;23(Suppl E):E128-E32.
112. Einarsen E, Cramariuc D, Lonnebakken MT, Boman K, Gohlke-Barwolf C, Chambers JB, et al. Comparison of Frequency of Ischemic Cardiovascular Events in Patients With Aortic Stenosis With Versus Without Asymmetric Septal Hypertrophy (from the SEAS Trial). Am J Cardiol. 2017;119(7):1082-7.
113. Ajmone Marsan N, Michalski B, Cameli M, Podlesnikar T, Manka R, Sitges M, et al. EACVI survey on standardization of cardiac chambers quantification by transthoracic echocardiography. Eur Heart J Cardiovasc Imaging. 2020;21(2):119-23.

114. Poon J, Leung JT, Leung DY. 3D Echo in Routine Clinical Practice - State of the Art in 2019. Heart Lung Circ. 2019;28(9):1400-10.

I

Ultrasound in Med. & Biol., Vol. 39, No. 6, pp. 1006–1014, 2013

0301-5629/$ - see front matter

http://dx.doi.org/10.1016/j.ultrasmedbio.2013.01.010

● *Original Contribution*

ACCURACY OF REAL-TIME SINGLE- AND MULTI-BEAT 3-D SPECKLE TRACKING ECHOCARDIOGRAPHY *IN VITRO*

JOHANNES JUST HJERTAAS,* HENRIK FOSSÅ,† GRETE LUNESTAD DYBDAHL,† RENATE GRÜNER,† PER LUNDE,† and KNUT MATRE*

*Institute of Medicine, University of Bergen, Bergen, Norway; and †Department of Physics and Technology, University of Bergen, Bergen, Norway

(*Received* 14 *July* 2012; *revised* 12 *December* 2012; *in final form* 16 *January* 2013)

Abstract—With little data published on the accuracy of cardiac 3-D strain measurements, we investigated the agreement between 3-D echocardiography and sonomicrometry in an *in vitro* model with a polyvinyl alcohol phantom. A cardiac scanner with a 3-D probe was used to acquire recordings at 15 different stroke volumes at a heart rate of 60 beats/min, and eight different stroke volumes at a heart rate of 120 beats/min. Sonomicrometry was used as a reference, monitoring longitudinal, circumferential and radial lengths. Both single- and multi-beat acquisitions were recorded. Strain values were compared with sonomicrometer strain using linear correlation coefficients and Bland–Altman analysis. Multi-beat acquisition showed good agreement, whereas real-time images showed less agreement. The best correlation was obtained for a heart rate 60 of beats/min at a volume rate 36.6 volumes/s. (E-mail: knut.matre@med.uib.no) **© 2013 World Federation for Ultrasound in Medicine & Biology.**

***Key Words: In vitro*, Phantom, Left ventricle, Echocardiography, Three-dimensional ultrasound, Strain, Sonomicrometer, Volume rate, Frame rate, Polyvinyl alcohol.**

INTRODUCTION

With several ultrasound vendors offering 3-D acquisition and 3-D analysis of myocardial strain with speckle tracking echocardiography (STE), an evaluation of the accuracy of these methods is needed. Several clinical studies have been published recently on 3-D strain values, including comparison with 2-D strain values (Ammar et al. 2012; Jasaityte et al. 2012; Perez de Isla et al. 2009; Saito et al. 2009; Yodwut et al. 2012), as well as animal studies comparing 3-D strain values against sonomicrometry (Duan et al. 2009; Papademetris et al. 2001; Seo et al. 2009). No study has shown *in vitro* measurements of strain accuracy of commercial methods using phantoms during controlled situations. One recent study has used a phantom setup to test the accuracy of a non-commercial 3-D strain algorithm against sonomicrometry (Heyde et al. 2012). Some clinical studies have also shown the importance of sufficient volume rate (VR) when using 3-D strain methods (Negishi et al. 2012). In a recent study, strain values using prototype software for 3-D and 2-D STE were compared in volunteers and patients with non-ischemic dilated cardiomyopathy (Yodwut et al. 2012). The authors found that the sufficient VR for 3-D STE strain was lower than that for 2-D STE frame rate (FR) to obtain corresponding values of strain.

In phantom studies, the accuracy of strain measurements can be evaluated over a wide range of strain values covering relevant values for both normal and dysfunctional myocardial segments. This range allows an investigation into the effect of important acquisition settings such as FR for 2-D methods (Korinek et al. 2007; Langeland et al. 2004; Lesniak-Plewinska et al. 2010; Mårtensson et al. 2008; Stigö et al. 2010).

For 3-D acquisitions, sufficient beam density is essential. Although *in vitro* studies have shown good accuracy for 3-D volume measurements (Mårtensson et al. 2011; Nguyen et al. 2003), no *in vitro* study has investigated the accuracy of 3-D strain measurements for different acquisition methods and VR. The effect of FR on strain accuracy for 2-D acquisition has been studied, and the optimal FR is found to be in the range of 50–100 frames/s (Edvardsen and Haugaa 2011; Sitia et al. 2010). New scanners easily obtain a FR close to 100 frames/s using 2-D probes. There is a trade-off between FR and spatial resolution. An optimal FR lies

Address correspondence to: Knut Matre, Institute of Medicine, University of Bergen, 5021 Bergen, Norway. E-mail: knut.matre@med.uib.no

between a low FR (large deformation between frames, but high spatial resolution) and high FR (small deformation between frames, but low spatial resolution). For 3-D acquisition, the VR for real-time or single beat recordings are lower than the FR for 2-D recordings; therefore, multi-beat techniques have been developed to record several heart beats to produce one 3-D heart cycle.

The present study describes a custom-developed setup based on a polyvinyl alcohol (PVA) left ventricular phantom, which is useful for testing deformation methods over a large range of stroke volumes and heart rates. Several other materials have been used for deformation studies (Hall et al. 1997; Mårtensson et al. 2008, 2011; Matre et al. 2003; Stigö et al. 2010), but PVA has shown good qualities for doing *in vitro* studies mimicking fluid filled organs, such as the left ventricle (Heyde et al. 2012; Lesniak-Plewinska et al. 2010). The hypothesis tested in this study was that optimal VR for 3-D strain measurements is lower than for typical FR for 2-D strain because of the volume tracking of speckles.

MATERIALS AND METHODS

Pump rig

The setup developed in this study consists of a custom-made rig, including a dual-cylinder pump and a phantom mimicking the left ventricle (Fig. 1). The pump was powered by a stepping motor and controlled by custom-made software developed in LabVIEW (LabVIEW 8.6, National Instruments, Austin, TX, USA), which allowed control of pump rate, here called heart rate (HR), and stroke volume of the phantom as well as the ratio of systole to diastole. A digital data logger (PowerLab 8/30, AD Instruments, Sydney, Australia) was used to record all the signals from the rig. The stepping motor control module generated a pulse for each pump cycle sampled by the digital logger for timing purposes. This signal was scaled and modified to mimic the QRS part of an electrocardiograph, in order to use the QRS detector of the ultrasound scanner.

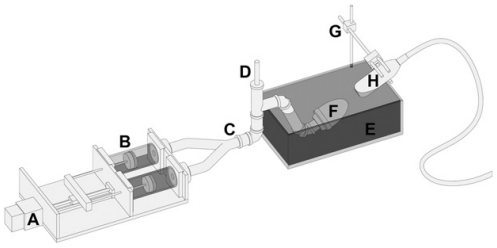

Fig. 1. Experimental setup. A = software-controlled stepping motor; B = dual-cylinder pump with pistons controlled by the stepping motor; C = rigid tubing from the pump to the phantom; D = air buffer to allow damping of each stroke (a surgical clamp was used to control the size of the buffer); E = water container (the walls and bottom of the container were covered with absorbing material to avoid artifacts); F = the phantom connected to the end of the tubing; G = rigid stand with clamp for holding the probe; H = ultrasound probe.

In vitro *phantom*

The phantom was made of PVA, which is able to mimic the contracting myocardium. The stiffness of the material and the compressional wave (sound) velocity can be controlled to an extent by the number of freeze–thaw cycles. The phantom was cast using an ellipsoidal mold of the left ventricle, which was symmetrical, and underwent two freeze–thaw cycles of 24 h. It was then fitted with pairs of sonomicrometer crystals (SL5-2, Triton Technologies Inc., San Diego, CA, USA), implanted at mid wall in the longitudinal and circumferential direction, each pair implanted with a distance between crystals of approximately 10 mm. One additional pair was glued to each opposite surface of the phantom wall to measure strain in the radial direction. The phantom was then submerged into a water container connected to the rig. When the pump was running, the water was pressed out of the pump's cylinders by the stepping motor, and the phantom expanded to a state defined as diastole. When the cylinders moved back, the volume of the phantom was reduced, and the wall thickness increased to a state defined as systole. This definition resembles the contracting left ventricle, although there is no active contraction in this passive phantom. The end systolic volume was 70 mL, and with a stroke volume setting of 50 mL the end diastolic volume was 120 mL. The digital data logger was used to record the output from the four-channel sonomicrometer (Type 120.2; Triton Technologies Inc., San Diego, CA, USA), pressure in the phantom generated by a micro-tip transducer (SPC-350, Millar Instruments, Houston, TX, USA) in addition to the timing pulses from the pump.

Ultrasound acquisition

The ultrasound probe (4V; GE Vingmed Ultrasound, Horten, Norway) was fixed to obtain apical views of the phantom and connected to an ultrasound scanner (Vivid E9; GE Vingmed Ultrasound). Figure 2 shows the phantom setup. The 3-D B-mode acquisition was performed using harmonic imaging. The image was optimized by adjusting the depth and sector angle for a large stroke volume setting. The resulting depth range was 0–12 cm and the sector angle was 75°, and these settings were kept constant throughout this study. Gain and other acquisition settings were also optimized and kept constant during the different recordings (Fig. 3).

Protocol

Two series of recordings were made: (1) one series at an HR of 60 beats/min, consisting of 15 different stroke

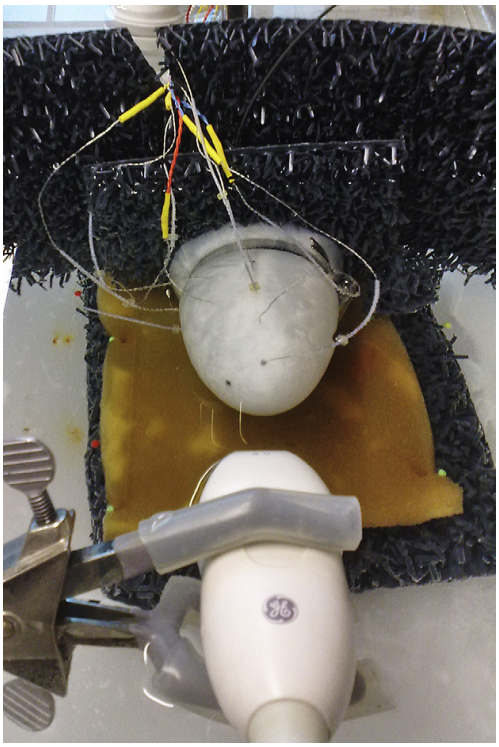

Fig. 2. Probe and phantom with implanted sonomicrometer crystals in the water tank.

volumes ranging 10–150 mL, and (2) one series at an HR of 120 beats/min, with stroke volumes ranging 10–80 mL. Each volume was tested once in this study. The maximum stroke volume of 80 mL at 120 beats/min was due to limitations of the flow rig at a high HR. The limitation of this pump to deliver large stroke volumes at high a HR was mainly due to a limited acceleration of the stepping motor, leading to position uncertainties that in turn shifted the starting position of the pumping action. The end systolic pressure in the phantom was kept constant for each stroke volume acquisition by adjusting the starting position of the pump cylinders before each acquisition. 3-D recordings, including real-time, 2– and 6–multi-beat recordings at different VRs, were then obtained for each of these situations. All the images were recorded with the same probe position and the same depth and sector angle to compare the strain values directly to each other. The scanner allows five different VRs to be chosen after the user has selected a specific probe sector angle and depth. In addition, the workstation does not accept VRs less than 12 volumes/s (VPS) for strain analysis; this imposes a limitation in the choice of VR.

The following acquisitions were performed using a selection of VRs:

1. Real-time (VR 21.9 VPS)
2. Multi-beat using 2-beat acquisition (VRs: 18.7 and 41.5 VPS)
3. Multi-beat using 6-beat acquisition (VRs: 30.2, 36.6, 52.3 and 124.4 VPS)

Sonomicrometer lengths were logged, showing the changes in segment lengths for each of these settings, serving as the reference measurement. The received sonomicrometer echoes were continuously monitored with an oscilloscope throughout the study to ensure correct triggering. The measurements by the two methods had to be taken in sequence, because interference made simultaneous measurements difficult.

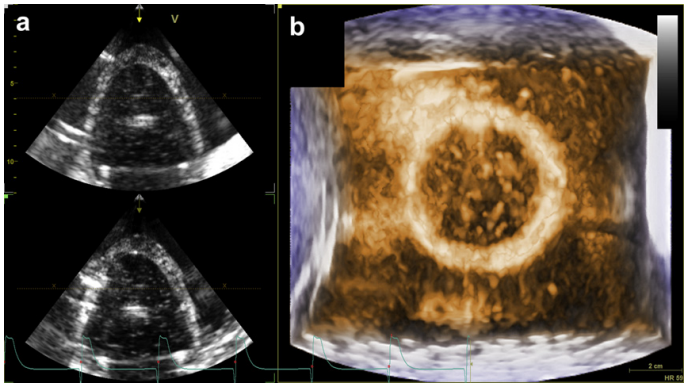

Fig. 3. 3-D image of the PVA phantom using 6–multi-beat recording at diastole. (a) Two perpendicular apical 2-D views. (b) 3-D image of phantom. At the bottom is the electrocardiogram signal generated by the data logger.

Data analysis

Sonomicrometry strain was calculated from the maximum and minimum values of sonomicrometry lengths. Post-processing of the echo-images was analyzed on a dedicated workstation using commercial software (EchoPac BT11; GE Vingmed Ultrasound). For analysis of the 3-D strain, the 4-D Auto LVQ tool was used. This tool in the software requires the user to define a region of interest (ROI) by tracing the inner and outer edges of the 3-D volume image at end systole and end diastole in a number of 2-D views. First, the 4-D Auto LVQ tool automatically places an initial ROI. The user then adjusts the endocardial and epicardial borders of the ROI while monitoring three long-axis and three short-axis planes (Fig. 4). Finally, the tissue inside the ROI is tracked in three dimensions, and the position and shape of the ROI are automatically adjusted to follow the tracking. The ROI is then segmented by the software into 17 segments with the 17th segment being the apex. The timing of end systole was chosen automatically by the program, based on the volume curve created by the software. All strain values were read at end systole. The algorithm used in this software estimated the strain from each ROI, and the results were presented as strain curves and as a bull's-eye plot of the ventricle with 17 strain segments (6 basal segments, 6 midventricular segments, 4 apical segments and 1 segment for the apex; Fig. 4; Crosby et al. 2009). The segment nearest the corresponding sonomicrometer crystals was chosen to avoid the strong echoes from crystals and leads, and it was compared with sonomicrometry at the time of end systole. Because the 3-D strain algorithm was unable to measure radial strain directly, radial strain was estimated from area strain. With this software, area strain (SA) is calculated as: $SA = 100 \times (A - A_0)/A_0$, where A is the instantaneous midwall area of the segment and A_0 is the initial area at end diastole (QRS).

Statistics

Linear correlation coefficients were calculated as a measure of association between the two methods. A Bland–Altman analysis (Altman and Bland 1983; Bland and Altman 1986) was performed to analyze the agreement between the methods.

Inter-observer variability was calculated as the mean difference between the two observers and as the intraclass correlation coefficient. The inter-observer variation refers to the off-line analysis only. This calculation was done because we believe that, for this controlled *in vitro* study, the variation was introduced by the investigators' placement of the endocardial and epicardial border

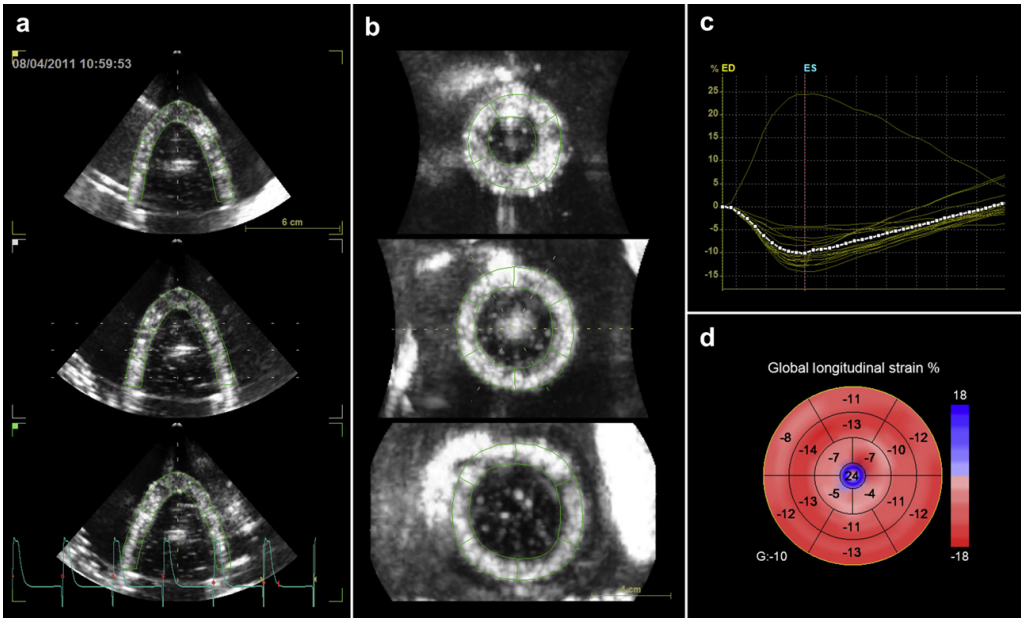

Fig. 4. Strain analysis using EchoPac BT11. (a) Three 2-D long-axis views of the phantom. (b) Three 2-D short-axis views at three different levels. (c) Time curve of longitudinal strain in 17 segments; positive strain curve from the apical segment. (d) Bull's-eye plot of end systolic longitudinal strain values.

(*i.e.,* the inner and outer surface echoes) during analysis. The second observer was blinded from the placement of the ROI and the strain values obtained by the first observer. Three data sets were used at different VRs (real-time recordings at 21.9 VPS and 6–multi-beat recordings at 36.6 and 52.3 VPS).

RESULTS

One hundred sixty-one 3-D recordings were analyzed. For recordings at 60 beats/min, values of longitudinal strain gave the best result, with a correlation coefficient of 0.990 and agreement 0.83% ± 1.54% (mean difference ± limits of agreement from the Bland–Altman analysis) at a VR of 36.6 VPS (Table 1). Best result for circumferential strain was also found at a VR of 36.6 VPS, with a correlation coefficient of 0.989 and agreement of −0.78% ± 1.75%. Radial strain also showed the best results at a VR of 36.6 VPS, with a correlation of 0.897 and agreement of 16.10% ± 22.26%.

For recordings at 120 beats/min, longitudinal strain again showed the best results at 36.6 VPS, with a correlation of 0.956 and agreement of 2.57% ± 2.40% (Table 2). Circumferential strain showed the best results at 30.2 VPS, with a correlation of 0.967 and agreement −1.20% ± 2.26%. Radial strain showed best result at 36.6 VPS, with a correlation of 0.993 and agreement of 5.08 ± 8.10%.

Figure 5 shows scatter plots and a Bland–Altman analysis of longitudinal strain for real-time (Fig. 5a, b) and 6–multi-beat recordings (Fig. 5c, d) at 60 beats/min. Multi-beat recordings show better correlation and better agreement than single beat recordings.

The mean difference between the two observers at 36.6 VPS using multi-beat recordings was −0.6% ± 1.4% (standard deviation) for longitudinal strain, −0.2% ± 0.7% for circumferential strain and 1.1% ± 2.0% for radial strain. The intra-class correlations were R_{ic} = 0.97, 0.99 and 0.99, respectively.

For a VR of 52.3 VPS using 6–multi-beat recordings, the mean difference between observers was 0.9% ± 1.4% (standard deviation) for longitudinal strain, −0.6% ± 1.8% for circumferential strain and −0.6% ± 3.4% for radial strain. The intra-class correlations were R_{ic} = 0.96, 0.83 and 0.94, respectively.

For a VR of 21.9 VPS using single-beat recordings, the mean difference between observers was 1.2% ± 5.1% (standard deviation) for longitudinal strain, −0.4% ± 2.5% for circumferential strain and −0.4% ± 7.5% for radial strain. The intra-class correlations were R_{ic} = 0.59, 0.57 and 0.65, respectively.

Table 1. Comparison of 3-D STE strain with sonomicrometer strain*

Direction	Mode	VPS	R	Bland–Altman Mean diff (%)	Bland–Altman ±1.96 SD (%)
Longitudinal strain	Single beat	21.9	0.791	2.16	7.26
	2 beat	41.5	0.941	1.41	3.89
	2 beat	18.7	0.863	3.03	5.65
	6 beat	124.4	0.918	3.97	6.22
	6 beat	52.3	0.954	2.92	3.86
	6 beat	36.6	0.990	0.83	1.54
	6 beat	30.2	0.978	−0.02	2.45
Circumferential strain	Single beat	21.9	0.169	6.04	11.83
	2 beat	41.5	0.867	1.81	6.21
	2 beat	18.7	0.938	4.90	6.00
	6 beat	124.4	0.954	−1.04	3.43
	6 beat	52.3	0.804	3.99	7.43
	6 beat	36.6	0.989	−0.78	1.75
	6 beat	30.2	0.965	−1.95	3.04
Radial strain	Single beat	21.9	0.750	4.43	13.86
	2 beat	41.5	0.884	10.84	13.15
	2 beat	18.7	0.713	4.52	15.87
	6 beat	124.4	0.841	11.60	15.24
	6 beat	52.3	0.883	5.81	10.29
	6 beat	36.6	0.897	16.10	22.26
	6 beat	30.2	0.912	19.32	24.44

Mean diff = mean of the differences between 3-D STE strain and sonomicrometer strain; R = linear correlation coefficient; VPS = volumes per second; ±1.96 SD = limits of agreement according to Bland and Altman analysis.

* HR = 60 beats/min for volumes of 10–150 mL (n = 15).

Table 2. Comparison of 3-D STE strain with sonomicrometer strain*

Direction	Mode	VPS	R	Bland–Altman Mean diff (%)	Bland–Altman ±1.96 SD (%)
Longitudinal strain	Single beat	21.9	0.588	3.23	6.50
	2 beat	41.5	0.948	1.13	2.59
	2 beat	18.7	−0.012	4.97	10.34
	6 beat	124.4	0.936	2.94	3.49
	6 beat	52.3	0.872	2.67	4.39
	6 beat	36.6	0.956	2.57	2.40
	6 beat	30.2	0.766	2.11	5.21
Circumferential strain	Single beat	21.9	0.729	3.08	5.28
	2 beat	41.5	0.344	3.49	7.15
	2 beat	18.7	0.854	4.20	4.61
	6 beat	124.4	0.843	−0.37	4.05
	6 beat	52.3	0.853	3.08	4.27
	6 beat	36.6	0.946	−0.39	2.43
	6 beat	30.2	0.967	−1.20	2.26
Radial strain	Single beat	21.9	0.789	−0.18	5.85
	2 beat	41.5	0.931	1.77	5.33
	2 beat	18.7	0.586	−3.45	7.89
	6 beat	124.4	0.928	4.30	5.54
	6 beat	52.3	0.962	0.58	3.47
	6 beat	36.6	0.993	5.08	8.10
	6 beat	30.2	0.969	6.63	7.53

Mean diff = mean of the differences between 3D STE strain and sonomicrometer strain; R = linear correlation coefficient; VPS = volumes per second; ±1.96 SD = limits of agreement according to Bland and Altman analysis.

* HR = 120 beats/min for volumes of 10–80 mL (n = 8).

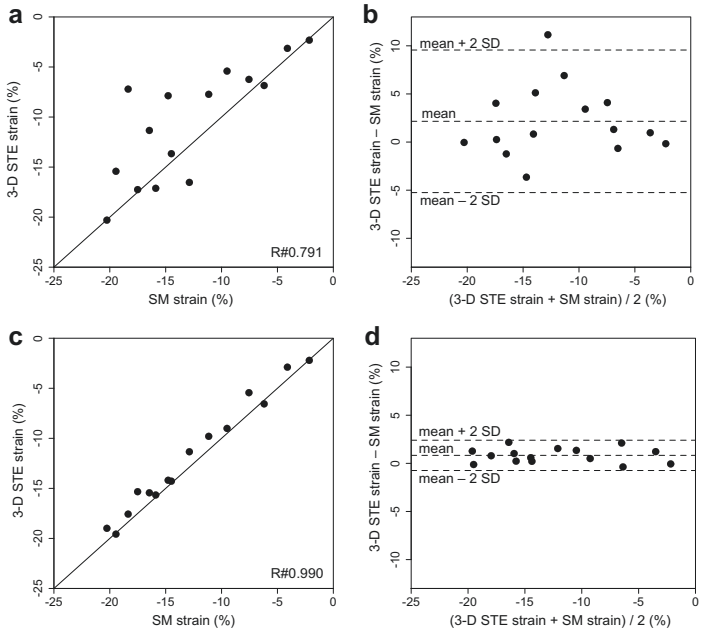

Fig. 5. Longitudinal strain at an HR of 60 beats/min. (a, c) Scatter plots showing 3-D STE strain along the y-axis and sonomicrometry (SM) strain along the x-axis. Line of unity is shown. (b, d) Bland–Altman analysis comparing longitudinal strain values from 3-D echocardiography and SM. (a, b) Recordings using single-beat at 21.9 VPS. (c, d) Recordings using 6-beat at 36.6 VPS.

DISCUSSION

Temporal versus spatial resolution

One of the objectives of this study was to determine the ultimate VR when performing 3-D strain analysis with STE, based on a comparison with sonomicrometry. Keeping in mind that by increasing the FR for 2-D or VR for 3-D at a fixed sector width and depth (better temporal resolution), the beam density is reduced (poorer spatial resolution), thus covering the same volume with fewer beams and resulting in reduced spatial resolution. The optimal VR might therefore be dependent on the HR, because a higher HR will require more frames per second to handle the fast movement of the myocardium. To achieve this VR, spatial resolution has to be sacrificed.

The ultrasound system used in this experiment keeps the beam density constant regardless of depth and sector angle. Adjusting these parameters affects only the VR. The beam density does, however, change when using different VR or multi-beat settings. The VR control of the system is actually a beam density control. Multi-beat linearly scales the beam density, whereas VR has an inverse linear relationship with the beam density. For example, for a fixed VR, the beam density is double in dual-beat compared with single-beat acquisition. In a fixed multi-beat setting, the beam density is double at 30 VPS compared with 60 VPS. Changing depth and sector angle does not change the spatial resolution; only VR rate and multi-beat settings do this. In this experiment, the 1-beat 21.9 VPS, 2-beat 41.5 VPS and 6-beat 124.4 VPS have similar low beam densities. The 2-beat 18.7 VPS and 6-beat 52 VPS have similar medium–low beam densities, whereas the-6 beat 36.6 VPS has medium–high beam density and the 6-beat 30.2 VPS has high beam density.

The reason for the poor accuracy at the highest VR is probably the low beam density, which gives poor image quality for speckle tracking. It is the combination of a relatively low VR and high multi-beat setting that enables the highest beam density. The optimal setting for speckle tracking is a trade-off between high beam density and high VR.

For a given multi-beat setting, the temporal and spatial resolutions are inversely proportional. The speckle tracking method suffers if the temporal resolution is too low, because the speckle pattern might change too much or move too far between frames. If the spatial

resolution is too low, the speckle pattern becomes too coarse to get a good match. Therefore, there must be an optimal trade-off between these settings. This experiment indicates that for 6–multi-beat, the optimal trade-off is at a temporal resolution of 36.6 VPS. The relation between temporal and spatial resolution depends on the multi-beat setting; therefore, the same VPS might give different results for different multi-beat settings.

Although Tables 1 and 2 show different results for the different acquisitions, there is a clear tendency for the single-beat acquisition to be the least accurate method and for a too low or too high VR to be inferior to the optimal 36.6 VPS.

Other studies

Previous animal studies in dogs have shown good agreement between 3-D STE and sonomicrometry *in vivo* (Duan et al. 2009; Papademetris et al. 2001), although these have been performed using non-commercial algorithms and equipment, whereas we used a commercially available scanner and software. Another study in sheep (Seo et al. 2009), using a VR of 30 VPS, achieved a global correlation of longitudinal strain of 0.89, circumferential strain of 0.90 and radial strain of 0.84, which are in the same order of magnitude for regional measurements as in this study. A recent clinical study by Yodwut et al. (2012) investigated 2-D and 3-D strain for different multi-beat acquisitions. Their study showed that 3-D strain can assess myocardial deformation at a lower VR than the corresponding FR for 2-D methods. In this experiment, the optimal 6-beat setting is always better than the optimal 2-beat setting (Tables 1 and 2, reading values for 6-beat at 36.6 VPS and 2-beat at 41.5 VPS); therefore, assuming that Yodwut et al. (2012) used optimal settings, the two experiments show similar findings. The studies are, however, not completely comparable because Yodwut et al. (2012) used 2-D strain as the method of comparison. In this study, implantable sonomicrometer crystals were used as an independent strain method, and different scanners were used.

It is difficult to do a direct comparison with previous studies because of different 3-D strain algorithms from different vendors, as well as different method of comparison and different species. Few studies are directly comparable to this study. Heyde et al. (2012) used a PVA phantom to evaluate a new 3-D strain algorithm and showed correlations of 0.96, 0.92 and 0.84 for longitudinal, circumferential and radial strain, respectively. In addition to showing the usefulness of PVA as a cardiac phantom, their results are better than our similar single-beat results. One reason for this difference could be different VR, in addition to a different algorithm. In our study the results showed less accuracy for radial strain at 60 beats/min, which is similar to their findings. This finding could be the result of calculating radial strain from area strain.

Phantom model

Several proposed materials for mimicking muscle have been proposed and used (Mukherjee et al. 2012; Zell et al. 2007). Agar gels have been used for the evaluation of cardiac deformation, but are mechanically weak and less suitable for fluid filled phantoms. Silicon rubber is stronger, but the sound velocity is low (1000 m/s) compared with biological soft tissue.

PVA has proved to be a useful material for phantom applications related to myocardium; however, it gives a different echo pattern compared with *in vivo* myocardium, with less visible speckles in the ultrasound image at frequencies used for cardiac scanning. The sound velocity and attenuation, however, is close to that of myocardium; it is also strong enough for fluid-filled phantoms and has been the material of choice in recent phantom studies (Heyde et al. 2012; Lesniak-Plewinska et al. 2010). An increase in speckle intensity can be achieved by adding glycerin to the PVA-fluid before the freeze–thaw cycles, thus giving a speckle pattern closer to myocardium (Heyde et al. 2012). This modification was not used in this study. The reflections from this PVA phantoms are not identical to the speckle pattern obtained from human myocardium. As seen from Figures 3 and 4, the speckle pattern is not as detailed and has somewhat larger speckles. However, noting that the 3-D probe used in this study has a lower transmitted frequency than most clinical 2-D sector probes, we believe that the speckle pattern produced by the PVA phantom used in this study is a good test object for testing the accuracy of this scanner and image analysis. In addition, the resulting strain curve resembles a clinically obtained curve.

Limitations

The PVA phantom was chosen to mimic the movement of the left ventricles during cardiac contraction. To do so, it is inflated using an increase in water pressure from the inside. One of the limitations of this phantom setup is the ability to expand in the longitudinal direction, resembling the human left ventricle. Especially at large stroke volumes, the phantom inflation resulted in a more spherical geometry, which is reflected in the limitation in longitudinal strain at maximal stroke volumes (Fig. 5). This limitation is difficult to overcome without an active contracting ventricle.

The use of PVA as a phantom material creates a slightly different sound velocity than *in vivo* myocardium. We measured the sound velocity to 1525 m/s after two freeze–thaw cycles. The sonomicrometer was

calibrated for the myocardium with a sound velocity of 1570 m/s, which would create a small error in length measurements when using sonomicrometry in PVA gel. However, strain measurements are relative and would not be influenced by the sound velocity.

The implanted sonomicrometer crystals and leads created strong echoes that were visible on the ultrasound images. Therefore, we did not measure strain in the same segment as the sonomicrometer crystals, but chose the nearest segment. This effect can be seen in Figure 4d, where the segment with crystals reads a strain of −8%, which is lower than the other basal segments (−11% to −13%). The phantom was cast to be symmetrical, but small changes in wall thickness and uneven mounting to the tube could give some variation in wall motion and thus strain values between the segments; however we believe this effect is small.

Measuring strain in segments will be less accurate for small segments, which includes a relatively low number of speckles. Measuring global or average strain of a large area will probably give a better accuracy for strain estimation because of the spatial averaging. We chose to compare one segment, only to obtain a value representative for the same region as that measured by the sonomicrometer, which was approximately 10 mm between the crystals for a crystal pair.

This study does not mimic the complex architecture and function of the intact left ventricle, including its twisting motion; however, there are no commercial phantom that does. One commercial phantom that includes a twisting apex has an apical attachment connected to a stepping motor and can mimic ventricular twist. However, because of this attachment, no apical ultrasound views can be recorded, and it is therefore not useful for apical 3-D recordings.

The PVA offers a good compromise between correct acoustic properties (velocity and attenuation) and being sufficiently elastic to withstand the volume loading necessary to obtain strain values similar to that found in the human left ventricle. The algorithm used in this study requires an apical geometry in the acquisition to work properly.

Inter-observer variability

Inter-observer variability showed excellent agreement for the tested multi-beat measurements (6-beat VR = 36.6 VPS and 52.3 VPS). A recent study by Gayat et al. (2011) using several scanners showed similar results for multi-beat acquisition, but with more differences between vendors than between observers. In this study, for single-beat acquisition, the agreement between the two observers was relatively poor, with larger limits of agreement and low correlation coefficient for all three strain directions.

Clinical implications

In the present study we evaluated one commercial 3-D strain algorithm using a controlled phantom setup. To obtain good spatial and temporal resolution, multi-beat recordings were used. The use of multi-beat recordings, especially 6 beats, requires conditions that might be difficult to obtain in some patients. Arrhythmias and patient or probe movement limits this acquisition method. However, 2-beat multi-beat recordings still gave acceptable results for most strain directions; this would be easier to use for such patients. The 3-D strain range in this experiment with the volume range used is −3% to −21% for peak longitudinal strain. Several studies have shown strain values in a normal population, Saito et al. (2009) gave a mean value of longitudinal strain in normal segments by 3-D STE to be −17.0% ± 5.5%, which is well within our tested values. Thus, the range of strain values tested in this study covers the typical strain values seen for both normal and dysfunctional myocardial segments.

The results from this study cannot be directly transferred to a clinical situation, but they provide a background for choosing a VR for 3-D acquisition. A feasibility study in patients is needed to test these measurements for clinical relevance.

CONCLUSION

This study demonstrates the relation between VR and 3-D strain accuracy. The images recorded as real-time single-beat images gave relatively poor agreement, whereas the 6–multi-beat recordings gave excellent agreement. The best longitudinal and circumferential recordings gave slightly better agreement than for radial strain, which indicates an optimal VR for 3-D strain measurement that is lower than for a typical corresponding FR for 2-D strain.

Acknowledgments—This work was supported by the Bergen University Heart Fund and the MedViz consortium, an inter-institutionary research and development program in medical visualization by the University of Bergen, Haukeland University Hospital and Christian Michelsen Research. There is no conflict of interest, and these institutions had no part in the development or approval of the manuscript.

REFERENCES

Altman DG, Bland JM. Measurement in medicine: The analysis of method comparison studies. J R Stat Soc 1983;32:307–317.

Ammar KA, Paterick TE, Khandheria BK, Jan MF, Kramer C, Umland MM, Tercius AJ, Baratta L, Tajik AJ. Myocardial mechanics: Understanding and applying three-dimensional speckle tracking echocardiography in clinical practice. Echocardiography 2012;29:861–872.

Bland JM, Altman DG. Statistical methods for assessing agreement between two methods of clinical measurement. Lancet 1986;1: 307–310.

Crosby J, Amundsen BH, Hergum T, Remme EW, Langeland S, Torp H. 3-D speckle tracking for assessment of regional left ventricular function. Ultrasound Med Biol 2009;35:458–471.

Duan Q, Parker KM, Lorsakul A, Angelini ED, Hyodo E, Homma S, Holmes JW, Laine AF. Quantitative Validation of Optical Flow Based Myocardial Strain Measures Using Sonomicrometry. Proc IEEE Int Symp Biomed Imaging 2009;2009:454–457.

Edvardsen T, Haugaa KH. Imaging assessment of ventricular mechanics. Heart 2011;97:1349–1356.

Gayat E, Ahmad H, Weinert L, Lang RM, Mor-Avi V. Reproducibility and inter-vendor variability of left ventricular deformation measurements by three-dimensional speckle-tracking echocardiography. J Am Soc Echocardiogr 2011;24:878–885.

Hall TJ, Bilgen M, Insana MF, Krouskop TA. Phantom materials for elastography. IEEE Trans Ultrason Ferroelectr Freq Control 1997; 44:1355–1365.

Heyde B, Cygan S, Choi HF, Lesniak-Plewinska B, Barbosa D, Elen A, Claus P, Loeckx D, Kaluzynski K, D'Hooge J. Regional cardiac motion and strain estimation in three-dimensional echocardiography: A validation study in thick-walled univentricular phantoms. IEEE Trans Ultrason Ferroelectr Freq Control 2012;59:668–682.

Jasaityte R, Heyde B, Ferferieva V, Amundsen B, Barbosa D, Loeckx D, Kiss G, Orderud F, Claus P, Torp H, D'Hooge J. Comparison of a new methodology for the assessment of 3D myocardial strain from volumetric ultrasound with 2-D speckle tracking. Int J Cardiovasc Imaging 2012;28:1049–1060.

Korinek J, Kjaergaard J, Sengupta PP, Yoshifuku S, McMahon EM, Cha SS, Khandheria BK, Belohlavek M. High spatial resolution speckle tracking improves accuracy of 2-dimensional strain measurements: An update on a new method in functional echocardiography. J Am Soc Echocardiogr 2007;20:165–170.

Langeland S, D'Hooge J, Claessens T, Claus P, Verdonck P, Suetens P, Sutherland GR, Bijnens B. RF-based two-dimensional cardiac strain estimation: A validation study in a tissue-mimicking phantom. IEEE Trans Ultrason Ferroelectr Freq Control 2004;51:1537–1546.

Lesniak-Plewinska B, Cygan S, Kaluzynski K, D'Hooge J, Zmigrodzki J, Kowalik E, Kordybach M, Kowalski M. A dual-chamber, thick-walled cardiac phantom for use in cardiac motion and deformation imaging by ultrasound. Ultrasound Med Biol 2010;36:1145–1156.

Mårtensson M, Bjällmark A, Brodin LÅ. Evaluation of tissue Doppler-based velocity and deformation imaging: A phantom study of ultrasound systems. Eur J Echocardiogr 2011;12:467–476.

Mårtensson M, Winter R, Cederlund K, Ripsweden J, Mir-Akbari H, Nowak J, Brodin LÅ. Assessment of left ventricular volumes using simplified 3-D echocardiography and computed tomography—a phantom and clinical study. Cardiovasc Ultrasound 2008;6:26.

Matre K, Ahmed AB, Gregersen H, Heimdal A, Hausken T, Ødegaard S, Gilja OH. In vitro evaluation of ultrasound Doppler strain rate imaging: Modification for measurement in a slowly moving tissue phantom. Ultrasound Med Biol 2003;29:1725–1734.

Mukherjee R, Sprouse C, Pinheiro A, Abraham T, Burlina P. Computing myocardial motion in 4-dimensional echocardiography. Ultrasound Med Biol 2012;38:1284–1297.

Negishi K, Negishi T, Agler DA, Plana JC, Marwick TH. Role of temporal resolution in selection of the appropriate strain technique for evaluation of subclinical myocardial dysfunction. Echocardiography 2012;29:334–339.

Nguyen LD, Leger C, Debrun D, Therain F, Visser J, Busemann Sokole E. Validation of a volumic reconstruction in 4-d echocardiography and gated SPECT using a dynamic cardiac phantom. Ultrasound Med Biol 2003;29:1151–1160.

Papademetris X, Sinusas AJ, Dione DP, Duncan JS. Estimation of 3D left ventricular deformation from echocardiography. Med Image Anal 2001;5:17–28.

Perez de Isla L, Balcones DV, Fernandez-Golfin C, Marcos-Alberca P, Almeria C, Rodrigo JL, Macaya C, Zamorano J. Three-dimensional-wall motion tracking: A new and faster tool for myocardial strain assessment: Comparison with two-dimensional-wall motion tracking. J Am Soc Echocardiogr 2009;22:325–330.

Saito K, Okura H, Watanabe N, Hayashida A, Obase K, Imai K, Maehama T, Kawamoto T, Neishi Y, Yoshida K. Comprehensive evaluation of left ventricular strain using speckle tracking echocardiography in normal adults: Comparison of three-dimensional and two-dimensional approaches. J Am Soc Echocardiogr 2009;22: 1025–1030.

Seo Y, Ishizu T, Enomoto Y, Sugimori H, Yamamoto M, Machino T, Kawamura R, Aonuma K. Validation of 3-dimensional speckle tracking imaging to quantify regional myocardial deformation. Circ Cardiovasc Imaging 2009;2:451–459.

Sitia S, Tomasoni L, Turiel M. Speckle tracking echocardiography: A new approach to myocardial function. World J Cardiol 2010;2:1–5.

Stigö A, Johansen P, Jensen MO, Sivesgaard K, Nygaard H, Sloth E. An automated in vitro model for the evaluation of ultrasound modalities measuring myocardial deformation. Cardiovasc Ultrasound 2010;8:40.

Yodwut C, Weinert L, Klas B, Lang RM, Mor-Avi V. Effects of frame rate on three-dimensional speckle-tracking-based measurements of myocardial deformation. J Am Soc Echocardiogr 2012;25:978–985.

Zell K, Sperl JI, Vogel MW, Niessner R, Haisch C. Acoustical properties of selected tissue phantom materials for ultrasound imaging. Phys Med Biol 2007;52:N475–N484.

II

Johannes Just Hjertaas* and Knut Matre

A left ventricular phantom for 3D echocardiographic twist measurements

https://doi.org/10.1515/bmt-2019-0096
Received April 25, 2019; accepted July 7, 2019

Abstract: Traditional two-dimensional (2D) ultrasound speckle tracking echocardiography (STE) studies have shown a wide range of twist values, also for normal hearts, which is due to the limitations of short-axis 2D ultrasound. The same limitations do not apply to three-dimensional (3D) ultrasound, and several studies have shown 3D ultrasound to be superior to 2D ultrasound, which is unreliable for measuring twist. The aim of this study was to develop a left ventricular twisting phantom and to evaluate the accuracy of 3D STE twist measurements using different acquisition methods and volume rates (VR). This phantom was not intended to simulate a heart, but to function as a medium for ultrasound deformation measurement. The phantom was made of polyvinyl alcohol (PVA) and casted using 3D printed molds. Twist was obtained by making the phantom consist of two PVA layers with different elastic properties in a spiral pattern. This gave increased apical rotation with increased stroke volume in a mock circulation. To test the accuracy of 3D STE twist, both single-beat, as well as two, four and six multi-beat acquisitions, were recorded and compared against twist from implanted sonomicrometry crystals. A custom-made software was developed to calculate twist from sonomicrometry. The phantom gave sonomicrometer twist values from 2.0° to 13.8° depending on the stroke volume. STE software tracked the phantom wall well at several combinations of temporal and spatial resolution. Agreement between the two twist methods was best for multi-beat acquisitions in the range of 14.4–30.4 volumes per second (VPS), while poorer for single-beat and higher multi-beat VRs. Smallest offset was obtained at six-beat multi-beat at 17.1 VPS and 30.4 VPS. The phantom proved to be a useful tool for simulating cardiac twist and gave different twist at different stroke volumes. Best agreement with the sonomicrometer reference method was obtained at good spatial resolution (high beam density) and a relatively low VR. 3D STE twist values showed better agreement with sonomicrometry for most multi-beat recordings compared with single-beat recordings.

Keywords: *in vitro*; myocardial twist; rotation; sonomicrometer; speckle tracking; three-dimensional echocardiography; volume rate.

List of abbreviations: 2D, two-dimensional; 3D, three-dimensional; ABS, acrylonitrile butadiene styrene; CAD, computer-aided design; CMR, cardiac magnetic resonance; ECG, electrocardiogram; FR, frame rate; HR, heart rate; PVA, polyvinyl alcohol; ROI, region of interest; STE, speckle tracking echocardiography; VPS, volumes per second; VR, volume rate.

Introduction

Left ventricular rotation and twist are important features of the normal left ventricular contraction and have shown to be modified by ischemia and hypertrophy [1–4]. Torsion, which in cardiology is calculated as twist divided by the end-diastolic left ventricular length, gives the possibility to compare the twisting action of hearts of different sizes. Peak systolic twist and torsion measurements by two-dimensional (2D) speckle tracking echocardiography (STE) have been published with a range of different values, also for normal hearts. As early as 2007, Weyman showed a span from 6.7° to 14.5° for twist in normal cohorts [5]. Newer publications also show large variation in twist values in normal individuals, where mean values of 7.9°–20° have been reported [6, 7]. The different result is believed to be caused by, in addition to possible variation between cohorts, limitations in the applied method. For 2D STE twist measurements, this includes variable image quality, the selection of the basal and apical planes, in- and out-of-plane motion, low frame rate (FR) as well as vendor differences in available acquisition methods and software algorithms [8]. For 2D STE torsion measurement, uncertainty in determining the end-diastolic distance between the selected planes can lead to inaccurate estimates. For three-dimensional (3D) STE methods, limitations in beam density and low volume rate (VR) could lead

***Corresponding author: Johannes Just Hjertaas,** Department of Clinical Science, University of Bergen, Haukeland University Hospital, 5021 Bergen, Norway, E-mail: johannes.hjertaas@gmail.com
Knut Matre: Department of Clinical Science, University of Bergen, Haukeland University Hospital, 5021 Bergen, Norway

to inaccurate strain measurements [9]. When comparing 2D with 3D STE measurements of torsion, studies have shown that 2D STE is not a reliable method to measure left ventricular torsion because of these limitations [10–12]. Measurements of twist and torsion are to be used with caution according to the current guidelines [13, 14]. Some studies have compared rotation and twist from STE to cardiac magnetic resonance (CMR) tagging. Generally it seems that CMR gives higher values for twist than 2D STE [15, 16]. However, CMR has its shortcoming with regard to especially temporal resolution.

To be able to assess the accuracy of rotation and twist measurements by STE, experimental studies have been performed comparing 2D STE with implanted crystals in dogs [15]. Other studies have used a rotating actuator for *ex vivo* hearts with a stepping motor for the control of basal rotation with a fixed apex [17, 18].

A synthetic twist phantom has been commercially available and has been used for *in vitro* evaluation of echocardiographic measurements [19], but is not suitable for apical views due to the apical attachment. Most 3D deformation algorithms are based on apical 3D views of the left ventricle, a twisting phantom should therefore not include an apical attachment. There is a need for a simplified synthetic phantom setup compared to the published animal and *ex vivo* setups. A twisting synthetic phantom with implantable sonomicrometry crystals for apical views is thus ideal to investigate and optimize 3D STE measurement of rotation and twist and has the advantage of enabling repetitive measurements over time with the same phantom in comparison to *ex vivo* setups. In previous studies, we used a pump rig with a phantom made of polyvinyl alcohol (PVA) to evaluate the accuracy of 2D and 3D strain measurements [9, 20]; however, these phantoms had no twist properties.

The aim of this study was to develop a twisting phantom which enabled different levels of twist to be simulated and further to quantify the effect of different acquisition methods. This includes both single-beat and multi-beat, as well as the accuracy of STE twist measurements against a reference method at different VRs.

It is important to emphasize that this phantom's single purpose was to generate twist for ultrasound measurements, not to mimic the physiology of the human heart.

Materials and methods

Left ventricular phantom construction

A phantom was designed to mimic a contracting and twisting left ventricle (Figure 1), using a similar technique as has been recently published for other cardiac simulation studies [21]. This phantom was entirely made from PVA with wall properties to introduce twist, thereby avoiding any apical deformation attachment. It has a truncated prolate spheroid shape and consists of two layers with different thickness and elastic properties in a spiral layout which forces it to twist when the phantom is inflated or deflated. This spiral structure is divided into eight continuous bands, with the inner layer differing in thickness from 0.1 to 8 mm at the base and from 0.1 to 4 mm at the apex. The internal diameter is 42 mm and the total length of the phantom is 92 mm (Figure 1A and B). These dimensions were based on our previous study [9]. The spiral structure is angled 45° to the longitudinal direction of the phantom, but narrows to 0° at the apex, which is necessary for the bands to meet. The outer layer gives the phantom a smooth surface and results in a total thickness of 12 mm at the base and 8 mm at the apex in the relaxed state (end systole). The thinner wall at the apex was found necessary to avoid spherical ballooning during water inflation (diastole). The phantom was casted using 3D printed molds in acrylonitrile butadiene styrene (ABS) plastic, with a one-part internal mold, a four-part external mold for the inner layer and a one-part external mold for the outer layer. The basal part of the phantom was anchored in a threaded mounting base, made of ABS plastic (Figure 1B). The molds were designed using computer-aided design (CAD) software (Rhino 5, Robert McNeel & Associates, Seattle, WA, USA). Both PVA layers were made of a material solution consisting of 10% by weight PVA (M_w 89K–98K, 99+% hydrolyzed, Sigma-Aldrich, Saint Louis, MO, USA) and 90% water. During casting, the solution was frozen for 12 h in –18°C, and then thawed at room temperature for 12 h. The inner layer first underwent five freezing cycles before it was taken out of the inner layer mold, which was replaced by the outer layer mold. Additional PVA material was then added to the mold, and it went through one more freezing cycle, which gave the inner layer a total of six cycles and the outer layer one. This made the inner layer rigid, which was necessary to make the phantom twist, ending up with a phantom with smooth inner and outer surfaces (Figure 1C).

Pump rig

The phantom was installed in a custom-made pump-rig similar to a previously published *in vitro* setup [22, 23]. The phantom itself was submerged in a water container with the apex pointing toward the surface, connected via rigid pipes to a dual-cylinder pump. Absorbing sheets covered the wall of the reservoir to reduce ultrasound reflections. The pump inflates and deflates the phantom using water, thus simulating the deformation of the left ventricle. The pump was driven by a stepper motor controlled by custom-made software, simulating heart cycles at different stroke volumes and pump rates, hereinafter referred to as heart rate (HR). More details about the pump rig can be found elsewhere [9, 20]. A 3D ultrasound probe (4V, GE Vingmed Ultrasound, Horten, Norway) was partially submerged 4 cm above the phantom apex, and connected to an ultrasound scanner (Vivid E9, GE Vingmed Ultrasound).

Sonomicrometry as the gold standard

Sonomicrometry has proven to be an accurate reference method for measuring dimensional changes for both *in vitro* and animal studies

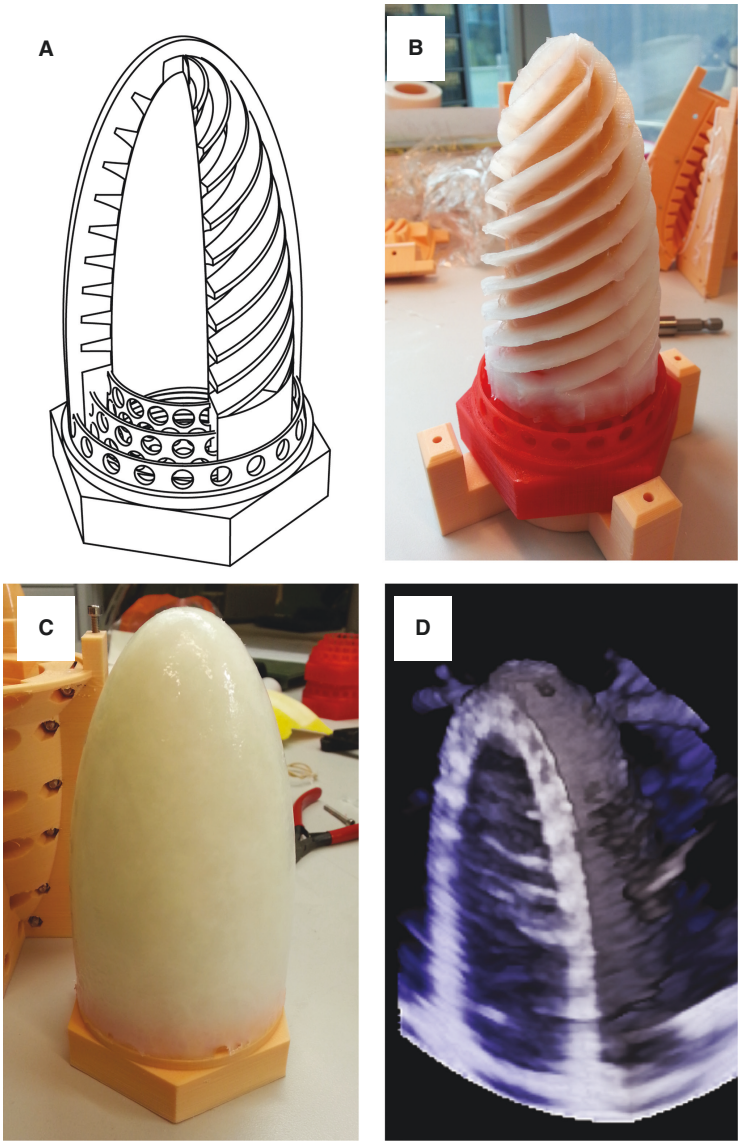

Figure 1: Design of the twisting ultrasound phantom.
(A) Schematic view of the phantom components. (B) Spiral layer and (C) final phantom including a smooth outer layer. (D) Appearance in 3D B-mode imaging.

[15, 23–25]. In this study, a total of six crystals were used. Three crystals were placed in an equilateral triangle at the base of the phantom, and three other crystals were placed in an opposite triangle at the apex, giving the crystal placement the shape of a triangular antiprism (Figure 2A). The crystals were placed at mid wall in the same planes as the ultrasound software would calculate twist, for direct comparison. A small drop of cyanoacrylate glue was used to fix each crystal in place during the complete protocol. The sonomicrometer method with six crystals defined two planes. A direct measurement of the distances between all crystals will correlate directly to strain, depending on the direction. The distances between all sonomicrometer crystals were logged at 192 samples/s using a commercial

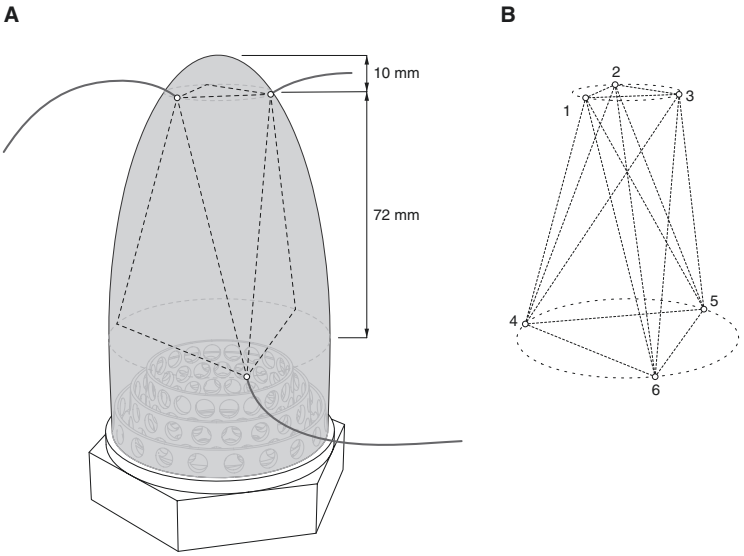

Figure 2: Sonomicrometer reference method.
(A) The two planes with three crystals in each plane. (B) Measured distances between all crystals make it possible to calculate the Cartesian coordinates by use of trilateration, which form the basis for twist estimation (see text for details).

sonomicrometer system (DS3-8 and LabChart Pro v7, Sonometrics Corporation, Ontario, Canada). Measurement resolution is specified by the manufacturer to be within 0.0124 mm given ideal conditions. In this study, our interest was to measure twist between the two planes of crystals. Measuring the angle rotation requires an external fixed reference for observation of the crystal movements and was not carried out. Torsion was not calculated in this one-size phantom study. A custom-made software application was written using MATLAB (MATLAB 2014b, MathWorks Inc., Natick, MA, USA) to calculate twist based on the distances measured by sonomicrometry (Figure 2B). This software used the method of trilateration to calculate the spatial coordinates of the crystals by knowing all the distances between them. Knowing the coordinates of the crystals, it then calculated the relative angles of the two planes using trigonometric functions. This was done for each sample from the sonomicrometer and a twist curve was produced where the peak twist value was selected for comparison with STE peak twist.

Acquisition protocol

The amount of twist was controlled by the stroke volume of the pump, which determined the amount of deformation of the phantom. A series of 21 different stroke volumes (5–105 ml with 5-ml intervals) were recorded using 11 recordings with different acquisition settings for each volume, 231 recordings in all. Recordings were obtained for single-beat using 25.5 volumes per second (VPS); for two-beat multi-beat using 14.4, 21.2 and 47.9 VPS; for four-beat multi-beat using 20.3, 27.0 and 42.4 VPS; and for six-beat multi-beat using 17.1, 30.4, 43.2 and 63.6 VPS. These acquisition settings were chosen because of hardware limitations and software requirements as well as for optimizing image quality. All recordings were done at HR 60 beats/min and with a systolic/diastolic time ratio of 30:70. Multi-beat recordings require an electrocardiography (ECG) signal to detect each heartbeat. This was achieved by sending the start/stop trigger pulse from the pump to a digital logger, corresponding to the start and end of injection (diastole). The signal was then modified and scaled to mimic the QRS of an ECG. This signal was connected to the ECG input of the scanner (Figure 3, lower left). To keep the same starting point of the deformation cycle (relaxed phantom or systole), a small positive starting pressure was given, keeping the same symmetric and slightly stretched phantom as the starting point for all 231 recordings.

All recordings were carried out with harmonic imaging at 1.7/3.3 MHz, and the quality of the B-mode recordings was optimized for a large stroke volume, resulting in settings for depth 0–14 cm and sector angle 75°. All acquisition settings were kept constant throughout all recordings.

Speckle tracking analysis of twist

Recorded ultrasound 3D images were analyzed using the 4D Auto LVQ tool of EchoPAC workstation software (EchoPAC BT201, GE Vingmed Ultrasound). The lumen of the phantom as well as the region of interest (ROI) were defined in end systole (relaxed phantom) and end diastole (expanded phantom). The software then calculated the rotational data in four different levels using STE, as shown in Figure 3. The rotational values of the basal segments were subtracted from the values of the apex segments, thus corresponding to the twist values from the same planes as measured by the sonomicrometer method.

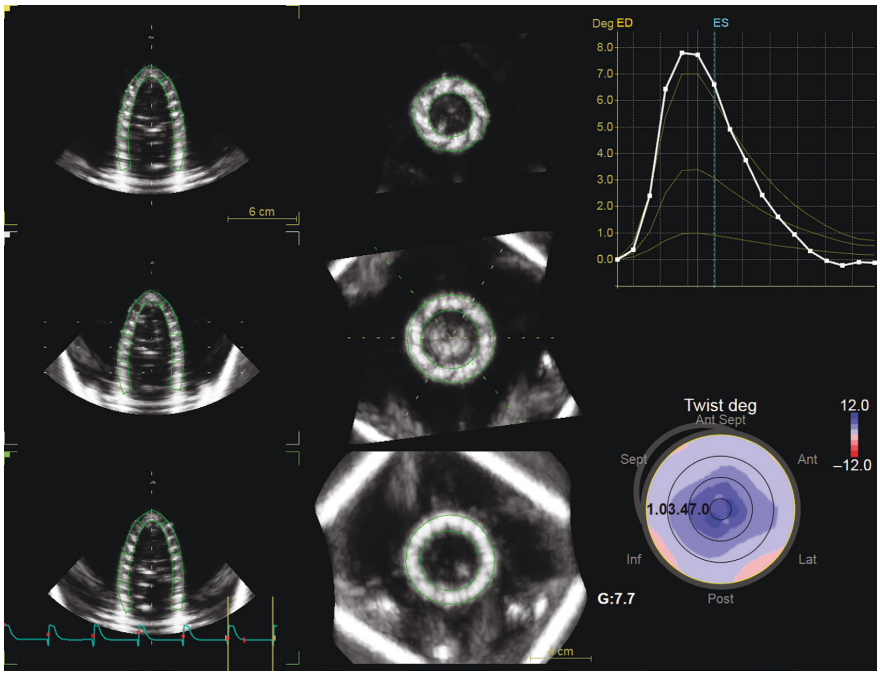

Figure 3: Speckle tracking of the twisting phantom.
From left, three long-axis views, three short-axis views, time-curve (upper, right) and the rotation at three levels, base, mid and apical. The values of the fourth level, apex, are not presented with a curve, but are provided with the software. The twist curve, which was used in this study, is calculated by subtracting base rotation from apex rotation, which gives 7.7° in this example.

Statistics

Linear correlation coefficient, giving the association between the two twist methods, and Bland-Altman analysis [26], giving the mean difference and limits of agreement [±1.96 standard deviation (SD)] as absolute differences between the methods, were calculated for each VR setting.

Results

The ultrasound appearance of the constructed phantom in B-mode is shown in Figures 1D and 3 and is close to a clinical recording but with somewhat more “spotty” echo appearance with less distinct speckles than myocardium. The current setup gave a range of sonomicrometer twist values from 2.0° to 13.8° (Figure 4). The EchoPAC software was able to track the movement of the phantom wall at low and medium VR (as in Figure 3), but had difficulties at the highest recorded VR, probably due to the reduced beam density with corresponding low spatial resolution,

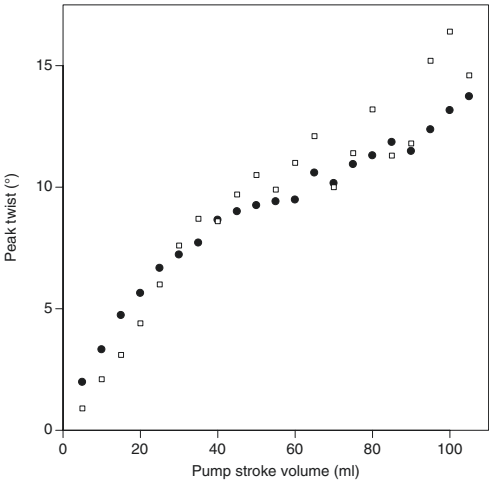

Figure 4: Peak twist vs. pump stroke volume measured with sonomicrometry (filled circles) and 3D STE using six-beat multi-beat acquisition at 17.1 VPS (open squares).
n = 21.

Table 1: Comparison of 3D STE twist with sonomicrometry.

Mode	Volume rate (VPS)	R	Bland-Altman	
			Mean diff (°)	±1.96 SD (°)
One beat	25.5	0.630	−4.62	2.46
Two beat	14.4	0.960	−1.19	1.00
	21.2	0.906	−3.94	1.38
	47.9	0.740	−5.52	2.23
Four beat	20.3	0.973	−0.17	1.91
	27.0	0.942	−1.21	1.18
	42.4	0.849	−5.03	1.67
Six beat	17.1	0.977	0.45	1.31
	30.4	0.944	−0.99	1.65
	43.2	0.941	−2.01	1.28
	63.6	0.603	−6.32	3.05

Mean diff, mean of the differences between 3D twist and sonomicrometer twist; R, linear correlation coefficient; ±1.96 SD, limits of agreement according to Bland-Altman analysis.

and also the appearance of the phantom wall at high VR. More details on this are provided in the Limitations section.

A total of 231 3D ultrasound recordings were analyzed for 21 different volumes at 11 different acquisition settings. A summary of the results from the correlation and Bland-Altman analysis is shown in Table 1. The best association between twist by 3D STE and sonomicrometry measured by correlation was achieved for six-beat multi-beat at 17.1 VPS with a correlation coefficient of 0.977. Best agreement between measurements based on mean difference was achieved for four-beat multi-beat at 20.3 VPS with a correlation coefficient of 0.973 and an agreement of −0.17° ± 1.91° (mean difference ± 1.96 SD), followed by six-beat multi-beat 17.1 VPS with an agreement of 0.45° ± 1.31°. Figures 5 and 6 show examples of scatter plots and corresponding Bland-Altman plots of the best results obtained

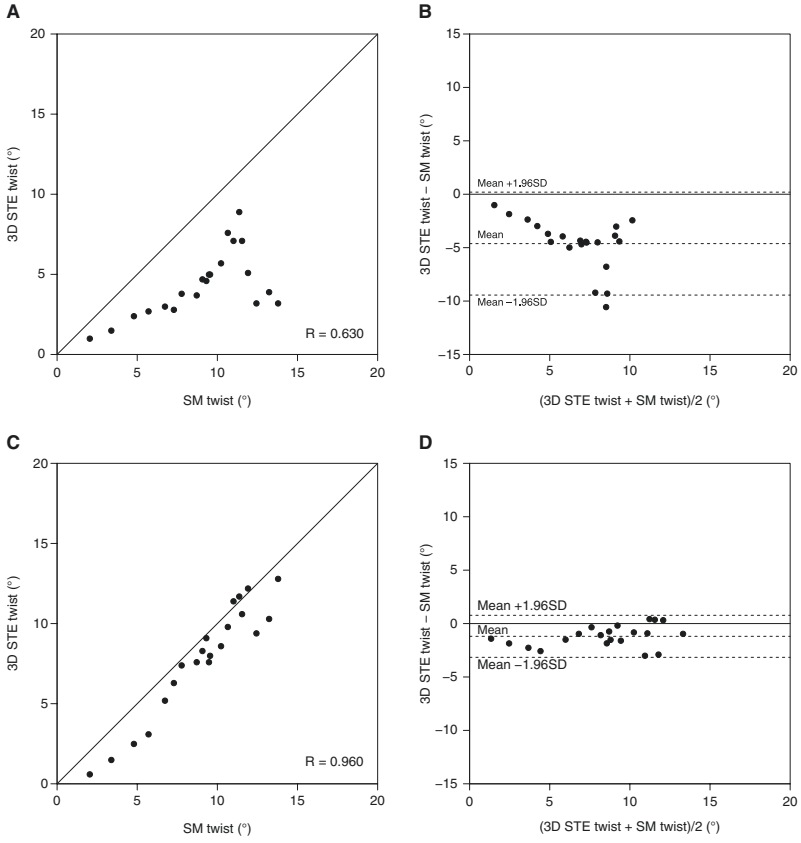

Figure 5: Scatter plots for 3D speckle tracking (STE) twist vs. sonomicrometer (SM) twist (left panels) and Bland-Altman plots (right panels). (A) and (B) show results for single-beat acquisition at 25.5 VPS, and (C) and (D) show results for two-beat multi-beat at 14.4 VPS. n = 21 for all scatter plots.

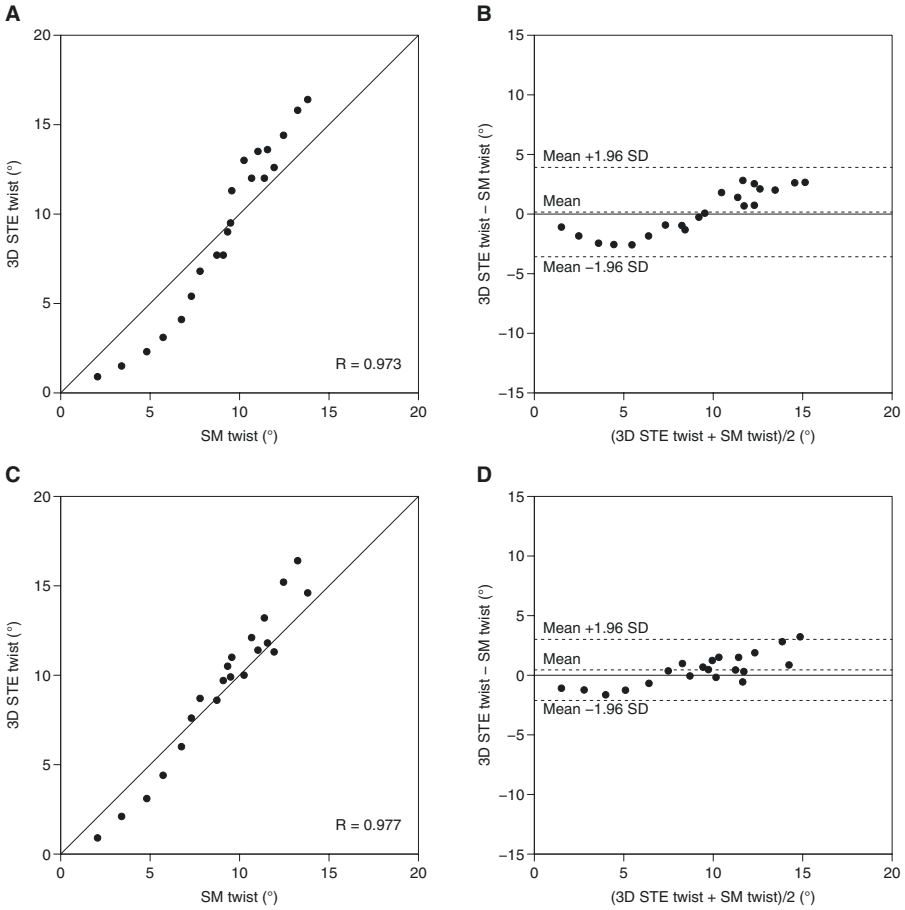

Figure 6: Scatter plots for 3D speckle tracking (STE) twist vs. sonomicrometer (SM) twist (left panels) and Bland-Altman plots (right panels). (A) and (B) show results for four-beat multi-beat acquisition at 20.3 VPS and (C) and (D) for six-beat multi-beat at 17.1 FPS. n = 21 for all scatter plots.

for each acquisition method, single-beat, two-, four- and six-beat multi-beat.

Discussion

The phantom developed in this study proved to be a useful tool for investigating the accuracy of twist measurement and gave a B-mode appearance similar to normal myocardium (Figures 1 and 3). Good speckle tracking as well as the ability to support large stroke volumes up to 120 ml were demonstrated. It had, however, some limitations in tracking at high scanner VR and some limitations in the achieved range of twist values. The measurement of 2D STE twist has been used for some years, but the accuracy of 2D derived twist measurements is debated [10, 11]. Using 3D STE for twist measurements is a relatively new method, and few studies have evaluated the accuracy of different 3D acquisition methods in animals and *ex vivo* investigations. The phantom developed in this study is an improvement compared to previous phantoms and *ex vivo* preparations because of the synthetic nature of the phantom. It has the ability to repeat and reproduce tests of acquisition methods and software over time, and eliminates the need for any external apical attachment [18, 19, 27].

Volume rate dependency

This study shows that high spatial resolution is as important as high temporal resolution for accurate 3D STE twist measurements (Table 1). The reason for this is two-fold. First, low spatial resolution for a cardiac sector probe, especially the lateral resolution at sector depths, gives large presentation of individual speckles, thus reducing the tracking accuracy. Second, for 3D acquisition, the speckles can be followed through an increased number of frames compared to 2D short-axis recordings, where speckles disappear out of the 2D plane due to the in- and out-of-plane motion. This is a limitation for any 2D left ventricular short-axis recording and will influence the measurement of circumferential strain as well as rotation, twist and torsion. This effect is reduced for 3D acquisitions [10, 11]. As seen from Table 1, good agreement was found for several multi-beat settings at relatively low VR compared to the FR of typical 2D recordings. Single-beat STE recordings (VR = 25.5 VPS) gave relatively poor agreement with sonomicrometry due to poor spatial resolution compared to any multi-beat recording. The best agreement between 3D STE and the reference method was achieved using four-beat multi-beat at 20.3 VPS and six-beat multi-beat at 17.1 VPS (Table 1). Sufficient VR for a 3D recording in a clinical setting must be seen relatively to the HR of the patient, and a better measure of sufficient VR is the VR/HR ratio corresponding to the FR/HR ratio for 2D acquisitions. In this study, all recordings were carried out at 60 strokes/min and thus the VR/HR ratio for VR = 20.3 VPS equals 0.34 which is lower than that recommended for 2D deformation measurements [28].

Being able to track speckles through more B-mode frames in a 3D dataset compared to a 2D dataset opens for less requirement for high temporal resolution, enabling an increased beam density and thus a better lateral resolution to be used. This is similar to the findings in our previous 3D phantom study on strain, where the best agreement with the same reference method was 36.6 VPS for longitudinal strain and 30.2 for circumferential strain [9].

The phantom and pump setup shown in this study is a useful utility for evaluating twist measurements. Rotation and torsion measurements are also possible to evaluate depending on the setup. The sonomicrometry system showed a reduced increment of peak twist at stroke volumes above 60 ml (Figure 4). This is probably caused by a reduced twist deformation when the phantom shape becomes more spherical.

Tracking limitations

Tracking was difficult especially at high VR and high stroke volumes. The results for high VR are thus not necessarily only a result of limitations of the STE algorithm but also a result of the changing properties of the PVA phantom. It was noted that at the highest stroke volumes the echo appearance of the phantom changed and included a stronger echo from the transition between the spiral layer and the smoothing layer of the phantom wall (Figure 3). This artificially strong echo was detected and followed by the tracking algorithm and could be the cause of the underestimation at high VR and large stroke volume.

The phantom appears with less defined speckles in the B-mode recording than myocardium in a good quality clinical recording. Adding particles to the PVA would increase the speckle appearance [23, 29, 30]. Based on several previous studies, sufficient backscatter from the PVA is present without additives [9, 20, 22], and too strong speckle appearance would make the phantom less relevant as a test object for clinical measurements where image quality varies between patients.

Other limitations

Clinical 2D twist studies have shown a great variation in twist, and a test phantom should produce all published twist values. As twist is load-dependent, this will result in twist variation in addition to vendor differences and the effect of different definition of selected planes [31]. It has been shown that ischemia reduces ventricular twist [2]; another study showed increased twist in the hypertrophic left ventricle with a mean value of twist angle for concentric hypertrophy measured to 19.4° [1]. In this study, we obtained 13.8° as our maximum twist value at 105 ml (Figure 4), covering the range of normal and ischemic values, but not for all peak values reported for hypertrophy. One possible solution for obtaining higher twist values would be to decrease the pressure in the phantom at the end of systole (relaxed phantom). We found this hard to reproduce because at this point in the pump cycle it was necessary to start injection of fluid with a symmetric phantom and slightly stretched phantom. A clinically measured peak systolic twist value is derived from the clockwise rotation of the base (as seen from the apex during systole), and the counter-clockwise rotation of the apex. This deformation is challenging to mimic in a physical phantom and it is easier to cover a larger range of twist values with an *ex vivo* preparation, as published

by Ashraf and coworkers [27]. Design improvements should be considered in the future, including increasing the number of spirals and the spiral angle.

Accuracy of the reference system

Sonomicrometry is considered the gold standard for experimental and laboratory measurement of dimensional changes. Applications include positioning the crystals at different levels of the left ventricle to measure twist and torsion in large animals [15]. Sonomicrometry relies on the receiving crystal being in the beam of the transmitted crystal and also on sufficient amplitude of the received RF pulse throughout the heart cycle to avoid triggering errors. In this study, the received crystal amplitude was carefully checked for all crystal combinations throughout the experiment. Any sonomicrometry triggering error was identified and corrected if needed. All crystals were implanted at mid-wall, as the EchoPAC software gives a mid-wall weighted measure of deformation.

Clinical implications

This study recommends a lower VR for twist measurement using 3D echocardiography than recommendations for 2D strain and twist measurements. The balance between temporal and spatial resolution is different for 3D STE because the speckles can be followed through more frames than for short-axis 2D recordings, where in- and out-of-plane motion is a major limitation. The setup in this study is not directly transferrable to a clinical situation, where the apex of the heart is almost stationary, and the atrioventricular plane is moving in the longitudinal chamber direction. In this setup, however, the base of the phantom is stationary, and the apex is moving and the purpose of this study is to evaluate twist measurements, not to simulate the heart contraction.

This study was carried out using equipment from one vendor only and is not directly transferrable to other vendors. However, the main conclusion should be relevant because the temporal and spatial resolution are limitations in all 3D echocardiography regardless of the vendor. A standardization of measurement of rotation, twist and torsion is strongly needed, such as the recent standardization of longitudinal strain measurements [13, 32]. These studies were carried out in collaboration with the industry, where newer versions of different software gave less variation in strain between vendors. Few, if any, similar studies exist on twist and torsion and this study shows a useful tool for testing different algorithms and for vendor comparison for the improvement of the accuracy of twist measurements.

Conclusion

The twisting left ventricular phantom developed in this study was a practical tool to study the accuracy of 3D echocardiographic measurements of twist. It gave a useful range of twist values at different stroke volumes and has the advantage of enabling measurements to be carried out over time due to synthetic material design. Best agreement between STE and sonomicrometer values using correlation coefficients was obtained for multi-beat acquisition using a VR between 17.1 and 30.4 VPS, while accuracy was reduced for single-beat at 25.5 VPS and multi-beat at a higher VR. Smallest offset and limits of agreement using a Bland-Altman analysis were obtained at 17.1 VPS using six-beat multi-beat acquisitions. Twist values showed good agreement with sonomicrometry with multi-beat giving better accuracy than single-beat.

Acknowledgments: Financial support was provided by the Bergen University Heart Foundation and from the MedViz consortium, an inter-institutionary R&D program in medical visualization by the University of Bergen, Haukeland University Hospital and Christian Michelsen Research. There is no conflict of interest and the above-mentioned institutions played no part in the development or approval of this manuscript.
Research funding: Authors state no funding involved.
Conflict of interest statement: Both authors declare that they have no competing interests concerning this study.
Informed consent: Informed consent is not applicable.
Ethical approval: The conducted research is not related to either human or animals use.

References

[1] Cameli M, Lisi M, Righini FM, Massoni A, Mondillo S. Left ventricular remodeling and torsion dynamics in hypertensive patients. Int J Cardiovasc Imaging 2013;29:79–86.
[2] Moen CA, Salminen PR, Grong K, Matre K. Left ventricular strain, rotation, and torsion as markers of acute myocardial ischemia. Am J Physiol Heart Circ Physiol 2011;300:H2142–54.
[3] Nagata Y, Takeuchi M, Wu VC, Izumo M, Suzuki K, Sato K, et al. Prognostic value of LV deformation parameters using 2D and

3D speckle-tracking echocardiography in asymptomatic patients with severe aortic stenosis and preserved LV ejection fraction. JACC Cardiovasc Imaging 2015;8:235–45.
[4] Russel IK, Gotte MJ, Bronzwaer JG, Knaapen P, Paulus WJ, van Rossum AC. Left ventricular torsion: an expanding role in the analysis of myocardial dysfunction. JACC Cardiovasc Imaging 2009;2:648–55.
[5] Weyman AE. The year in echocardiography. J Am Coll Cardiol 2007;49:1212–9.
[6] Sugimoto T, Dulgheru R, Bernard A, Ilardi F, Contu L, Addetia K, et al. Echocardiographic reference ranges for normal left ventricular 2D strain: results from the EACVI NORRE study. Eur Heart J Cardiovasc Imaging 2017;18:833–40.
[7] Kocabay G, Muraru D, Peluso D, Cucchini U, Mihaila S, Padayattil-Jose S, et al. Normal left ventricular mechanics by two-dimensional speckle-tracking echocardiography. Reference values in healthy adults. Rev Esp Cardiol (Engl Ed) 2014;67:651–8.
[8] Opdahl A, Helle-Valle T, Skulstad H, Smiseth OA. Strain, strain rate, torsion, and twist: echocardiographic evaluation. Curr Cardiol Rep 2015;17:568.
[9] Hjertaas JJ, Fossa H, Dybdahl GL, Gruner R, Lunde P, Matre K. Accuracy of real-time single- and multi-beat 3-d speckle tracking echocardiography *in vitro*. Ultrasound Med Biol 2013;39:1006–14.
[10] Parisi V, Losi MA, Contaldi C, Chiacchio E, Pastore F, Scatteia A, et al. Speckle-tracking analysis based on 2D echocardiography does not reliably measure left ventricular torsion. Clin Physiol Funct Imaging 2013;33:117–21.
[11] Wu VC, Takeuchi M, Otani K, Haruki N, Yoshitani H, Tamura M, et al. Effect of through-plane and twisting motion on left ventricular strain calculation: direct comparison between two-dimensional and three-dimensional speckle-tracking echocardiography. J Am Soc Echocardiogr 2013;26:1274–81.e4.
[12] Park CM, March K, Williams S, Kukadia S, Ghosh AK, Jones S, et al. Feasibility and reproducibility of left ventricular rotation by speckle tracking echocardiography in elderly individuals and the impact of different software. PLoS One 2013;8:e75098.
[13] Voigt JU, Pedrizzetti G, Lysyansky P, Marwick TH, Houle H, Baumann R, et al. Definitions for a common standard for 2D speckle tracking echocardiography: consensus document of the EACVI/ASE/Industry Task Force to standardize deformation imaging. J Am Soc Echocardiogr 2015;28:183–93.
[14] Lang RM, Badano LP, Mor-Avi V, Afilalo J, Armstrong A, Ernande L, et al. Recommendations for cardiac chamber quantification by echocardiography in adults: an update from the American Society of Echocardiography and the European Association of Cardiovascular Imaging. J Am Soc Echocardiogr 2015;28:1–39.e14.
[15] Helle-Valle T, Crosby J, Edvardsen T, Lyseggen E, Amundsen BH, Smith HJ, et al. New noninvasive method for assessment of left ventricular rotation: speckle tracking echocardiography. Circulation 2005;112:3149–56.
[16] Kleijn SA, Brouwer WP, Aly MF, Russel IK, de Roest GJ, Beek AM, et al. Comparison between three-dimensional speckle-tracking echocardiography and cardiac magnetic resonance imaging for quantification of left ventricular volumes and function. Eur Heart J Cardiovasc Imaging 2012;13:834–9.
[17] Zhou W, Benharash P, Ho J, Ko Y, Patel NA, Mahajan A. Left ventricular twist and untwist rate provide reliable measures of ventricular function in myocardial ischemia and a wide range of hemodynamic states. Physiol Rep 2013;1:e00110.
[18] Ashraf M, Zhou Z, Nguyen T, Ashraf S, Sahn DJ. Apex to base left ventricular twist mechanics computed from high frame rate two-dimensional and three-dimensional echocardiography: a comparison study. J Am Soc Echocardiogr 2012;25:121–8.
[19] Wood PW, Gibson PH, Becher H. Three-dimensional echocardiography in a dynamic heart phantom: comparison of five different methods to measure chamber volume using a commercially available software. Echo Res Pract 2014;1:51–60.
[20] Khan U, Hjertaas JJ, Greve G, Matre K. Optimal acquisition settings for speckle tracking echocardiography-derived strains in infants: an *in vitro* study. Ultrasound Med Biol 2016;42:1660–70.
[21] Jansen-Park SH, Hsu PL, Muller I, Steinseifer U, Abel D, Autschbach R, et al. A mock heart engineered with helical aramid fibers for *in vitro* cardiovascular device testing. Biomed Tech (Berl) 2017;62:139–48.
[22] Lesniak-Plewinska B, Cygan S, Kaluzynski K, D'Hooge J, Zmigrodzki J, Kowalik E, et al. A dual-chamber, thick-walled cardiac phantom for use in cardiac motion and deformation imaging by ultrasound. Ultrasound Med Biol 2010;36:1145–56.
[23] Heyde B, Cygan S, Choi HF, Lesniak-Plewinska B, Barbosa D, Elen A, et al. Regional cardiac motion and strain estimation in three-dimensional echocardiography: a validation study in thick-walled univentricular phantoms. IEEE Trans Ultrason Ferroelectr Freq Control 2012;59:668–82.
[24] Bouchez S, Heyde B, Barbosa D, Vandenheuvel M, Houle H, Wang Y, et al. *In-vivo* validation of a new clinical tool to quantify three-dimensional myocardial strain using ultrasound. Int J Cardiovasc Imaging 2016;32:1707–14.
[25] Urheim S, Edvardsen T, Torp H, Angelsen B, Smiseth OA. Myocardial strain by Doppler echocardiography. Validation of a new method to quantify regional myocardial function. Circulation 2000;102:1158–64.
[26] Bland JM, Altman DG. Measuring agreement in method comparison studies. Stat Methods Med Res 1999;8:135–60.
[27] Ashraf M, Myronenko A, Nguyen T, Inage A, Smith W, Lowe RI, et al. Defining left ventricular apex-to-base twist mechanics computed from high-resolution 3D echocardiography: validation against sonomicrometry. JACC Cardiovasc Imaging 2010;3:227–34.
[28] Rösner A, Barbosa D, Aarsaether E, Kjonas D, Schirmer H, D'Hooge J. The influence of frame rate on two-dimensional speckle-tracking strain measurements: a study on silico-simulated models and images recorded in patients. Eur Heart J Cardiovasc Imaging 2015;16:1137–47.
[29] Mårtensson M, Bjallmark A, Brodin LA. Evaluation of tissue Doppler-based velocity and deformation imaging: a phantom study of ultrasound systems. Eur J Echocardiogr 2011;12:467–76.
[30] Larsson M, Heyde B, Kremer F, Brodin LA, D'Hooge J. Ultrasound speckle tracking for radial, longitudinal and circumferential strain estimation of the carotid artery – an *in vitro* validation via sonomicrometry using clinical and high-frequency ultrasound. Ultrasonics 2015;56:399–408.
[31] A'Roch R, Gustafsson U, Poelaert J, Johansson G, Haney M. Left ventricular twist is load-dependent as shown in a large animal model with controlled cardiac load. Cardiovasc Ultrasound 2012;10:26.
[32] Yang H, Marwick TH, Fukuda N, Oe H, Saito M, Thomas JD, et al. Improvement in strain concordance between two major vendors after the strain standardization initiative. J Am Soc Echocardiogr 2015;28:642–8.e7.

Graphic design: Communication Division, UiB / Print: Skipnes Kommunikasjon AS

uib.no

ISBN: 9788230854228 (print)
9788230851111 (PDF)